CTU
CZECH TECHNICAL UNIVERSITY IN PRAGUE

FACULTY OF ELECTRICAL ENGINEERING
Department of Control Engineering

Doctoral Thesis

Measures and LMIs

for V&V of Adaptive Control

November 2020

Daniel Wagner

Czech Technical University in Prague

Faculty of Electrical Engineering
Department of Control Engineering

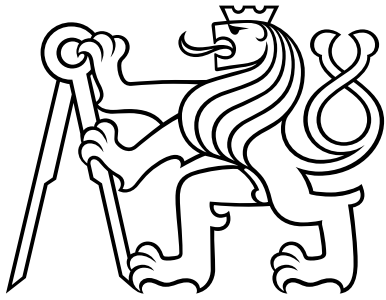

Doctoral Thesis

Measures and LMIs

for V&V of Adaptive Control

by Ing. Daniel Wagner

presented to the Faculty of Electrical Engineering,
Czech Technical University in Prague,
in partial fulfillment of the requirements
for the degree of
Doctor of Philosophy

Ph.D. program: Electrical Engineering and Information Technology
Branch of study: Control Engineering and Robotics
Supervisor: Prof. Ing. Didier Henrion, Ph.D.
Co-supervisor: Doc. Ing. Martin Hromčík, Ph.D.

November 2020

Acknowledgement

From trail's end can you look back to reflect on your journey, your fortune, and the people that brought you here. First and foremost, I would like to thank both of my advisers: Dr. Didier Henrion and Dr. Martín Hromčík. Didier, your patience and incredible insight have made me into a better student and a better person. Martin, your wisdom and encouragement have helped me overcome all adversity. I enjoyed those constructive discussions about research in aerospace. Both of you served as my feedback loop for my PhD. It was a privilege working with both of you. I couldn't have picked better advisers. I also wish to thank Czech Technical University and GAČR for providing me financial support during my PhD.

My work is unfinished without mentioning those who helped me from across the ocean at University of South Florida and Embry-Riddle. Dr. Tansel Yucelen and Dr. K Merve Dogan, I give you my thanks. Tansel, you were an amazing supervisor during my Master's degree. I was elated to still collaborate with you during my PhD. Dr. Merve Dogan, it was a pleasure having you both as a lab partner and as a friend. Thank you both for collaborating with me and providing feedback.

Lastly, I extend my thanks out to my friends and family. Without them, I would have never went on that trail less traveled. All of you have made making this far away place feel a little closer to home.

Declaration

This dissertation is submitted in partial fulfillment of the requirements for the degree of doctor of philosophy (Ph.D.). The work submitted here is the result of my own investigation, except when stated otherwise. I hereby declare that the contents of this dissertation were produced by the author, unless stated otherwise. Any sources contained in this document are cited in accordance with the methodical instructions in in regards to ethical principles for writing academic thesis for CTU in Prague. I also declare that the material herein are not concurrently submitted for any other degree.

Czech Technical University in Prague
November 2020

Daniel Wagner

Abstract

Verification and Validation remains a critical and costly process in the field of aerospace. The current state-of-the-art relies on linear analysis and Monte-Carlo to identify worst case behavior and the existence of unsafe trajectories in the model. These methods remain applicable only to aircraft models with linear feedback. In practice, aircraft dynamics are seldom linear. This is due to inherent aerodynamic nonlinearities and actuators with rate/deflection saturation that do not follow the first order model. In that sense, adaptive control remains promising since it can, by design, reject exogenous disturbances and alleviate shortcomings with modeling accuracy. However, the added complexity makes it impossible to numerically validate using traditional methods. New state-of-the-art tools are required. This thesis utilizes occupation measures and LMI relaxations (called the moment sums of squares or Lasserre hierarchy) on nonlinear aircraft models with nonlinear feedback and piecewise constraints. This framework can be used in conjunction with Lyapunov analysis to impose strict transient/terminal performance guarantees on the closed-loop. This thesis provides the flight controls community with a powerful set of tools that can build confidence in using nonlinear controllers to reduce fatalities and loss-of-control events.

Abstrakt

Validace a verifikace zákonů řízení zůstává na poli leteckého a kosmického průmyslu nadále kritickým a nákladným procesem. Nejmodernější postupy se při identifikaci nejhorších scénářů a existence riskantních trajektorií v rámci modelu spoléhají na lineární analýzy a Monte-Carlo metody. Tyto metody lze použít pouze pro modely letounů s lineární zpětnou vazbou. V praxi je však dynamika letounu jen zřídkakdy lineární. Důvodem jsou základní aerodynamické nelinearity a a saturace akčních členů. V tomto smyslu představuje adaptivní řízení slibnou metodu, jelikož již z principu vylučuje vnější vlivy a zmírňuje nedostatky v rámci přesností modelu. Větší komplexita však znemožňuje numerické ověření pomocí tradičních metod. Jsou vyžadovány nové a moderní nástroje. Tato diplomová práce využívá okupační míry a relaxace LMI (nazývané momentové součty čtverců nebo Lasserrova hierarchie) na nelineárních modelech letounů s nelineární zpětnou vazbou a částečnými omezeními. Tento rámec lze ve spojení s Ljapunovovou analýzou použít k zavedení záruk stability a kvality řízení. Tato práce poskytuje komunitě zabývající se řízením letounů výkonnou sadu nástrojů, které mohou zvyšovat jistotu při používání nelineárního řízení a redukovat tak počet obětí a situace ztráty kontroly nad řízením.

List of Symbols

The following list specifies the most important symbols used in this doctoral thesis. Symbols excluded from this list are defined later in the text. Note that some symbols might have multiple meanings depending to the context.

Uppercase Latin letters

A	system matrix
A_{r}	reference system matrix
B	system input matrix
B_{r}	reference system input matrix
C	system output matrix
C_{r}	reference system output matrix
D	normalizing matrix
I	identity matrix
K_1	state feedback gain matrix
K_2	state feedforward gain matrix
$\mathscr{M}$	measures of a cone
$\mathscr{M}_+$	positive measures of a cone
$\mathbb{R}_+$	set of real positive numbers
$\mathbb{R}$	set of real numbers
S	wing area $\left[\mathrm{ft}^2\right]$
T	total thrust [lbs]
V_T	total velocity [ft/s]
$\mathcal{V}(\mathbf{x}(t))$	Lyapunov candidate function of state vector $\mathbf{x}(t)$
$\hat{\mathbf{W}}(t)$	weight update law vector field

$\hat{W}_i(t)$	ith element of weight update law vector field $\hat{\mathbf{W}}(t)$
P	positive-definite solution matrix for Lyapunov equality
Q	positive-definite tuning matrix for Lyapunov equality

Lowercase Latin letters

div$\mathbf{f}$	divergence operator of vector field $\mathbf{f}$
$\mathbf{f}(\mathbf{x}(t))$	vector field of the state vector $\mathbf{x}(t)$
$f(\mathbf{x}(t))$	scalar function of the state vector $\mathbf{x}(t)$
g	gravitational constant $\left[\text{ft/s}^2\right]$
k	bounded uncertain parameter
m	mass [slugs]
$p(t)$	roll rate [deg/s]
$q(t)$	pitch rate [deg/s]
$\bar{q}$	dynamic pressure $\left[\text{lbs/ft}^2\right]$
$r(t)$	yaw rate [deg/s]
t	time [sec]
$\triangle t$	sampling time step size [sec]
$\mathbf{u}(t)$	system control input vector
$u(t)$	control scalar
$\mathbf{x}(t)$	system state vector
$\mathbf{x_p}(t)$	system state vector for aircraft longitudinal dynamics
$\mathbf{x_q}(t)$	system state vector for aircraft lateral dynamics
$x(t)$	state scalar
$\mathbf{x_r}(t)$	system reference vector
$\mathbf{y}(t)$	system output or state vector, depending on the context
$y(t)$	state or output scalar, depending on context
$\mathbf{z}(t)$	unmodeled dynamics system state vector
$z(t)$	unmodeled state system scalar

Uppercase Greek letters

Γ	adaptation learning rate matrix
$\Phi\big(\mathbf{x}(t)\big)$	known basis function of the state vector $\mathbf{x}(t)$
$\Phi\big(\mathbf{x}(t)\big)_{\mathbf{x}}$	partial derivative known basis function of the state vector $\mathbf{x_p}(t)$ with respect to state vector $\mathbf{x}(t)$

Lowercase Greek letters

$\alpha(t)$	angle of attack
$\beta(t)$	sideslip angle
$\delta_{\mathrm{a}}(t)$	aileron deflection angles
$\delta_{\mathrm{a}}(t)$	elevator deflection angles
$\delta_{\mathrm{r}}(t)$	rudder deflection angles
ϵ	small positive constant
γ	bounded uncertain parameter
$\lambda_{\max}(M)$	the largest eigenvalue of matrix M
$\lambda_{\min}(M)$	the smallest eigenvalue of matrix M
μ_0	initial measure
μ	occupation measure
μ_T	terminal measure
$\phi(t)$	roll angle
$\theta(t)$	pitch angle

Contents

List of Figures

List of Tables

1

Introduction

Verification and Validation (V&V) of the flight control system remains a critical and costly process in aerospace. An error in the flight control software that makes it beyond the testing phase can result in astronomical costs to correct. Loss-Of-Control (LOC) event contribute to 35 percent of fatalities and 22 percent of accidents in commercial aviation [1]. Currently, flight control law development, combined with software implementation and flight testing, now comprise up to 60 percent of the development costs for a modern aircraft [2].

Traditional V&V for flight control laws typically involves Monte-Carlo. This technique involves numerical step integration and random sampling of a hi-fidelity closed-loop model to determine quality properties of the aircraft such as Probability-Loss-Of-Control (PLOC). These events are simulated as they would occur naturally, for each initial condition. Since the number of samples required versus probability of an event happening are inversely proportional, these simulations are prohibitively costly for medium to large scale systems. NASA has developed RASCLE, which combines Monte-Carlo simulation and search tools to only identify the worst case behavior of the plant [3].

For aircraft, there are two types of nonlinearities:

1. Aerodynamic nonlinearities at high angles of attack;
2. Rate and magnitude saturations in the control surfaces of the aircraft.

These nonlinearities can be strongly present, especially near the boundary of the flight envelope for the aircraft. They can be invoked by weather, wind or turbulence, changes to the dynamics of the aircraft, or extreme maneuvers.

Even with hi-fidelity modeling and extensive V&V testing, it is entirely possible for an aircraft LOC event to circumvent detection. For example, LOC caused by the falling-leaf mode on the F/A-18 led to crashes and a complete rewriting of its baseline control laws [4].

Modern control design methods typically involve Lyapunov stability analysis [3]. From a certification perspective, a weakness to this approach is the requirement for a polynomial representation of the plant. This stability analysis usually represents worst case behavior in the aircraft dynamics. Furthermore, Lyapunov analysis can only provide information about the long-range behavior of the learning algorithm. For non-autonomous systems, which are very common in aerospace, the best guarantee is infinite time convergence. From a real-world perspective, it is of more importance to show the nominal system and flight control law converge in finite time.

The increased demand for added functionality from the flight controller has increased its overall size, complexity, and cost to certify. Although traditional methods, such as Monte-Carlo, have consistently produced sufficiently safe and reliable flight control laws, they will be insufficient for V&V of future intelligent systems [5]. Other methods, such as planned test automation, have been proven to reduce test hours but may not do so effectively for newer flight control system requirements.

The current state-of-the-art is using sum-of-squares (SOS) hierarchies with available off-the-shelf-software for V&V. A good implementation is described in [4, 6] where the authors focus on SOS Lyapunov functions to approximate the Region Of Attraction (ROA) of polynomial aircraft models and their linear control laws. A drawback to this approach is that there exists no means of guaranteeing control law convergence in finite time nor V&V of aircraft with nonlinear controllers and/or actuator dynamics.

Model reference adaptive control (or MRAC for short) arises from the fact that, without exception, every physical dynamical system is subject to exogenous disturbances and/or inherent system uncertainties. These phenomena can arise from exogenous forces such as wind and turbulences, or system uncertainties inherited by idealized assumptions, linearization, and/or degraded modes of operation. From a classical controls point of view, there remains a persistent trade-off between modeling uncertainty and the performance of the controller. MRAC bypasses that completely by matching the true nonlinear system to its idealized reference model.

The origins of MRAC can be traced back to [7, 8]. It has since expanded to include additional control modifications that either address uncertain dynamical systems with specific structures or improve robustness and/or tracking performance. See also books [9, 10, 11, 12, 13, 14, 15, 16] and relatively recent surveys [17, 18, 19, 20] that outline the current state-of-the-art. Although the architecture of these controllers can vary, each MRAC is made up of two basic components: a reference system and a parameter adjustment mechanism.

The reference model is designed a priori. In other words, the reference model represents the ideal linearized system we wish to follow. This desired closed loop system is then compared to the true nonlinear model. This comparison

drives the parameter adjustment mechanism in real time. Depending on the structure of the uncertainties, the MRAC can drive the nonlinear system to the trajectories of the reference model asymptotically, or at least remains in a defined a priori bound.

One of the earliest of adaptive control in flight testing was the NASA X-15 [21]. NASA has also implemented a neural net intelligent flight control system on a modified F-15 aircraft [22] and the X-36 tailless fighter [23]. The US Air Force and Boeing have implemented a direct adaptive controller on the Joint Direct Attack Munitions (JDAM) [24]. More recently, NASA has implemented adaptive control for its Space Launch System [25].

There exist several challenges in development of MRAC for aerospace which are discussed extensively in [3, 26]. For example, it is well known that adaptive control subject to unmodeled dynamics can lead to instability [27].

As such, there exists formal no procedure for V&V of MRAC by the Federal Aviation Administration for national air and space. New state-of-the-art tools are required for V&V of adaptive controllers prior to flight testing.

The concept of using optimization techniques for synthesis of adaptive control is relatively recent. Linear Matrix Inequalities (LMIs) have been used compute find allowable bandwidths for MRAC with the presence of actuator dynamics [28]. The results yield conservative bounds of convex Lyapunov-like functionals with uncertain parameters, and cannot deal with nonlinearities such as actuator rate/angle saturation. The convergence guarantees provided by these solutions at best remain asymptotic.

1.1 Thesis Contributions

The scope of this work is to utilize occupation measures and LMI relaxations (called the moment SOS or Lasserre hierarchy) for verification and validation of polynomial aircraft models with adaptive control laws. This can be achieved with off-the-shelf-software (such as Gloptipoly 3 [29]) and SDP solvers (MOSEK [30] or SeDuMi [31]). The main advantage is a guaranteed finite time convergence for non-autonomous systems. This is a significant improvement over Barbalat's Lemma [32], which informs us about the long range stability of a non-autonomous closed-loop system.

By doing so, we can directly optimize over admissible trajectories to ensure properties such as safety (all trajectories starting from a set of initial conditions never reach a set of bad states), avoidance (at least one trajectory starting from initial conditions will never reach a set of bad states), eventuality (at least one trajectory starting from a set of initial conditions will reach a set of good states in finite time), reachability (at least one trajectory starting from a set of initial conditions will reach a set of good states in finite time), and robustness (all trajectories from a set of initial conditions guarantee acceptable

performance subject to disturbances and/or unmodeled dynamics). This is achieved by representing the complete closed-loop system as a polynomial dynamical optimization problem. From there we can write it as its equivalent infinite dimensional LP problem of measures. Lastly, we relax the LP problem of measures and solve using truncated moment LMI sequences.

With our framework, the solutions provided in the proceeding sections are primal since we are optimizing over admissible trajectories. The Lyapunov certificate achieved in the MRAC design is also readily available. We also make direct comparisons to solutions obtained using traditional Monte-Carlo methods. The content and the contributions of each chapter are outlined below:

- **chapter 3** presents V&V problem of a polynomial of the longitudinal dynamics of an F-16 fighter aircraft complete with MRAC. We first present the problem as a polynomial dynamical optimization problem and then discuss the steps necessary to convert it into a feasible moment SOS relaxations problem. Three cases with piecewise disturbances are considered. Since the reference dynamics penalizes the problem with additional states, we approximate the reference dynamics using piecewise polynomials that depend on time.

- **chapter 4** introduces a novel method approximating the reference trajectory in MRAC by exploiting sparsity for Ordinary Differential Equations (ODEs). We then validate a lateral F-16 polynomial model with MRAC with piecewise disturbance at large roll angle. The main contribution of this paper is the validation of a nonlinear controller with a large number of states.

- **chapter 5** considers the V&V problem of model reference adaptive control in the presence of unmodeled flexible dynamics. Since unmodeled dynamics can adversely affect the closed-loop stability with MRAC, they cannot be safely neglected. However, uncertain parameters have an explicit representation in the space of occupation measures. In other words, In our example, an F-16 with linear/polynomial longitudinal dynamics and MRAC is considered with uncertain parameters coupling its longitudinal dynamics to its aeroelastic modes. In our results, we show that there exist sufficiently small parameters that do not incite unsafe trajectories.

- **chapter 6** presents a problem of uncertain higher order actuator dynamics in adaptive control. It is well known that MRAC with the presence degraded actuator performance can lead to closed-loop instability and control departure. An F-16 longitudinal model is considered with higher order actuator dynamics containing uncertain parameters. These uncertain parameters are expressed explicitly in the space of occupation measures.

Then we show that the MRAC can tolerate small uncertainties in the damping and natural frequency of the actuator.

2

Theoretical preliminaries

We begin by briefly stating the standard notation where $\mathbb{R}$ denotes the set of real numbers, $\mathbb{R}^n$ denotes the set of $n \times 1$ column vectors, $\mathbb{R}^{n\times m}$ denotes the set of $n \times m$ real matrices, $\mathbb{R}_+$ denotes the set of positive real numbers, $\|\cdot\|_2$ denotes the Euclidean norm, $\lambda_{\min}(A)$ (respectively, $\lambda_{\max}(A)$) denotes the minimum (respectively, maximum) eigenvalue of a real and square matrix $A \in \mathbb{R}^{n\times m}$. We also use the following definitions taken from [33]. If X is a compact subset of $\mathbb{R}^n$, $\mathscr{C}(X)$ denotes the space of continuous functions on X and $\mathscr{M}(\mathbf{x})$ (respectively, $\mathscr{M}_+(X)$) denotes the cone of (respectively, non-negative) measures. Since any measure $\mu \in \mathscr{M}(X)$ can be viewed as an element of the dual space $\mathscr{C}(X)$, the duality pairing of μ on a test function $v \in \mathscr{C}(\mathbf{x})$ is

$$\int_X v(z)\mu(z). \tag{2.1}$$

For any measure $\mu \in \mathscr{M}_+(X)$, we denote its support as $\mathrm{spt}(\mu)$. A probability measure is a non-negative measure whose integral is exactly one.

2.1 Polynomial Dynamical Optimization

Consider the nonlinear ordinary differential equation (ODE)

$$\dot{\mathbf{x}}(t) = \mathbf{f}(t, \mathbf{x}(t)) \tag{2.2}$$

for all $t \in [0, T]$ and given terminal time $T > 0$, where $\mathbf{x} : [0, T] \to \mathbb{R}^n$ is a time dependent state vector, and vector field $\mathbf{f} : [0, T] \times \mathbb{R}^n \to \mathbb{R}^n$ is a smooth map.

Consider now the following polynomial dynamical optimization problem

$$\begin{aligned} J = \inf_{h_T,\, h} \quad & h_T(T, \mathbf{x}(T)) + \int_0^T h(t, \mathbf{x}(t))dt \\ \text{s.t.} \quad & \dot{\mathbf{x}}(t) = \mathbf{f}(t, \mathbf{x}(t)), \quad \mathbf{x}(t) \in X, \quad t \in [0, T] \\ & \mathbf{x}(0) \in X_0, \quad \mathbf{x}(T) \in X_T \end{aligned} \tag{2.3}$$

with given polynomial dynamics $\mathbf{f} \in \mathbb{R}[t, \mathbf{x}]^n$ and costs $h, h_T \in \mathbb{R}[t, \mathbf{x}]$, and state trajectories $\mathbf{x}(t)$ constrained in the compact basic semialgebraic set $X = \{\mathbf{x} \in \mathbb{R}^n : \quad p_k(\mathbf{x}) \geq 0, k = 1, \ldots, n_X\}$ for given polynomials $p_k \in \mathbb{R}[\mathbf{x}]$. Finally, the initial and terminal states are constrained in the compact basic semialgebraic sets $X_0 = \{\mathbf{x} \in \mathbb{R}^n : \quad p_{0k}(\mathbf{x}) \geq 0, k = 1, \ldots, n_0\}$, and $X_T = \{\mathbf{x} \in \mathbb{R}^n : p_{Tk}(\mathbf{x}) \geq 0, \quad k = 1, \ldots, n_T\} \subset X$ for given polynomials $p_{0k}, p_{Tk} \in \mathbb{R}[\mathbf{x}]$.

The evolution of a family of trajectories solving (2.2) is formalized as follows: First consider one admissible trajectory x on $t \in [0, T]$, we define its occupation measure (denoted $\mu(\cdot|\mathbf{x})) \in \mathscr{M}_+([0, T] \times X)$ as

$$\mu(A \times B|\mathbf{x}) \triangleq \int_0^T I_{A\times B}(t, \mathbf{x}(t))dt \tag{2.4}$$

for all subsets $A \times B$ in the Borel σ-algebra of $[0, T] \times X$, where $I_{A\times B}(\cdot)$ is the indicator function on a set $A \times B$ and is defined as the following: The indicator function of a set A is the function $\mathbf{x} \mapsto I_A(\mathbf{x})$ such that $I_A(\mathbf{x}) = 1$ when $\mathbf{x}(t) \in A$ and $I_A(\mathbf{x}) = 0$ when $\mathbf{x}(t) \notin A$. The quantity $\mu(A \times B|\mathbf{x})$ corresponds to the amount of time the graph (for example, as illustrated in Fig. 2.1) of its trajectory, $(t, \mathbf{x}(t))$, spends in $A \times B$. Similarly, the initial measure can be defined as

$$\mu_0(A \times B) \triangleq I_{A\times B}(0, \mathbf{x}(0)) \tag{2.5}$$

and its terminal measure

$$\mu_T(A \times B) \triangleq I_{A\times B}(T, \mathbf{x}(T)). \tag{2.6}$$

Although the cost function in (2.3) can potentially be nonlinear, it becomes linear when it is formulated with occupation measures. In fact, a similar analog holds true for the dynamics of the system. In other words, the occupation measure associated with an admissible pair satisfy a linear equation over measures [33]. Conversely, all supported measures correspond to the solutions of (2.3).

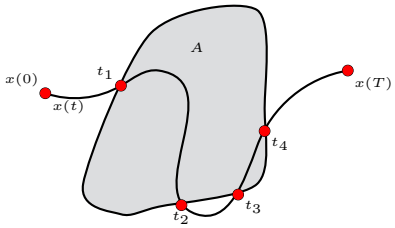

Figure 2.1: Occupation Measure $\mu([0,T]\times A|x) = (t_2 - t_1) + (t_4 - t_3)$

The nonconvex optimization problem (2.3) can be expressed as a convex infinite dimensional LP problem of measures

$$\begin{aligned} J_\infty = \inf \quad & \int h_T(T,\mathbf{x}(T))d\mu_T + \int h(t,\mathbf{x}(t))d\mu \\ \text{s.t.} \quad & \frac{\partial \mu}{\partial t} + \text{div}\mathbf{f}\mu + \mu_T = \mu_0 \\ & \int \mu_0 = 1 \end{aligned} \tag{2.7}$$

where div is the divergence operator and the infimum is with respect to the occupation measure $\mu \in \mathscr{M}_+([0,T]\times X)$, terminal measure $\mu_T \in \mathscr{M}_+(\{T\}\times X_T)$, and terminal time $T > 0$. It may happen that minimum in (2.7) is strictly less than the infimum in (2.3), so we make the following critical assumption:

Assumption 2.1.1. *There is no relaxation gap between (2.7) and (2.3). In other words, $J_\infty = J$.*

Since we assume X_0, X, and X_T are compact, the infinite dimensional LP problem 2.7 can be approximated as the finite dimensional moment LMI relaxations problem

$$\begin{aligned} J_d = \inf \quad & \sum_{i=1}^{3}\sum_{\alpha} c_{i\alpha}y_{i\alpha} \\ \text{s.t.} \quad & \sum_{i=1}^{3}\sum_{\alpha} a_{ij\alpha}y_{i\alpha} = b_j, \quad j = 1,\dots,m \\ & M(y_i) \succeq 0, \quad M(p_{ik}\, y_i) \succeq 0, \quad i = 1,\dots,3, \quad k = 1,\dots,n_i, \end{aligned} \tag{2.8}$$

where the three moment sequences $y_{i\alpha}$, $i = 1,\dots,3$ correspond to the initial, terminal, and occupation measures, respectively,. The constraints $\sum_{i=1}^{3}\sum_{\alpha} a_{ij\alpha}y_{i\alpha} = b_j$, $j = 1,\dots,m$ model the linear transport equations on the moments of the measures. Moment matrix $M(y_i)$ is positive semidefinite

symmetric and linear in y. Symmetric matrices $M(p_{ik}\ y_i)$ are also positive semidefinite and linear in y. They are called the localizing matrices. They ensure that the moments correspond to measures with the appropriate supports. The LMI constraints of this problem are truncated, or relaxed versions of the infinite dimensional problem LMI constraints 2.7, using Lasserre's LMI hierarchy [34]. When relaxation order $d \in \mathbb{N}$ tends to infinity, it holds that $J_d \leq J_{d+1} \leq J_\infty$ and $\lim_{d\to\infty} J_d = J_\infty$.

2.2 Piecewise Polynomial Dynamical Optimization

In this section we extend the results from section 2.1 to a case where the dynamics of the polynomial from (2.3) are piecewise [35]. Consider the following dynamical optimization problem with piecewise polynomial differential constraints

$$\begin{aligned} J = \inf_{h_T,\ h} \quad & h_T(T, \mathbf{x}(T)) + \int_0^T h(t, \mathbf{x}(t))dt \\ \text{s.t.} \quad & \dot{\mathbf{x}}(t) = \mathbf{f_j}(t, \mathbf{x}(t)), \quad \mathbf{x}(t) \in X_j, \quad j = 1, \ldots, N \\ & \mathbf{x}(0) \in X_0, \quad \mathbf{x}(T) \in X_T, \quad t \in [0, T], \end{aligned} \tag{2.9}$$

with given polynomial dynamics $\mathbf{f_j} \in \mathbb{R}[t, \mathbf{x}]^n, \quad j = 1, \ldots, N$ and costs $h, h_T \in \mathbb{R}[t, \mathbf{x}]$, and state trajectory $\mathbf{x}(t)$ constrained in compact basic semialgebraic sets X_j. We assume that the state space partitioning sets, or cells X_j, are such that all of their respective intersections have zero Lebesgue measure, and they belong to a given compact semialgebraic set X. Initial and terminal states are constrained in a given compact basic semialgebraic sets X_0 and X_T.

We then extend the LP problem framework to several measures μ_j, one supported on each cell X_j, so that the global occupation measure is

$$\mu = \sum_{j=1}^{N} \mu_j. \tag{2.10}$$

The new measure LP problem reads as

$$\begin{aligned} J_\infty = \inf \quad & \int h_T(T, \mathbf{x}(T))d\mu_T + \sum_{j=1}^{N} \int h(t, \mathbf{x}(t))d\mu_j \\ \text{s.t.} \quad & \sum_{j=1}^{N} \left(\frac{\partial \mu_j}{\partial t} + \text{div}\mathbf{f_j}\mu_j \right) + \mu_T = \mu_0 \\ & \int \mu_0 = 1, \end{aligned} \tag{2.11}$$

and it can be solved numerically with the hierarchy of LMI relaxations as shown in section 2.1.

2.3 Piecewise Polynomial Dynamical Optimization with Parsimony

The nonconvex optimization problem (2.9) can be approximated as a generic convex infinite dimensional LP problem of measures using parsimony

$$\begin{aligned} J_\infty = \inf \quad & \int h_T(T, \mathbf{x}(T)) d\mu_T + \int h(t, \mathbf{x}(t)) d\mu \\ \text{s.t.} \quad & \left(\frac{\partial \mu}{\partial t} + \text{div} \mathbf{f}_j \mu_j \right) + \mu_T = \mu_0 \\ & \left(\frac{\partial \nu}{\partial t} + \text{div} \mathbf{f}_k \nu_k \right) + \nu_T = \nu_0 \\ & \sum_{j=1}^{N} \pi_{t,\mathbf{y}} \# \mu_j = \sum_{k=1}^{M} \pi_{t,\mathbf{y}} \# \nu_k \\ & \int \mu_0 = 1, \quad \int \nu_0 = 1, \end{aligned} \tag{2.12}$$

where div is the divergence operator and the infimum is with respect to the occupation measure $\mu,\ \nu \in \mathscr{M}_+([0,T] \times X)$, initial measure $\mu_0,\ \nu_0 \in \mathscr{M}_+(\{0\} \times X_0)$, terminal measure $\mu_T,\ \nu_T \in \mathscr{M}_+(\{T\} \times X_T)$, terminal time $T > 0$. Each measure μ_j (resp. ν_k) supported on their respective cell X_j (respectively, V_k) so that the global occupation measure becomes

$$\mu = \sum_{j=1}^{N} \mu_j, \quad \nu = \sum_{k=1}^{M} \nu_k,$$

with marginal $\pi_{t,\mathbf{y}} \# \mu$ (respectively, $\pi_{t,\mathbf{y}} \# \nu$) of measure μ (respectively, ν) with respect to variables t, $\mathbf{y}$. As noted in [36], this approach allows flexibility with the computational limit caused by the largest moment SDP block. With appropriate partitioning strategies, we can solve problems with medium to large number of states.

2.4 Standard Model Reference Adaptive Control

We now briefly state the standard model reference control problem. Consider the uncertain dynamical system given by

$$\dot{\mathbf{x}}(t) = A\mathbf{x}(t) + B\big(\mathbf{u}(t) + \Delta(\mathbf{x}(t))\big), \quad \mathbf{x}(0) = \mathbf{x}_0, \tag{2.13}$$

where $\mathbf{x}(t) \in \mathbb{R}^n$ is is the state vector available for feedback, $\mathbf{u}(t) \in \mathbb{R}^m$ is the control input restricted to the class of admissible controls consisting of

measurable functions, $A \in \mathbb{R}^{n\times n}$ is a known system matrix, $B \in \mathbb{R}^{n\times m}$ is a known input matrix, and $\Delta(\mathbf{x}(t)) : \mathbb{R}^n \to \mathbb{R}^m$. For well-posedness of the problem, we also assume the pair (A, B) is controllable.

Assumption 2.4.1. *It is assumed that each individual component $\Delta_i(\mathbf{x}(t))$ of $\Delta(\mathbf{x}(t))$ is a linear combination of N known locally Lipschitz continuous basis functions $\Phi\big(\mathbf{x}(t)\big)$. In other words,*

$$\Delta(\mathbf{x}(t)) = \mathbf{W}^T\Phi\big(\mathbf{x}(t)\big) \tag{2.14}$$

where $\mathbf{W} \in \mathbb{R}^{N\times m}$ is an unknown but bounded weight matrix and $\Phi\big(\mathbf{x}(t)\big) = \begin{bmatrix}\Phi\big(\mathbf{x}(t)\big)_1 & \dots & \Phi\big(\mathbf{x}(t)\big)_N\end{bmatrix}$ is a known basis function.

We are interested in the design of a *combined* nominal and adaptive feedback control law

$$\mathbf{u}(t) = \mathbf{u_n}(t) + \mathbf{u_a}(t) \tag{2.15}$$

that asymptotically tracks the reference state vector $\mathbf{x_r}(t) \in \mathbb{R}^n$ of the *desired closed-loop* reference model

$$\dot{\mathbf{x}}_\mathbf{r}(t) = A_\mathrm{r}\mathbf{x_r}(t) + B_\mathrm{r}\mathbf{c}(t) \tag{2.16}$$

where $A_\mathrm{r} \in \mathbb{R}^{n\times n}$ is Hurwitz, $B_\mathrm{r} \in \mathbb{R}^{n\times m}$ is the command input matrix, $\mathbf{c}(t) \in \mathbb{R}^m$ is a given piecewise continuous bounded command signal.

Assumption 2.4.2. *There exists an unknown matrix $K_1 \in \mathbb{R}^{m\times n}$ and known matrix $K_2 \in \mathbb{R}^{m\times m}$ such that $A_\mathrm{r} = A - BK_1$ and $B_\mathrm{r} = BK_2$ hold.*

Now subjecting (2.13) to Assumptions 2.4.1 and 2.4.2 yields

$$\dot{\mathbf{x}}(t) = A_\mathrm{r}\mathbf{x}(t) + B_\mathrm{r}\mathbf{c}(t) + B\big(\mathbf{u_a}(t) + \mathbf{W}^T\Phi\big(\mathbf{x}(t)\big)\big)+B_\mathrm{r}\mathbf{c}(t) \tag{2.17}$$

where $\mathbf{W}$ remains unknown. Our adaptive feedback law is chosen to dominated the system matched uncertainties such that

$$\mathbf{u_a}(t) = \hat{\mathbf{W}}^T(t)\Phi\big(\mathbf{x}(t)\big) \tag{2.18}$$

where $\hat{\mathbf{W}}(t) \in \mathbb{R}^{N\times m}$ follows the weight update law

$$\dot{\hat{\mathbf{W}}}(t) = \Gamma\big(\Phi\big(\mathbf{x}(t)\big)\mathbf{e}^T(t)PB + \dot{\hat{\mathbf{W}}}_m(t)\big) \tag{2.19}$$

with error dynamics $\mathbf{e}(t) = \mathbf{x}(t) - \mathbf{x_r}(t)$, learning rate $\Gamma \in \mathbb{R}^{N\times N}$ adaptive control modification term $\dot{\hat{\mathbf{W}}}_m(t)$ (for example, the error modifcation [37] or adaptive loop recovery [38]), and unique positive definite $P \in \mathbb{R}^{n\times n}$ that satisfies the Lyapunov equality

$$A_\mathrm{r}^TP + PA_\mathrm{r} + Q = 0, \quad Q \geq 0. \tag{2.20}$$

It is well known for any $Q \geq 0$ that $\hat{\mathbf{W}}(t)$ remains bounded and $\lim_{t\to\infty}\mathbf{e}(t) = 0$. Theorems that highlight the boundedness and closed-loop stability of this configuration can be found in [32].

3

F-16 Longitudinal Dynamics with MRAC

3.1 INTRODUCTION

Traditional V&V methods are costly and inefficient. A popular method is Monte-Carlo, which is widely used in V&V because it is very robust. However, it becomes intractable when there are large uncertainties in the state space or when more sophisticated control laws are used. It is presumed that traditional V&V methods, such as Monte-Carlo, will be insufficient for intelligent systems [5].

Using moment SOS hierarchies with available off-the-shelf-software is a state of the art technique for V&V, see e.g. [4, 6] where the authors focus on polynomial dynamical models and polynomial SOS Lyapunov functions. More recently, this V&V methodology is used for assessing robust stability of space launcher control laws within the SAFE-V project [40]. However, these V&V techniques have been thus far limited to cases where there are a small number of states and/or simple controllers.

MRAC has been researched extensively by the aerospace community for the last five decades. Examples of successful flight testing include the X-36 Tailless fighter [23] and the JDAM guided munitions [24]. One of the main benefits of adaptive controllers is their capability of handling adverse conditions and/or inherent uncertainty in the aircraft dynamics. The main barrier to the

Content of this chapter appeared in the Proceedings of the 58th IEEE Conference on Decision and Control [39].

application of adaptive controllers is that there exists no formal procedure by the Federal Aviation Administration (FAA) to validate MRACs for national air and space [3]. One research direction is extending Monte-Carlo methods to adaptive control systems. The current state of the art is to search for "worst case" operating points within the flight envelope. However, there is little room for uncertainty and complexity without leaving large areas of the state space unexplored or rendering the V&V problem intractable.

Our main goal is to validate existing MRAC and state feedback architecture for a nonlinear aircraft model in the presence of uncertainties using off-the-shelf-software. In particular, we are interested in qualitative properties such as safety (all trajectories starting from a set of initial conditions never reach a set of bad states), avoidance (at least one trajectory starting from initial conditions will never reach a set of bad states), eventuality (at least one trajectory starting from a set of initial conditions will reach a set of good states in finite time), reachability (at least one trajectory starting from a set of initial conditions will reach a set of good states in finite time), and robustness (all trajectories from a set of initial conditions guarantee acceptable performance subject to disturbances and/or unmodeled dynamics).

As sketched in chapter 2, the procedure follows directly from [40], see also [33] for a broader perspective. We first rephrase our validation problem as a robustness analysis problem and then as a nonconvex nonlinear optimization problem over admissible trajectories. Then the problem is expressed equivalently as an infinite dimensional linear programming (LP) problem by introducing occupation measures supported over admissible trajectories. We finally relax the infinite dimensional LP problem of measures to a finite dimensional linear matrix inequality (LMI) problem of moments. The solutions to our V&V problem are primal in the sense that we optimize directly over the system trajectories. The well-established Lyapunov certificates can also be retrieved from the dual SOS LP problem.

The main contributions of this chapter are as follows:

- We start with the familiar longitudinal polynomial F-16 model completed with the closed-loop dynamics of the MRAC augmentation obtained by solving directly the Lyapunov equation. Then the existing control architecture is simplified by relaxing MRAC control law. The absolute value contained within the adaptation law is replaced with a quadratic function. Additionally, the total number of adaptive states is reduced to one. This is considered desirable for practical implementation. We also demonstrate the validity of this approach with our V&V framework.

- Then we use our V&V framework to provide numerical certificates for various flight conditions of interest in section 3.3, which include: Reduced control effectiveness, matched uncertainties, and adverse changes in the

flight dynamics. Disturbances and nonlinearities that are otherwise difficult to model can be addressed explicitly. For comparison, numerical certificates are given for an existing baseline LQR controller without the MRAC augmentation.

- For comparison, Monte-Carlo analysis is also done for all of our flight conditions of interest. We also provide an example where a region of instability caused by certain combinations of parameters may not be detected if the state space is not sufficiently explored with simulation. We also show how our V&V framework can detect these unsafe trajectories without additional computation time.

- Our new V&V framework reduces a complicated control law validation problem to numerically solving a simple moment LMI relaxations problem which is solvable directly with off-the-shelf-software (namely, Gloptipoly 3 for MATLAB [29]) and a SDP solver (such as MOSEK [30] or SeDuMi [31]).

The V&V framework developed in [4] and [6] is restrictive. It can only be used to solve problems that contain autonomous polynomial systems. Convergence in finite time also cannot be guaranteed. Conversely, the use of moments in our V&V framework enables us to deal with systems that have non-autonomous piecewise polynomials. We can further show in our numerical examples that all states, including the reference system tracking errors, converge to the origin in finite time. This result is significantly better than existing asymptotic guarantees provided by using Barbalat's Lemma, which describes the stability of non-autonomous ODEs, for the closed-loop system [32].

The organization of this chapter is as follows: section 3.2 discusses the nonlinear polynomial F-16 model we developed for purposes of validation and the control system architecture, and section 3.3 contains the main numerical results. Lastly, section 3.4 contains our conclusions with a small discussion on future results.

3.2 F-16 SHORT PERIOD DYNAMICS

The various parameters used for implementing the longitudinal F-16 aircraft can be found in Table 3.1:

Table 3.1: Properties of the Aircraft Model

Parameter	Values
Mass m	636.94 slugs
Wing area S	300.0 ft^2
Mean aerodynamic chord $\bar{c}$	11.32 ft
Reference center of gravity location Δ	$0.35\bar{c}$ ft
Thrust T	8000 lbf
Total velocity V_T	502 $\frac{\text{ft}}{\text{s}}$
Dynamic Pressure $\bar{q}$ at 0 ft	299.0027 ft
Gravitational pull of the Earth g	32.17 $\frac{\text{ft}}{\text{s}^2}$
Pitch-axis moment of inertia J_y	55814 slug $\cdot$ ft^2

For an F-16 traveling at wings-levels steady-state flight, the longitudinal short period mode [41], with elevator input $\delta_{\text{e}}(t) \in \mathbb{R}$, can be expressed as

$$\begin{aligned}
\dot{\alpha}(t) = &\big(1 + \frac{\bar{q}S\bar{c}}{2mV_T^2}(C_{zq}(\alpha(t))cos(\alpha(t)) \\
&- C_{xq}(\alpha(t))sin(\alpha(t))\big)q(t) \\
&+ \frac{\bar{q}S}{mV_T}\big(C_z(\alpha(t), \delta_{\text{e}}(t), \beta(t))cos(\alpha(t)) \\
&- C_x(\alpha(t), \delta_{\text{e}}(t))sin(\alpha(t))\big) \\
&- \frac{T}{mV_T}sin(\alpha(t)) + \frac{g}{V_T}cos(\theta(t) - \alpha(t)) \\
\dot{q}(t) = &\frac{\bar{q}S\bar{c}}{2J_yV_T}\big(\bar{c}C_{mq}(\alpha(t)) + \Delta C_{zq}(\alpha(t))\big)q(t) \\
&+ \frac{\bar{q}S\bar{c}}{J_y}\big(C_m(\alpha(t), \delta_{\text{e}}(t)) + \frac{\Delta}{\bar{c}}C_z(\alpha(t), \delta_{\text{e}}(t), \beta(t))\big)
\end{aligned} \tag{3.1}$$

where $\alpha(t)$ is the angle of attack, $q(t)$ is the pitchrate, $\theta(t)$ is the pitch angle, and $\beta(t)$ is the sideslip. We assume that the roll rate and yaw rate of the aircraft are minimal. We also assume that for small angles ($\theta(t) \approx 0$) the velocity of the aircraft remains constant and that the axis of thrust coming from the engine is fixed.

The aerodynamic coefficients $C_{zq}(\alpha(t))$, $C_{xq}(\alpha(t))$, $C_x(\alpha(t), \delta_{\text{e}}(t))$, $C_{mq}(\alpha(t))$, $C_m(\alpha(t), \delta_{\text{e}}(t))$, and $C_z(\alpha(t), \delta_{\text{e}}(t), \beta(t))$ are approximated by their polynomials using aerodynamic data taken from [42].

The vehicle angle of attack was selected to represent the system *controlled output* $y(t) = \alpha(t)$. Thus, the control goal is to asymptotically track any bounded

set point command $c(t) = \alpha_{\text{cmd}}(t)$, in the presence of system uncertainties. Let

$$e_y(t) = \alpha(t) - c(t) \tag{3.2}$$

be the system output tracking error. Augmenting (3.1) with the integrated output tracking error

$$\dot{e}_{y,\text{int}}(t) = e_y(t) = \alpha(t) - c(t) \tag{3.3}$$

yields the *extended closed-loop dynamics*.

3.2.1 Model Reference Adaptive Control with Adaptive Loop Recovery

We make substantial use of adaptive control framework in this subsection, and the unfamiliar reader may wish to consult [43, 38]. Consider *augmented* longitudinal flight model (3.1) to (3.3) in the form of

$$\begin{aligned}\dot{\mathbf{x}}(t) = A\mathbf{x}(t) + B\Lambda(u(t) + \Delta(\mathbf{x}(t))) \\ + g(\mathbf{x}(t), \delta_{\text{e}}(t), \beta(t)) + B_{\text{r}}c(t), \quad \mathbf{x}(0) = \mathbf{x}_0\end{aligned} \tag{3.4}$$

where $\mathbf{x}(t) = \begin{bmatrix} e_{y,\text{int}}(t) & \alpha(t) & q(t) \end{bmatrix}$, $u(t) = \delta_{\text{e}}(t)$, $A \in \mathbb{R}^{3\times3}$ is known, $B \in \mathbb{R}^{3\times1}$ is known, $\Lambda \in \mathbb{R}_+$ is an unknown control effectiveness, $B_{\text{r}} \in \mathbb{R}^{3\times1}$ is a known command input matrix, $c(t)$ is a given piecewise continuous bounded command, $g(\mathbf{x}(t), \delta_{\text{e}}(t), \beta(t)) \in \mathbb{R}^{3\times1}$ contains all the higher order polynomials, and $\Delta(\mathbf{x}(t)) \in \mathbb{R}$ represents additional unknown matched disturbances.

Next, consider the reference system capturing the desired, ideal closed-loop dynamical performance given by

$$\dot{\mathbf{x}}_{\mathbf{r}}(t) = A_{\text{r}}\mathbf{x}_{\mathbf{r}}(t) + B_{\text{r}}c(t), \quad \mathbf{x}_{\mathbf{r}}(0) = \mathbf{x}_{\mathbf{r}0}, \tag{3.5}$$

where $\mathbf{x}_{\mathbf{r}}(t) \in \mathbb{R}^3$ is the reference state vector and $A_{\text{r}} \in \mathbb{R}^{3\times3}$ is the reference system matrix (we shall assume that it is Hurwitz).

The objective of the model reference adaptive control problem is to construct an adaptive feedback control law $u(t)$ such that the state vector $\mathbf{x}(t)$ asymptotically follows the reference state vector $\mathbf{x}_{\mathbf{r}}(t)$. Now consider the augmented adaptive feedback control law given by

$$u(t) = u_{\text{n}}(t) + u_{\text{a}}(t), \tag{3.6}$$

where $u_{\text{n}}(t) \in \mathbb{R}$ is control signal generated by the nominal feedback control law and $u_{\text{a}}(t) \in \mathbb{R}$ is related to the adaptive feedback control law. Additionally, let the nominal feedback control law be given by

$$u_{\text{n}}(t) = -K_1\mathbf{x}(t), \tag{3.7}$$

where $K_1 \in \mathbb{R}^{1\times 3}$ is the nominal feedback gain such that $A_{\mathrm{r}} = A - BK_1$. Next, let the adaptive feedback control law be given by

$$u_{\mathrm{a}}(t) = -\hat{\mathbf{W}}^T(t)\Phi\big(\mathbf{x}(t)\big), \tag{3.8}$$

where $\Phi\big(\mathbf{x}(t)\big) \in \mathbb{R}^{3\times 1}$ is a known basis function and $\hat{\mathbf{W}}(t) \in \mathbb{R}^{3\times 1}$ is the estimate of $W(t)$ satisfying the weight update law

$$\dot{\hat{\mathbf{W}}}(t) = \Gamma\big(\Phi\big(\mathbf{x}(t)\big)e^T(t)PB + \kappa_w \Phi\big(\mathbf{x}(t)\big)_{\mathbf{x}} \Phi\big(\mathbf{x}(t)\big)_{\mathbf{x}}^T \hat{\mathbf{W}}(t) - k_e |e^T(t)PB| \hat{\mathbf{W}}(t)\big), \tag{3.9}$$

where $\Gamma \in \mathbb{R}^{3\times 3}$ is a positive definite learning rate matrix, $k_e > 0$ is the e modification gain, $k_w >> 1$ is the adaptive loop recovery gain, $\mathbf{e}(t) \triangleq \mathbf{x}(t) - \mathbf{x_r}(t)$ is the system error state vector, $\Phi\big(\mathbf{x}(t)\big)_{\mathbf{x}} = \frac{\partial}{\partial x}\Phi(x) \in \mathbb{R}^{3\times 1}$, and positive definite $P \in \mathbb{R}^{3\times 3}$ is the unique solution to the Lyapunov equation

$$0 = A_{\mathrm{r}}^T P + P A_{\mathrm{r}} + Q, \tag{3.10}$$

where $Q \in \mathbb{R}^{3\times 3}$ is positive definite and can viewed as an additional learning rate. Note that because A_{r} is Hurwitz, it follows from the converse Lyapunov theory [32] that there exists a unique P satisfying (3.10) for a given R.

This controller is the same as described in chapter 2 with the inclusion of an unmatched uncertainty. Theorems that highlight the boundedness of the closed-loop system errors $\mathbf{e}(t)$ and $\tilde{W} \triangleq W - \hat{\mathbf{W}}(t)$, for the adaptive loop recovery and error modification, can be found in [38, 37]. In practice, Lyapunov analysis only informs us about the ultimate stability of the closed-loop system [3]. For non-autonomous systems in particular, the theoretical performance of the MRAC provided by the Lyapunov analysis is strictly asymptotic. This proof usually employs Barbalat's Lemma with the prerequisite assumptions [32]. It is interesting to note that, for our main results in section 3.3, all states converge to the origin in finite time.

Reference matrix A_{r} and the corresponding *baseline LQR feedback gains* $K_1 = \begin{bmatrix} -10.0000 & -10.8756 & -6.0565 \end{bmatrix}$ were taken from [44]. To reduce the number of constraints for the optimization problem, we simplify the absolute value function in (3.9) such that

$$\dot{\hat{\mathbf{W}}}(t) = \Gamma\big(\Phi\big(\mathbf{x}(t)\big)e^T(t)PB + \kappa_w \Phi\big(\mathbf{x}(t)\big)_{\mathbf{x}} \Phi\big(\mathbf{x}^T(t)\big)_{\mathbf{x}} \hat{\mathbf{W}}(t) - k_e \left[e^T(t)PB\right]^2 \hat{\mathbf{W}}(t)\big). \tag{3.11}$$

We will demonstrate the validity of this approach in section 3.3. To help visualize the longitudinal controller, a block diagram is provided in Fig. 3.1.

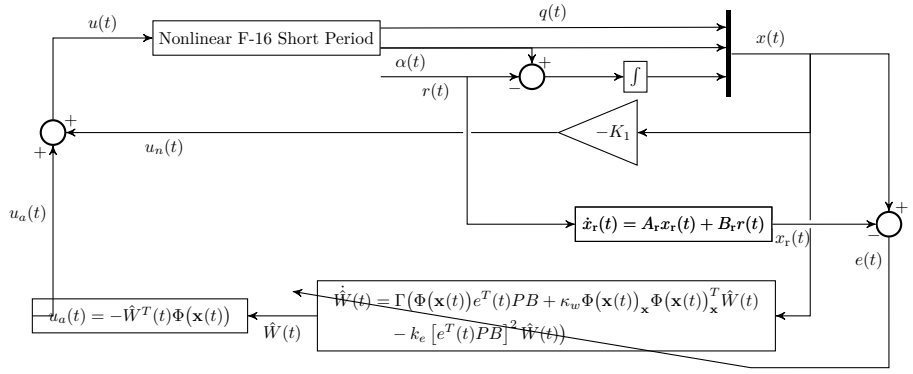

Figure 3.1: Longitudinal MRAC Block Diagram

3.3 NUMERICAL EXAMPLES

We now present the main numerical results. For the numerical examples used throughout this section, we use the same MRAC configuration with $Q = \text{diag}(\begin{bmatrix}0.1 & 100 & 100\end{bmatrix})$, $\Gamma = \text{diag}(\begin{bmatrix}0 & 2000 & 0\end{bmatrix})$, $k_e = 0.001$, and $k_w = 12$. For sake of convenience, we also assume $\hat{W}(0) = \mathbf{0}_{3\times 1}$.

All states, including the time domain, must be normalized on the interval $\begin{bmatrix}-1 & 1\end{bmatrix}$. For this we use normalizing matrix $D = \text{diag}(\begin{bmatrix}\frac{1}{10} & \frac{1}{30} & \frac{1}{50} & \frac{1}{30}\end{bmatrix})$ and given terminal time T. We write all of normalized our state equations, complete with our augmented feedback (3.6) and weight update laws (3.11), in the compact form

$$\dot{\mathbf{x}}_{\mathbf{opt}}(t) = TD\mathbf{f}\big(t, D^{-1}\mathbf{x}_{\mathbf{opt}}(t), \Lambda(u(t) + \Delta(\mathbf{x}(t))), \beta(t)\big), \tag{3.12}$$

where $\mathbf{x}_{\mathbf{opt}}(t) = \begin{bmatrix}e_{y,\text{int}}(t) & \alpha(t) & q(t) & \hat{W}^T(t)\end{bmatrix}$. We can interpret (3.12) as the collection of all admissible trajectories we wish to optimize over.

Our objective is to find the initial state maximizing the norm of the terminal state. A concave quadratic term $J = -[c(t) - \alpha(T)]^2$ is used. If we can certify that for every chosen initial state $\mathbf{x}_{\mathbf{opt}}(0) \in X_0$, where X_0 is the box $X_0 \triangleq \begin{bmatrix}-\epsilon, & \epsilon\end{bmatrix} \times \begin{bmatrix}-10, & 10\end{bmatrix}\frac{\pi}{180} \times \begin{bmatrix}-10, & 10\end{bmatrix}\frac{\pi}{180} \times \begin{bmatrix}-\epsilon, & \epsilon\end{bmatrix}, \epsilon << 1$, such that all trajectories remain bounded in the box $X \triangleq \begin{bmatrix}-10, & 10\end{bmatrix}\frac{\pi}{180} \times \begin{bmatrix}-30, & 30\end{bmatrix}\frac{\pi}{180} \times \begin{bmatrix}-50, & 50\end{bmatrix}\frac{\pi}{180} \times \begin{bmatrix}-30, & 30\end{bmatrix}$, until they reach final state belonging to a set $X_T \triangleq \{J \leq 3 \cdot 10^{-3}\} \subset X$, then the control law is validated. The choice of initial conditions represent reasonable maneuvers of the aircraft.

Three cases are considered for control validation:

- $c(t) = 0$, $\Lambda = 1$, $\Delta(\mathbf{x}(t)) = 0$, $\beta(t) = 0$

- $c(t) = 0$, $\Lambda = 0.4$, $\Delta(\mathbf{x}(t)) = d(\alpha(t))$, $\beta(t) = 0$
- $c(t) = 5$, $\Lambda = 0.4$, $\Delta(\mathbf{x}(t)) = 0$, $\beta(t) = 15\alpha(t) + 0.1$

where $\Delta(\mathbf{x}(t)) \in \mathbb{R}$ can be viewed as unknown nonlinearities in the aerodynamic Z-force and pitching moments, and $\beta(t)$ is the sideslip.

We evaluate each case using LQR feedback with and without ($u_{\mathrm{a}}(t) = 0$) the MRAC augmentation. The main results are compared with upper bounds for J obtained directly using Monte-Carlo on the same F-16 polynomial mode. For the setup, we used Newton's Method (step time 0.0001 s) and evenly spaced initial conditions for the nested loops.

3.3.1 First Case

For this case, we use command signal $c(t) = 0$, reference signal $\mathbf{x_r}(t) = \mathbf{0}_{3\times 1}$, final time $T = 10$, and the control effectiveness $\Lambda = 1$. Under normal flight conditions we also assume $\Delta(\mathbf{x}(t)) = 0$, $\beta(t) = 0$. The polynomial dynamical optimization problem (2.3) becomes

$$\begin{aligned} J = \inf_{\alpha(T)} \quad & -[c(t) - \alpha(T)]^2 \\ \text{s.t.} \quad & \dot{\mathbf{x}}_{\mathbf{opt}}(t) = TD\mathbf{f}\big(t, D^{-1}\mathbf{x_{opt}}(t), u(t)\big) \\ & \mathbf{x_{opt}}(t) \in X, \quad t \in [0,1] \\ & \mathbf{x_r}(t) = \mathbf{0}_{3\times 1} \\ & \mathbf{x_{opt}}(0) \in X_0, \quad \mathbf{x_{opt}}(T) \in X_T, \end{aligned} \tag{3.13}$$

with given polynomial dynamics $f \in \mathbb{R}[t, x]$. The primal problem on measures (2.7) and finite dimensional moment LMI relaxations problem are modified accordingly.

Fig. 3.2 compares the simulations of the LQR with and without the MRAC augmentation. The maximum upper bounds were obtained by taking the maximum absolute value of all the trajectories at $\alpha(10)$. For the LQR with and without MRAC, they were determined as $J = 2.37 \times 10^{-6}$ and $J = 3.92 \times 10^{-16}$, respectively,.

With Gloptipoly 3 and the SDP solver MOSEK, we obtained the following sequence of upper bounds in Table 3.2 using the cost function from (3.13). Both control laws are validated since all initial conditions reach the pre-specified set within finite time.

3.3.2 Second Case

For this case, we use command signal $c(t) = 0$, reference signal $\mathbf{x_r}(t) = \mathbf{0}_{3\times 1}$, final time $T = 10$, and the reduced control effectiveness $\Lambda = 0.4$. We also let

$\beta(t) = 0$ and $\Delta(\mathbf{x}(t)) = d(\alpha(t))$ is a step function centered at $\alpha(t) = 0$ with the width $|\alpha(t)| \leq 0.0233$.

To include the disturbance, we reformulate the optimization problem with the system dynamics defined as locally affine functions in three cells X_j, $j = 1, 2, 3$ corresponding respectively, to the regimes of the disturbance $X_1 \triangleq \{\mathbf{x_{opt}}(t) \in \mathbb{R}^4 : |\alpha(t)| \leq 0.0233\}, \dot{\mathbf{x}}_{\mathbf{opt}}(t) = TD\mathbf{f}_1\big(t, D^{-1}\mathbf{x_{opt}}(t), \Lambda(u(t)+1)\big)$, $X_2 \triangleq \{\mathbf{x_{opt}}(t) \in \mathbb{R}^4 : \alpha(t) \leq -0.0233\}, \dot{\mathbf{x}}_{\mathbf{opt}}(t) = TD\mathbf{f}_2\big(t, D^{-1}\mathbf{x_{opt}}(t), \Lambda u(t)\big)$, and $X_3 \triangleq \{\mathbf{x_{opt}}(t) \in \mathbb{R}^4 : \alpha(t) \geq 0.0233\}, \dot{\mathbf{x}}_{\mathbf{opt}}(t) = TD\mathbf{f}_3\big(t, D^{-1}\mathbf{x_{opt}}(t), \Lambda u(t)\big)$.

The polynomial dynamical optimization problem (2.3) becomes

$$\begin{aligned} J = \inf_{\alpha(T)} \quad & -[c(t) - \alpha(T)]^2 \\ \text{s.t.} \quad & \dot{\mathbf{x}}_{\mathbf{opt}}(t) = TD\mathbf{f}_j\big(t, D^{-1}\mathbf{x_{opt}}(t), \\ & \qquad \Lambda(u(t) + d(\alpha(t)))\big) \\ & \mathbf{x_{opt}}(t) \in X_j, \quad j = 1, \ldots, 3, \quad t \in [0, 1] \\ & \mathbf{x_r}(t) = \mathbf{0}_{3\times 1} \\ & \mathbf{x_{opt}}(0) \in X_0, \quad \mathbf{x_{opt}}(T) \in X_T, \end{aligned} \tag{3.14}$$

with given polynomial dynamics $\mathbf{f}_j \in \mathbb{R}[t, x]$. The primal problem on measures (2.7) and the finite dimensional moment LMI relaxations problem are modified accordingly.

Numerical simulations can be found in Fig. 3.3. The maximum upper bounds were found by taking the maximum absolute value of all the trajectories at $\alpha(10)$. For the LQR with and without MRAC, they were determined as $J = 1.50 \times 10^{-3}$ and $J = 1.64 \times 10^{-16}$, respectively,.

We obtained the following sequence of monotonically decreasing upper bounds J_d, $d = 1, \ldots, 5$ in Table 3.3. The LQR with MRAC achieves a consistent lower maximum bound and reaches the set by the fourth relaxation order.

3.3.3 Third Case

For the final case we use final time $T = 30$ and the reduced control effectiveness $\Lambda = 0.4$. We also assume $\Delta(\mathbf{x}(t)) = 0$. For command signal $c(t) = 5$, we have to build a reference signal $\mathbf{x_r}(t)$. Since the dynamics of $\mathbf{x_r}(t)$ are purely linear, we can approximate their states via piecewise polynomials over a partitioned time domain. We also include sideslip buildup $\beta(t) = 15\alpha(t) + 0.1$ as it appears in $C_z(\alpha(t), \delta_e(t), \beta(t))$.

To include the reference trajectory dynamics $\mathbf{x_r}(t)$, we reformulate the optimization problem with the system dynamics defined as locally affine functions in three cells X_j, $j = 1, 2, 3$ corresponding to the first time partition $X_1 \triangleq \{t \in \mathbb{R} : 0 \leq t \leq 3\}, \mathbf{x_r}(t) = P_1(t)$, with trajectories

Table 3.2: Gloptipoly 3 + MOSEK Upper Bounds for Case 1

	LQR		LQR + MRAC	
Rel Ord	Upper Bnd J	CPU [s]	Upper Bnd J	CPU [s]
1	2.74×10^{-1}	2.54	2.74×10^{-1}	2.29
2	1.59×10^{-1}	2.13	7.61×10^{-2}	7.06
3	6.67×10^{-5}	6.71	3.25×10^{-5}	5.31×10^{1}
4	3.72×10^{-6}	2.34×10^{1}	4.96×10^{-6}	3.53×10^{2}
5	1.25×10^{-6}	1.01×10^{2}	1.47×10^{-6}	2.58×10^{3}

$\dot{\mathbf{x}}_{\mathbf{opt}}(t) = TD\mathbf{f}_1\big(t, D^{-1}\mathbf{x}_{\mathbf{opt}}(t), \Lambda u(t), \beta(t)\big)$, the second time partition $X_2 \triangleq \{t \in \mathbb{R} : 3 \leq t \leq 9\}, \mathbf{x}_{\mathbf{r}}(t) = P_2(t), \dot{\mathbf{x}}_{\mathbf{opt}}(t) = TD\mathbf{f}_2\big(t, D^{-1}\mathbf{x}_{\mathbf{opt}}(t), \Lambda u(t), \beta(t)\big)$, and the final time partition $X_3 \triangleq \{t \in \mathbb{R} : 9 \leq t \leq T\}, \mathbf{x}_{\mathbf{r}}(t) = P_3(t), \dot{\mathbf{x}}_{\mathbf{opt}}(t) = TD\mathbf{f}_3\big(t, D^{-1}\mathbf{x}_{\mathbf{opt}}(t), \Lambda u(t), \beta(t)\big)$. The polynomial dynamical optimization problem (2.3) becomes

$$\begin{aligned} J = \inf_{\alpha(T)} \quad & -[c(t) - \alpha(T)]^2 \\ \text{s.t.} \quad & \dot{\mathbf{x}}_{\mathbf{opt}}(t) = TD\mathbf{f}_j\big(t, D^{-1}\mathbf{x}_{\mathbf{opt}}(t), \Lambda u(t), \beta(t)\big) \\ & \mathbf{x}_{\mathbf{opt}}(t) \in X_j, \quad j = 1, \ldots, 3, \quad t \in [0, 1] \\ & \mathbf{x}_{\mathbf{r}}(t) = P_j(t) \\ & \mathbf{x}_{\mathbf{opt}}(0) \in X_0, \quad \mathbf{x}_{\mathbf{opt}}(T) \in X_T, \end{aligned} \tag{3.15}$$

with given polynomial dynamics $\mathbf{f}_j \in \mathbb{R}[t, x]$. The primal problem on measures (2.7) and the finite dimensional moment LMI relaxations problem are modified accordingly.

Numerical simulations can be found in Fig. 3.3. The maximum upper bounds were found by taking the maximum absolute value of all the trajectories at $\alpha(30)$. Some of the trajectories of the standalone LQR were omitted, because they were unstable. In particular, the trajectories beginning with large combinations of $\alpha(0)$ and $q(0)$ values are unbounded. The upper bound for the LQR without MRAC is $J = \infty$, and with the MRAC it is $J = 5.18 \times 10^{-15}$.

We obtained the following sequence of monotonically decreasing upper bounds J_d, $d = 1, \ldots, 5$ in Table 3.4. The standalone LQR upper bound remains large. Conversely, the LQR with MRAC upper bound obtains a sufficiently small value by the fourth relaxation order.

3.4 CONCLUSIONS AND FUTURE WORKS

In this chapter, we validated both LQR and MRAC control laws using moment LMI relaxations and off-the-shelf-software. An F-16 polynomial model was implemented to ensure that the MRAC model matches the LMI framework. We took steps to simplify the MRAC architecture for practical implementation.

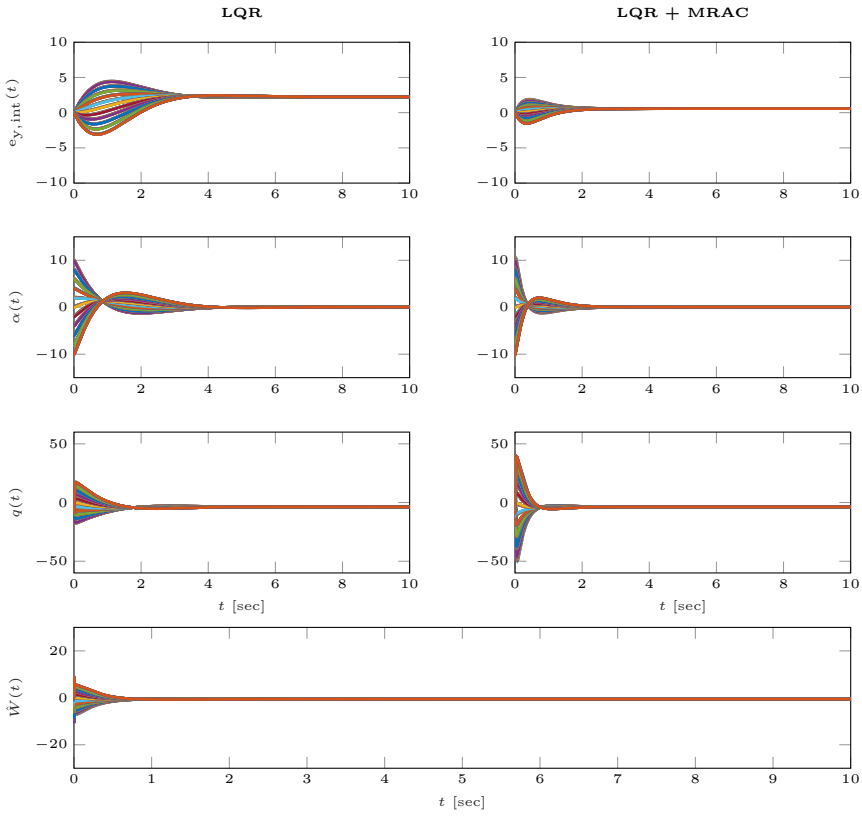

Figure 3.2: Numerical Results for Case 1

Table 3.3: Gloptipoly 3 + MOSEK Upper Bounds for Case 2

	LQR		LQR + MRAC	
Rel Ord	**Upper Bnd J**	**CPU [s]**	**Upper Bnd J**	**CPU [s]**
1	6.26×10^{-2}	2.80	2.74×10^{-1}	2.53
2	7.44×10^{-3}	3.51	4.52×10^{-3}	1.91×10^{1}
3	4.05×10^{-3}	1.96×10^{1}	8.02×10^{-4}	2.05×10^{2}
4	3.74×10^{-3}	2.64×10^{1}	7.24×10^{-4}	1.31×10^{3}
5	3.61×10^{-3}	6.41×10^{2}	7.04×10^{-4}	9.74×10^{3}

Then the entire system (the polynomial F-16 model complete with the LQR with and without the MRAC augmentation) was then validated under various flight conditions of interest. These results were compared with those obtained numerically using Monte-Carlo. The main challenge was adapting these control laws to our V&V framework. Derivative-free model reference adaptive control

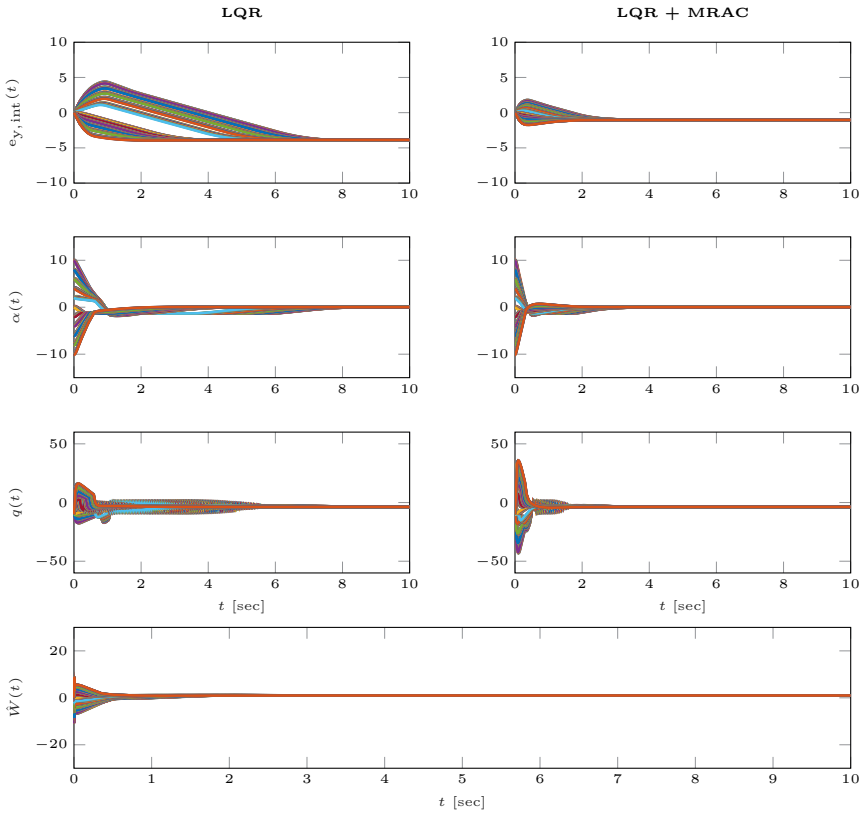

Figure 3.3: Numerical Results for Case 2

Table 3.4: Gloptipoly 3 + MOSEK Upper Bounds for Case 3

	LQR		LQR + MRAC	
Rel Ord	**Upper Bnd J**	**CPU [s]**	**Upper Bnd J**	**CPU [s]**
1	3.73×10^{-1}	1.65	3.73×10^{-1}	7.57
2	1.97×10^{-1}	1.54	2.14×10^{-1}	1.07×10^{2}
3	1.90×10^{-1}	5.39	1.91×10^{-1}	9.24×10^{2}
4	1.90×10^{-1}	2.48×10^{1}	2.59×10^{-2}	1.05×10^{4}
5	1.90×10^{-1}	9.81×10^{1}	2.98×10^{-3}	5.39×10^{4}

(DF-MRAC) could yield promising results as it does not impose additional states on the dynamics. Another topic of interest is validating adaptive control laws in the presence of actuator dynamics. Their sparsity can be exploited. We also wish to consider other types of nonlinear control laws have similar properties.

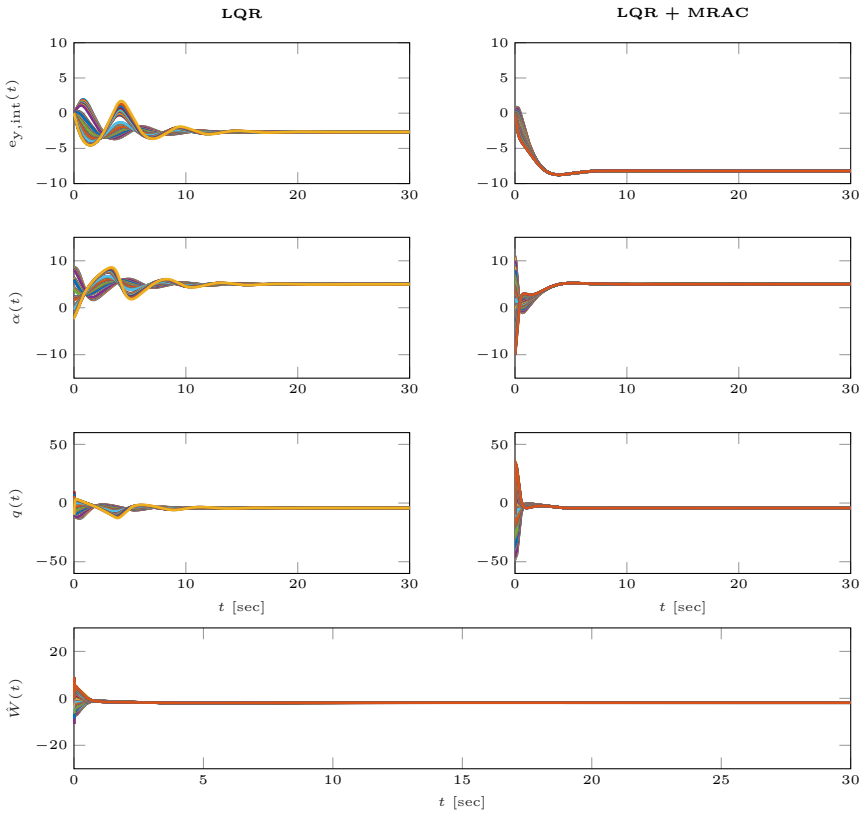

Figure 3.4: Numerical Results for Case 3

4

F-16 Lateral Dynamics with MRAC

4.1 INTRODUCTION

This chapter considers V&V of a lateral F-16 dutch-roll polynomial model with reduced control effectiveness at large roll angles. A closed-loop model is derived using the standard LQR + MRAC augmentation. The controller is simplified by building the adaptive feedback around the aileron channel.

Like our work in chapter 3, we wish to close the numerical gap by validating closed-loop models with MRAC controllers using our V&V framework. We also use new theoretical framework provided by [36] where the complexity of solving the LMI relaxations is reduced by exploiting sparsity of ODEs. With this approach, we can solve aerospace models of medium-to-large scale.

For the LQR + MRAC augmentation problem is solved by exploiting sparsity [36] for ODEs. This is done by approximating the reference trajectories with a given roll angle command signal. This procedure reduces the size of the largest SDP block. Compared to chapter 3, we double the amount of states (from 4 states to 9 total) that can be validated.

Our V&V framework is used to certify the closed-loop model subject to normal and reduced control effectiveness. We compare the baseline LQR closed-loop model to the same model using the LQR + MRAC augmentation. Likewise, we certify the same closed-loop model using Monte-Carlo methods.

Content of this chapter appeared in the Proceedings Proceedings of the 2020 American Control Conference [45].

$$\Delta(\mathbf{x_q}(t),\mathbf{u}(t)) = \begin{bmatrix} (1-4.26\beta^2(t))(9.00\times10^{-7}\delta_{\mathrm{a}}(t)-6.00\times10^{-7}\delta_{\mathrm{a}}(t)+1\times10^{-3}\delta_{\mathrm{a}}(t)) \\ (1-4.26\beta^2(t))(3.63\times10^{-4}\delta_{\mathrm{r}}(t)+2.42\times10^{-4}\delta_{\mathrm{r}}(t)+1\times10^{-3}\delta_{\mathrm{r}}(t)) \\ \quad +7.50\times10^{-2}(-1.25\times10^{-1}+7.85\times10^{-2}p(t)-1.37\times10^{-3}p^2(t))(5.24\times10^{-2}r(t)+1) \\ \quad +4.50\times10^{-1}(-1.25\times10^{-1}+7.85\times10^{-2}p(t)-1.37\times10^{-3}p^2(t))(5.24\times10^{-2}r(t)+1) \end{bmatrix} \tag{4.4}$$

The organization of this chapter is as follows: section 4.2 discusses the nonlinear closed-loop F-16 polynomial model and the MRAC augmentation, section 4.3 contains our main numerical results, and section 4.4 contains a small discussion of our conclusions and future results.

4.2 F-16 DUTCH-ROLL DYNAMICS

The trimmed nonlinear dutch-roll dynamics of an F-16 traveling at 502 ft/s and $\alpha = 2.11$ deg is given by

$$\begin{aligned} \dot{\mathbf{x}}_{\mathbf{q}}(t) &= A\mathbf{x}_{\mathbf{q}}(t) + B\Lambda\big(\mathbf{u}(t) \\ &\qquad + \Delta(\mathbf{x}_{\mathbf{q}}(t),\mathbf{u}(t))\big), \quad \mathbf{x}_{\mathbf{q}}(0) = \mathbf{x}_{\mathbf{q0}} \\ \mathbf{y}(t) &= C\mathbf{x}_{\mathbf{q}}(t), \end{aligned} \tag{4.1}$$

where

$$A = \begin{bmatrix} -0.3220 & 0.0640 & 0.0364 & -0.9917 \\ 0 & 0 & 1 & 0.0393 \\ -30.6490 & 0 & -3.6784 & -0.6646 \\ 8.3595 & 0 & -0.0254 & -0.4764 \end{bmatrix}, \tag{4.2}$$

$$B = \begin{bmatrix} 0 & 0 \\ 0 & 0 \\ -0.7331 & 0.1315 \\ -0.0319 & -0.0620 \end{bmatrix}, \quad C = \begin{bmatrix} 1 & 0 & 0 & 0 \\ 0 & 1 & 0 & 0 \end{bmatrix}, \tag{4.3}$$

$\mathbf{x}_{\mathbf{q}}(t) = \begin{bmatrix}\beta(t) & \phi(t) & p(t) & r(t)\end{bmatrix} \in \mathbb{R}^4$ is the lateral state vector, $\mathbf{u}(t) = \begin{bmatrix}\delta_{\mathrm{a}}(t) & \delta_{\mathrm{r}}(t)\end{bmatrix} \in \mathbb{R}^2$ are the measurable control inputs, $\mathbf{y}(t) \in \mathbb{R}^2$ is the output, $\Lambda = \lambda I_{2\times2}$, $\lambda \in \mathbb{R}_+$ is the control effectiveness, and $\Delta(\mathbf{x}_{\mathbf{q}}(t),\mathbf{u}(t)) \in \mathbb{R}^2[x]$, found below in (4.4), contains unknown higher order dynamics which include dead-zone and loss-of-control effectiveness for large $\beta(t)$. The open-loop flight model, coefficients, and the nonlinearities were taken from [44]. The higher order terms in $\Delta(\mathbf{x}_{\mathbf{q}}(t),\mathbf{u}(t))$ were derived by taking the Taylor series of hyperbolic functions. In the proceeding subsection we discuss the derivation of the nominal and adaptive control law used in the closed-loop model.

4.2.1 Closed-Loop Configuration

Consider the lateral dynamics in the form of (4.1). Our control objective is to asymptotically track the reference trajectory

$$\begin{aligned} \dot{\mathbf{x}}_{\mathbf{r}}(t) &= A_{\mathrm{r}}\mathbf{x}_{\mathbf{r}}(t) + B_{\mathrm{r}}\mathbf{c}(t), \quad \mathbf{x}_{\mathbf{r}}(0) = \mathbf{x}_{\mathbf{r0}} \\ \mathbf{y}_{\mathbf{r}}(t) &= C\mathbf{x}_{\mathbf{r}}(t) \end{aligned} \tag{4.5}$$

where $\mathbf{c}(t) = \begin{bmatrix} \beta_{\mathrm{cmd}} & \phi_{\mathrm{cmd}} \end{bmatrix} \in \mathbb{R}^2$ are the given piecewise continuous bounded yaw/roll command signals, and $\mathbf{x}_{\mathbf{r}}(t) \in \mathbb{R}^4$ is the reference state vector. Nominal controller gains

$$K_1 = \begin{bmatrix} 10.6901 & -9.5824 & -2.0328 & -6.1944 \\ -0.3982 & -0.2043 & -0.4170 & -27.0142 \end{bmatrix},$$
$$K_2 = \begin{bmatrix} -2.9031 & -9.9924 \\ 156.5907 & -2.4300 \end{bmatrix},$$

were derived using the LQR-method [46] such that $A_{\mathrm{r}} = A - BK_1$ is Hurwitz, $B_r = BK_2$, and the DC gain between the command signals $\mathbf{c}(t)$ and output $\mathbf{y}(t)$ is unity as $t \to \infty$. Now consider the combined nominal/adaptive feedback law

$$\mathbf{u}(t) = \mathbf{u}_{\mathbf{n}}(t) + \mathbf{u}_{\mathbf{a}}(t), \tag{4.6}$$

with *baseline* nominal control law $\mathbf{u}_{\mathbf{n}}(t) = K_1\mathbf{x}_{\mathbf{q}}(t) + K_2\mathbf{c}(t) \in \mathbb{R}^2$ and adaptive control law $\mathbf{u}_{\mathbf{a}}(t) = -\hat{\mathbf{W}}^T(t)\Phi\big(\mathbf{x}(t)\big)$. Basis function $\Phi\big(\mathbf{x}_{\mathbf{q}}(t)\big)_i = (1 + e^{x_{q,i}})^{-1}$, $i = 1, \ldots, 4$ is known and $\hat{\mathbf{W}}(t) \in \mathbb{R}^1$ satisfies the weight update law

$$\dot{\hat{\mathbf{W}}}(t) = \underbrace{\begin{bmatrix} \epsilon & & & \\ & 300 & & \\ & & \epsilon & \\ & & & \epsilon \end{bmatrix}}_{\Gamma} \Phi\big(\mathbf{x}_{\mathbf{q}}(t)\big)\mathbf{e}^T(t)P \underbrace{\begin{bmatrix} 0 & 0 \\ 0 & 0 \\ -0.7331 & 0 \\ -0.0319 & 0 \end{bmatrix}}_{B_{\mathrm{ail}}},$$
$$\hat{\mathbf{W}}(0) = \hat{\mathbf{W}}_{\mathbf{0}} \tag{4.7}$$

where $\epsilon << 1$, $\mathbf{e}(t) = \mathbf{x}_{\mathbf{q}}(t) - \mathbf{x}_{\mathbf{r}}(t)$, and positive definite symmetric $P \in \mathbb{R}^{4\times4}$ is the unique solution to the Lyapunov equation

$$0 = A_{\mathrm{r}}^T P + PA_{\mathrm{r}} + 100I_{4\times4}. \tag{4.8}$$

Theorems that highlight the boundedness and performance of this configuration can be found in [47].

States containing small gain ϵ are removed in this configuration because they contribute little to the feedback. There is only adaptive feedback through

the aileron channel in (4.6) and (4.7). This is done to reduce the total number of states in the system. We will demonstrate the validity of our approach in the proceeding section.

We can now write the closed-loop model with (4.1) and (4.5) to (4.7) in their compact form

$$\dot{\mathbf{x}}(t) = \mathbf{f}\big(t, \mathbf{x}(t), \Lambda\mathbf{u}(t)\big), \tag{4.9}$$

where $\mathbf{x}(t) = \begin{bmatrix}\mathbf{x_q}(t) & \hat{\mathbf{W}}(t) & \mathbf{x_r}(t)\end{bmatrix} \in \mathbb{R}^9$. The unused rudder states in the weight update law (4.7) are discarded. A block diagram of the complete closed-loop model is provided in Fig. 4.1.

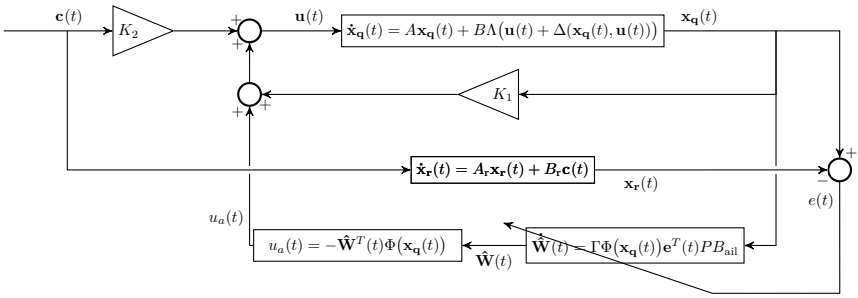

Figure 4.1: Dutch-Roll Closed-Loop Configuration

4.3 MAIN NUMERICAL RESULTS

We wish to validate our existing closed loop polynomial aircraft model (4.9) by finding the initial state that maximizes of the norm of the concave cost function $J = -\|\mathbf{c}(t) - \mathbf{y}(T)\|_2^2$ with given terminal time $T = 10$ s and $\mathbf{c}(t) = \begin{bmatrix}0 & +10\end{bmatrix}\frac{\pi}{180}$. If we can show that for every chosen initial state

$$\mathbf{x}(0) \in X_0 \triangleq \begin{bmatrix}-10 & 10\end{bmatrix}^4 \frac{\pi}{180} \times \begin{bmatrix}-0.001 & 0.001\end{bmatrix} \times \begin{bmatrix}-0.001 & 0.001\end{bmatrix}^4 \frac{\pi}{180}$$

that all trajectories remain bounded in

$$\mathbf{x}(t) \in X \triangleq \begin{bmatrix}-30 & 30\end{bmatrix}^8 \frac{\pi}{180} \times \begin{bmatrix}-80 & 80\end{bmatrix}$$

until they reach the final state belonging to a set $\mathbf{x}(T) \in \{J \leq 3 \times 10^{-3}\}$, then the control law is validated.

The main results of this section rely heavily on theoretical background discussed extensively in [33, 39, 35]. The procedure consists of writing our validation problem as a piecewise polynomial dynamical optimization problem

$$\begin{aligned} J = \inf_{h_T,\, h} \quad & h_T(T, \mathbf{x}(T)) + \int_0^T h(t, \mathbf{x}(t))dt \\ \text{s.t.} \quad & \dot{\mathbf{x}}(t) = \mathbf{f}_j(t, \mathbf{x}(t)), \quad j = 1, 2, \\ & \mathbf{x}(t) \in X_j, \quad \mathbf{x}(0) \in X_0, \quad \mathbf{x}(T) \in X_T, \quad t \in [0, T] \end{aligned} \tag{4.10}$$

with given polynomial dynamics $f \in \mathbb{R}[t, x]$ and costs $h, h_T \in \mathbb{R}[t, x]$, and state trajectories $\mathbf{x}(t)$ constrained in the compact basic semialgebraic sets X, X_0, and X_T.

We then write (4.10) as its infinite-dimensional measure-LP problem

$$\begin{aligned} J_\infty = \inf_{\mu_T,\, \mu} \quad & \int h_T(T, \mathbf{x}(T))d\mu_T + \int h(t, \mathbf{x}(t))d\mu \\ \text{s.t.} \quad & \frac{\partial \mu}{\partial t} + \text{div}\mathbf{f}_j\mu_j + \mu_T = \mu_0 \\ & \int \mu_0 = 1 \end{aligned} \tag{4.11}$$

where div is the divergence operator and the infimum is with respect to the occupation measure $\mu \in \mathscr{M}_+([0, T]\times X)$, terminal measure $\mu_T \in \mathscr{M}_+(\{T\}\times X_T)$, and terminal time $T > 0$. This infinite dimensional problem of measures can be relaxed to a finite moment LMI problem of truncated sequences sequences, using Lasserre's LMI hierarchy [34]. When relaxation order $d \in \mathbb{N}$ tends to infinity, it holds that $J_d \leq J_{d+1} \leq J_\infty$ and $\lim_{d\to\infty} J_d = J_\infty$.

A piecewise disturbance is also included where the aircraft experiences reduced control effectiveness at large roll angles. To include the disturbance, we reformulate the optimization problem with the system dynamics defined as locally affine functions in two cells X_j, $j = 1, 2$ corresponding respectively, to the regimes of the disturbance

$$\begin{aligned} X_1 &\triangleq \{\mathbf{x}(t) \in \mathbb{R}^7 : |\phi| \leq \phi_{\max}\}, \quad \lambda = 1 \\ X_2 &\triangleq \{\mathbf{x}(t) \in \mathbb{R}^7 : |\phi| \geq \phi_{\max}\}, \quad \lambda = 0.2 \end{aligned} \tag{4.12}$$

such that $\phi_{\max} \in \mathbb{R}_+$.

For our main results, we consider two cases: $\phi_{\max} = 1$ and $\phi_{\max} = 3.14 \times 10^{-1}$. We first consider (4.9) without the MRAC augmentation ($\mathbf{u_a}(t) = 0$) for both cases. Then in section 4.3.1 we discuss our main contribution for implementing (4.9) with the MRAC augmentation by reducing the total number of states using parsimony. Lastly, the results for (4.9) with adaptive feedback are presented in section 4.3.3 and compared against the baseline control law from section 4.3.1 for both cases.

If (4.10) can be written in the form of (4.11), it can be solved directly using off-the-shelf-software. In our examples, we used GloptiPoly 3 [29] and MOSEK [30] to solve a hierarchy of moment LMI relaxations. Additional steps must be taken to reduce numerical problems. In (4.9), we employ a normalizing matrix $D = \text{diag}[a_1, \ldots, a_9]$, $a_1, \ldots, a_9 \in \mathbb{R}_+$ such that

$$\dot{\mathbf{x}}(t) = TD\mathbf{f}_j\big(t, D^{-1}\mathbf{x}(t), \Lambda\mathbf{u}(t)\big). \tag{4.13}$$

and all trajectories, including the time domain, are normalized within the interval $\begin{bmatrix}-1 & 1\end{bmatrix}$.

Our numerical results can all be found in Tables 4.1 and 4.2. Then the results obtained with our framework are compared against Monte-Carlo. The Monte-Carlo simulations in Figs. 4.3 and 4.4 were built by using Newton's Method ($t_{\text{step}} = 0.001$ s) and nested for-loops with evenly spaced initial conditions. The green lines denote the desired closed-loop performance. The numerical maximum upper bounds found in Table 4.3 were obtained by searching for the largest J generated by every initial condition.

4.3.1 Baseline Controller Problem

The baseline controller configuration can be obtained by setting $\Gamma = 0$ and $\mathbf{u_a}(t) = 0$. The closed-loop model does not depend on the error dynamics $\mathbf{e}(t)$ in this form, so we also negate the reference dynamics (4.5). Given (4.9), the polynomial dynamical optimization problem becomes

$$\begin{aligned} J = \inf_{\mathbf{y}(T)} \quad & -\|\mathbf{c}(t) - \mathbf{y}(T)\|_2^2 \\ \text{s.t.} \quad & \dot{\mathbf{x}}(t) = TD\mathbf{f}_j\big(t, D^{-1}\mathbf{x}(t), \Lambda_j\mathbf{u}(t)\big) \\ & \mathbf{x}(t) \in X_j, \quad t \in [0,1], \quad j = 1,2 \\ & \mathbf{x}(0) \in X_0, \quad \mathbf{x}(T) \in X_T, \end{aligned} \tag{4.14}$$

and its measure LP

$$\begin{aligned} J_\infty = \inf_{\mu_T} \quad & -\int \|\mathbf{c}(t) - \mathbf{y}(T)\|_2^2 \, \mu_T \\ \text{s.t.} \quad & \frac{\partial \mu_j}{\partial t} + \text{div}\mathbf{f}_j\mu_j + \mu_T = \mu_0 \\ & \int \mu_0 = 1. \end{aligned} \tag{4.15}$$

The moment LMI relaxations problem can now be obtained directly from (4.15).

As shown in the Monte-Carlo simulations Figs. 4.3 and 4.4 and Table 4.3, there is no degradation in tracking performance when $\phi_{\max} = 1$. When $\phi_{\max} = 3.14 \times 10^{-1}$, trajectory overshoot is heavily penalized. Only 2% of the

trajectories fail to achieve proper tracking performance in Fig. 4.4. Insufficient sampling of the state-space in the Monte-Carlo simulations could result these trajectories remaining undetected.

On the other hand, our framework can extract directly the unsafe trajectories. Tables 4.1 and 4.2 contains the Gloptipoly 3 + MOSEK results for both cases. For $\phi_{\max} = 1$, the baseline controller achieves our desired terminal cost. This is not reflected for $\phi_{\max} = 3.14 \times 10^{-1}$, which produces a significantly larger upper bound. This indicates a loss in tracking performance.

4.3.2 Exploiting Sparsity for ODEs

Consider the polynomial dynamics in the form of

$$\begin{aligned} \dot{\mathbf{x}}_{\mathbf{1}}(t) &= \mathbf{f}_{\mathbf{1}}\big(t, \mathbf{x}_{\mathbf{1}}(t), \mathbf{y}(t)\big) \\ \dot{\mathbf{x}}_{\mathbf{2}}(t) &= \mathbf{f}_{\mathbf{2}}\big(t, \mathbf{x}_{\mathbf{2}}(t)\big), \quad \mathbf{y}(t) = C_2 \mathbf{x}_{\mathbf{2}}(t) \end{aligned} \tag{4.16}$$

where $\mathbf{x}_{\mathbf{1}}(t),\ \mathbf{x}_{\mathbf{2}}(t) \in \mathbb{R}^n$, $\mathbf{y}(t) \in \mathbb{R}^m$, and $m < n$. The dynamics of $\mathbf{f}_{\mathbf{2}}(\cdot)$ are *autonomous* and serves as a control input for $\mathbf{f}_{\mathbf{1}}(\cdot)$. In this configuration, (4.16) can be *approximated* using the sparse measure LP

$$\begin{aligned} J_\infty = \inf_{\mu_T} \quad & \int h_T(T, \mathbf{x}(T)) d\mu_T + \int h(t, \mathbf{x}(t)) d\mu \\ \text{s.t.} \quad & \left(\frac{\partial \mu}{\partial t} + \text{div}\mathbf{f}_1 \mu\right) + \mu_T = \mu_0 \\ & \left(\frac{\partial \nu}{\partial t} + \text{div}\mathbf{f}_2 \nu\right) + \nu_T = \nu_0 \\ & \pi_{t,\mathbf{y}\#}\mu = \pi_{t,\mathbf{y}\#}\nu \\ & \int \mu_0 = 1, \quad \int \nu_0 = 1, \end{aligned} \tag{4.17}$$

with marginal $\pi_{t,\mathbf{y}\#}\mu$ respectively, $\pi_{t,\mathbf{y}\#}\nu$ of measure μ respectively, ν with respect to variables t, $\mathbf{y}$. This form was first derived in [36] and is useful for applications where there are a large number of states in (4.10) (the new maximum problem size is $1+n+m$ variables versus $1+2n$). The main advantage of this approach is that the complexity of the problem depends on the size of the largest SDP block. This effectively allows us to use our framework to solve much larger problems.

For our case, the derivation of the MRAC closed-loop validation problem with sparsity begins by looking at the desired closed-response of (4.5) in Fig. 4.2. With the given command signal, we can try approximating the error dynamics

using

$$\hat{\mathbf{e}}(t) = \begin{bmatrix} \beta(t) - \beta_{ss} \\ \phi(t) - \phi_{\mathrm{r}}(t) \\ p(t) - p_{\mathrm{r}}(t) \\ r(t) - r_{ss} \end{bmatrix} \approx \mathbf{e}(t) \tag{4.18}$$

where $\beta_{ss} = \lim_{t\to\infty} \beta_{\mathrm{r}}(t)$ and $r_{ss} = \lim_{t\to\infty} r_{\mathrm{r}}(t)$.

Since $\mathbf{x_r}(t)$ is both linear and *autonomous*, we can go directly to (4.17) by using (4.9), piecewise polynomial dynamical optimization [35] with respect to global occupation measure μ

$$\mu = \mu_1 + \mu_2, \tag{4.19}$$

and the approximated error dynamics (4.18). The main takeaway of using (4.18) is that we reduce the total number of equality constraints in (4.17) and further simplify the problem. We are now ready to write the MRAC closed-loop problem.

4.3.3 MRAC Controller Problem

Given (4.17) and the polynomial dynamical optimization problem

$$\begin{aligned} J = \inf_{\mathbf{y}(T)} \quad & -\|\mathbf{c}(t) - \mathbf{y}(T)\|_2^2 \\ \text{s.t.} \quad & \dot{\mathbf{x}}(t) = TD\mathbf{f}_j\big(t, D^{-1}\mathbf{x}(t), \Lambda_j \mathbf{u}(t)\big) \\ & \dot{\mathbf{x}}_{\mathbf{r}}(t) = A_{\mathrm{r}}\mathbf{x}_{\mathbf{r}}(t) + B_{\mathrm{r}}\mathbf{c}(t) = \mathbf{f}_{\mathbf{r}}\big(\mathbf{x}_{\mathbf{r}}(t), \mathbf{c}(t)\big) \\ & \mathbf{x}(t) \in X_j, \quad \mathbf{x}_{\mathbf{r}}(t) \in X_{\mathrm{r}}, \quad t \in [0,1], \quad j = 1,2 \\ & \mathbf{x}(0) \in X_0, \quad \mathbf{x}(T) \in X_T, \\ & \mathbf{x}_{\mathbf{r}}(0) \in X_{\mathrm{r}0}. \quad \mathbf{x}_{\mathbf{r}}(T) \in X_{\mathrm{r}T} \end{aligned} \tag{4.20}$$

the new measure-LP for the closed-loop model with MRAC becomes

$$\begin{aligned} J_\infty = \inf_{\mathbf{y}(T)} \quad & -\|\mathbf{c}(t) - \mathbf{y}(T)\|_2^2 \\ \text{s.t.} \quad & \left(\frac{\partial \mu_j}{\partial t} + \mathrm{div}\mathbf{f}_j\mu_j\right) + \mu_T = \mu_0, \quad j = 1,2 \\ & \left(\frac{\partial \nu}{\partial t} + \mathrm{div}\mathbf{f}_{\mathbf{r}}\nu\right) + \nu_T = \nu_0 \\ & \pi_{t,\mathbf{y}\#}\mu_1 + \pi_{t,\mathbf{y}\#}\mu_2 = \pi_{t,\mathbf{y}\#}\nu \\ & \int \mu_0 = 1, \quad \int \nu_0 = 1, \end{aligned} \tag{4.21}$$

where $\mathbf{x}(t) = \big[\mathbf{x_q}(t), \quad \hat{\mathbf{W}}(t), \quad \mathbf{x_r}(t)\big]$. We also have marginal $\pi_{t,\mathbf{y}\#}\mu$ respectively, $\pi_{t,\mathbf{y}\#}\nu$ of measure μ respectively, ν with respect to variables

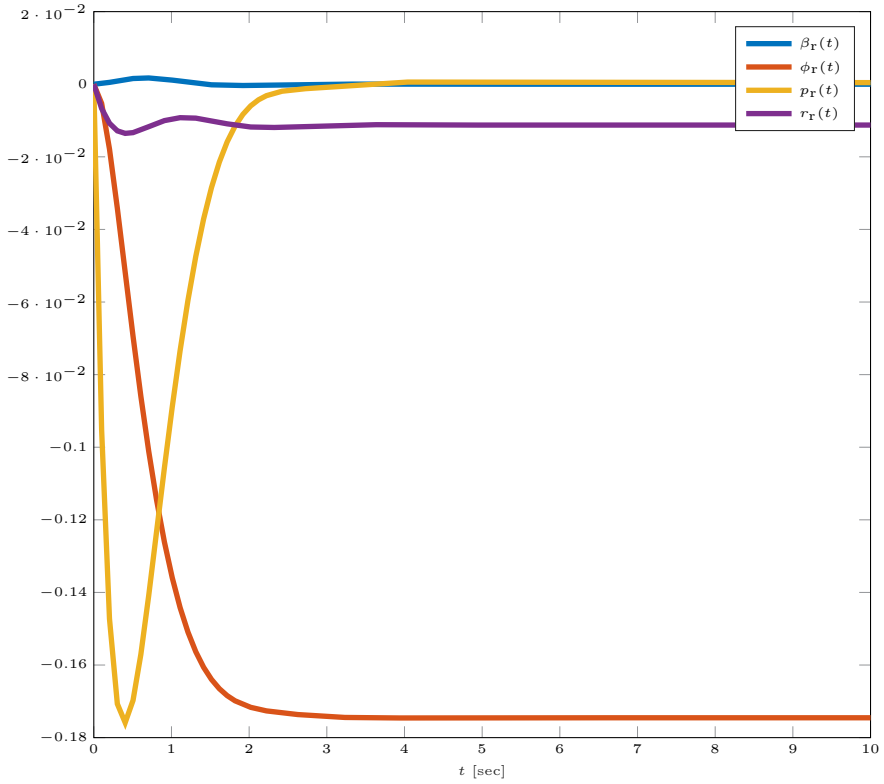

Figure 4.2: Reference Trajectory $\mathbf{x_r}(t)$ Given $\mathbf{c}(t)$

t, $\mathbf{y}$. With the moment equality constraints and the appropriate supports, the moment LMI relaxation problem of (4.21) provides a useful upper bound for the cost function J given in (4.20).

For both values of $\phi_{\max}$, good tracking performance was achieved for our LQR + MRAC configuration. This is reflected in our Monte-Carlo simulations Figs. 4.3 and 4.4 and Table 4.3. Likewise, desirable upper bounds are achieved in our Gloptipoly 3 + MOSEK results Tables 4.1 and 4.2. The main takeaway is that even a simple LQR + MRAC closed-loop configuration can reject exogenous disturbances and initial condition mismatches.

It is also possible to achieve improved transient performance using MRAC modifications, such as the error modification [37] or adaptive loop recovery [38], and are discussed extensively in chapter 3.

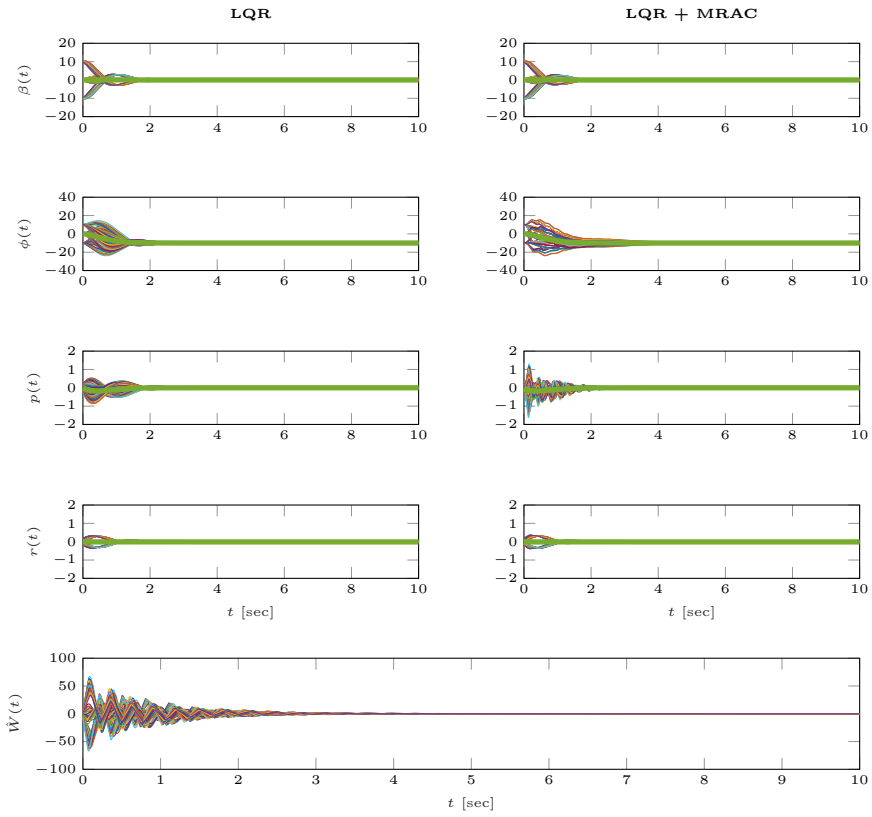

Figure 4.3: F-16 Monte-Carlo with safe trajectories ($\phi_{\max} = 1$)

Table 4.1: Gloptipoly 3 + MOSEK Upper Bounds ($\phi_{\max} = 1$)

	LQR		LQR + MRAC	
Rel Ord	**Upper Bnd J**	**CPU [s]**	**Upper Bnd J**	**CPU [s]**
1	2.59	2.33	2.36×10^{-1}	3.24×10^{1}
2	9.78×10^{-2}	2.05	6.41×10^{-4}	1.22×10^{3}
3	1.44×10^{-3}	1.33×10^{1}	1.40×10^{-5}	2.65×10^{5}
4	2.81×10^{-5}	1.17×10^{2}	-	-

4.4 CONCLUSIONS AND FUTURE WORKS

We considered a nonlinear dutch-roll F-16 closed-loop model complete with a baseline LQR and MRAC augmentation. To reduce the size of the problem,

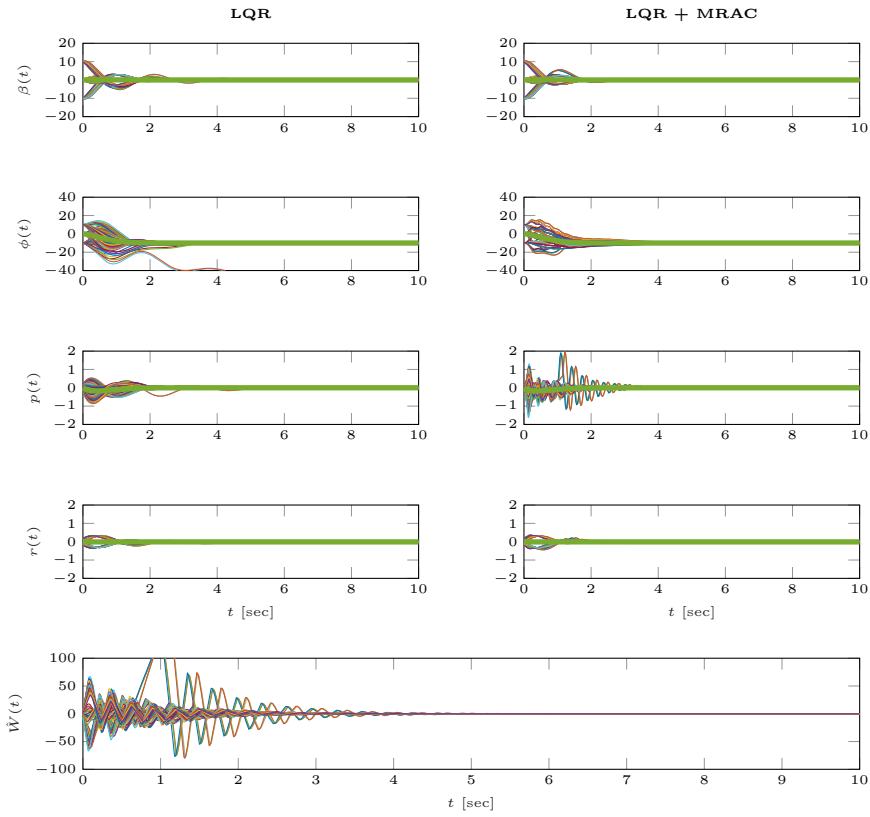

Figure 4.4: F-16 Monte-Carlo with unsafe trajectories in baseline LQR ($\phi_{\max} = 3.14 \times 10^{-1}$)

we exploited sparsity in our framework. These models were then validated using moment LMI relaxations and existing off-the-shelf software. We compared the performance of the closed-loop model baseline LQR controller to the same model with the MRAC. These results were then compared with upper bounds obtained using Monte-Carlo simulations. For future work, we wish to use our framework to consider aircraft models with unknown flexible dynamics.

Table 4.2: Gloptipoly 3 + MOSEK Upper Bounds ($\phi_{\max} = 3.14 \times 10^{-1}$)

	LQR		LQR + MRAC	
Rel Ord	**Upper Bnd J**	**CPU [s]**	**Upper Bnd J**	**CPU [s]**
1	2.59	1.43	2.29×10^{-1}	2.20×10^{1}
2	6.58×10^{-1}	1.53	6.47×10^{-4}	1.25×10^{3}
3	4.68×10^{-1}	9.62	1.52×10^{-5}	2.21×10^{5}
4	4.59×10^{-1}	8.25×10^{1}	-	-

Table 4.3: Monte-Carlo Upper Bounds for section 4.3

$\phi_{\max}$	Upper Bound J (LQR)	Upper Bound J (LQR + MRAC)	CPU [s]
1	1.87×10^{-10}	5.07×10^{-7}	1.18×10^{1}
3.14×10^{-1}	4.46×10^{-1}	5.07×10^{-7}	1.20×10^{1}

5

Flexible Aircraft with MRAC

5.1 Introduction

It is well established that MRAC is susceptible to closed-loop instability in the presence of system uncertainties and unmodeled dynamics [27]. To address this phenomenon, the authors of [48, 49, 50, 51, 52] proposed the use of "intelligent adaptive control". See also [53, 54, 55] where the authors propose an MRAC which can maintain closed-loop stability in the presence of uncertain parameters and unmodeled dynamics with respect to a set of initial conditions or under the assumption of persistency of excitation. Recently, the authors of [56, 57, 58, 59, 60] utilized an MRAC modification that permitted closed-loop stability in the presence of large uncertainties.

Since MRAC cannot tolerate the presence large system uncertainties, they cannot be safely neglected in the design phase. For example, the coupling between the static and flexible modes in an aircraft is very difficult to model precisely and can lead to instability with MRAC. Model identification of the static and flexible modes is usually carried out separately through wind tunnel and vibration testing. The rest must be achieved by extensive simulation and flight testing.

To illustrate this problem, an F-16 model with unmodeled flexible dynamics and LQR + MRAC is considered. This procedure is similar to that in chapter 3. The closed-loop performance requirements can be expressed as a V&V problem

Contents of this chapter were submitted for publication to International Journal of Control

of polynomial dynamical optimization. These uncertain, bounded parameters in the unmodeled dynamics can be written explicitly in the space of occupation measures and do not require improved modeling accuracy. To reduce issues with scaling, exploiting parsimony for ODEs in introduced to partition the dynamics. Then the V&V problem is solved with our framework.

In chapter 3 we used polynomials to approximate the reference trajectory. This required partitioning the dynamics over several intervals in the time domain. For chapter 4, using parsimony approximating the reference was introduced for the first time. As far as we know, this is the first time that a fully integrated V&V framework is proposed for aircraft with flexible dynamics and MRAC.

Monte-Carlo simulations scale very poorly with the number of these uncertain parameters in the unmodeled system. If the state-space is not sufficiently explored for all uncertain parameters, there is good chance the simulations will not reveal unexplored, unsafe trajectories. This point is illustrated in a side-by-side comparison is made between the Monte-Carlo simulations and our framework for the F-16.

In the numerical examples, the ability for the LQR + MRAC to maintain acceptable command following in the presence of uncertain, unmodeled flexible dynamics is reflected in a cost function. If the uncertain parameters in the flexible dynamics are sufficiently small, it follows that the upper bound of this cost function is sufficiently small. Conversely, a cost function with a large upper bound is indicative of large unmodeled dynamics and unsafe trajectories.

Unlike the results of [53, 54, 55], we do not rely on a set of initial conditions or persistency of excitation. Compared to [56, 57, 58, 59, 60], control modifications are not used to address the unmodeled dynamics. Instead, it is demonstrated numerically that the upper tolerances of simple MRAC configuration using our V&V framework. This is achieved by exploiting parsimony for ODEs similar to our results in chapter 4. Any uncertain parameters or initial condition mismatch can be addressed explicitly with our framework.

The organization of this chapter is as follows: section 5.2 illustrates our main contribution by using a simple example, section 5.3 considers a closed-loop linear F-16 model coupled with uncertain flexible dynamics and MRAC, section 5.4 considers the model from chapter 3 coupled with uncertain flexible dynamics, and section 5.5 contains a small discussion of our conclusions and future work.

5.2 Illustrative Simple Example

The proceeding problem draws directly the theoretical contributions provided in [34]. See also chapter 3 for a practical example. The procedure for validating our uncertain models is illustrated in the simple example below. Consider the

closed-loop linear parameter varying (LPV) system in the form of

$$\begin{bmatrix}\dot{\mathbf{x}}(t)\\ \dot{\mathbf{z}}(t)\end{bmatrix} = \begin{bmatrix} 0 & -1+k & 0 & 0 & 0\\ 1+k & -5 & 0 & 0 & 0\\ 0 & 0.1 & -10 & 0.1 & 0\\ 0 & 0 & 0.1 & -1 & -0.1\\ 0 & 0 & 0 & 1 & -1 \end{bmatrix} \begin{bmatrix}\mathbf{x}(t)\\ \mathbf{z}(t)\end{bmatrix} = \mathbf{f}(t,\mathbf{x}(t),\mathbf{z}(t),k),$$
$$\begin{matrix}\mathbf{x}(0)=\mathbf{x}_0,\\ \mathbf{z}(0)=\mathbf{z}_0,\end{matrix} \quad (5.1)$$

where $\mathbf{x}(t) = \begin{bmatrix}x_1(t) & x_2(t)\end{bmatrix} \in \mathbb{R}^2$, $\mathbf{z}(t) = \begin{bmatrix}z_1(t) & z_2(t) & z_3(t)\end{bmatrix} \in \mathbb{R}^3$, and parameter $k \in \begin{bmatrix}-k_{max} & k_{max}\end{bmatrix}, k_{max} \in \mathbb{R}_+$ is uncertain. Now suppose that (5.1) is a closed loop model of some dynamical system such that the state trajectory of $x_1(T)$ reaches a smaller subset in finite time. In other words, we want find the initial state maximizing the norm of the terminal state with the concave quadratic term $J = \inf_{x_1(T)} -x_1(T)^2$ and given terminal time $T = 10$. There are also the initial constraints

$$\mathbf{x}(0) \in \begin{bmatrix}-0.1 & 0.1\end{bmatrix}^2 \triangleq X_0,$$
$$\mathbf{z}(0) \in \begin{bmatrix}-0.1 & 0.1\end{bmatrix}^3 \triangleq Z_0,$$

the trajectory constraints

$$\mathbf{x}(t) \in \begin{bmatrix}-1 & 1\end{bmatrix}^2 \triangleq X,$$
$$\mathbf{z}(t) \in \begin{bmatrix}-1 & 1\end{bmatrix}^3 \triangleq Z,$$

and the terminal constraints

$$\mathbf{x}(T) \in \begin{bmatrix}-1 & 1\end{bmatrix}^2 \triangleq X_T,$$
$$\mathbf{z}(T) \in \begin{bmatrix}-1 & 1\end{bmatrix}^3 \triangleq Z_T.$$

This overall problem description can be collectively written as the polynomial dynamical optimization problem

$$\begin{aligned} J = \inf_{x_1(T)} \quad & -x_1(T)^2 \\ \text{s.t.} \quad & \begin{bmatrix}\dot{\mathbf{x}}(t)\\ \dot{\mathbf{z}}(t)\end{bmatrix} = \mathbf{f}(t,\mathbf{x}(t),\mathbf{z}(t),k), \\ & \mathbf{x}(0) \in X_0, \quad \mathbf{x}(t) \in X, \quad \mathbf{x}(T) \in X_T, \\ & \mathbf{z}(0) \in Z_0, \quad \mathbf{z}(t) \in Z, \quad \mathbf{z}(T) \in Z_T, \\ & t \in \begin{bmatrix}0, & T\end{bmatrix}, \quad k \in \begin{bmatrix}-k_{max} & k_{max}\end{bmatrix}. \end{aligned} \quad (5.2)$$

Table 5.1: Gloptipoly 3 + MOSEK Upper Bounds for section 5.2

	$k_{\max} = 0.1$		$k_{\max} = 0.5$		$k_{\max} = 5$	
Rel Ord	**Upper Bnd** J	**CPU [s]**	**Upper Bnd** J	**CPU [s]**	**Upper Bnd** J	**CPU [s]**
1	1.41×10^{-2}	2.18	1.71×10^{-2}	2.17	1	2.08
2	8.03×10^{-4}	5.13	1.44×10^{-3}	5.46	1	4.68
3	2.84×10^{-4}	1.22×10^{2}	8.39×10^{-4}	1.08×10^{2}	1	1.25×10^{2}
4	2.67×10^{-4}	2.13×10^{3}	8.30×10^{-4}	2.88×10^{3}	1	3.90×10^{3}
5	-	-	-	-	-	-

and is equivalent to the problem in the infinite-dimensional space of measures

$$\begin{aligned} J_\infty = \inf_{\mu_T} \quad & -\int x_1(T)^2 d\mu_T \\ \text{s.t.} \quad & \frac{\partial \mu}{\partial t} + \text{div}\mathbf{f}\mu(t,\mathbf{x},\mathbf{z},k) + \mu_T = \mu_0 \\ & \int \mu_0 = 1 \end{aligned} \tag{5.3}$$

where div is the divergence operator and the infimum is with respect to the occupation measure $\mu \in \mathscr{M}_+([0,T]\times X)$, terminal measure $\mu_T \in \mathscr{M}_+(\{T\}\times X_T)$, and terminal time $T > 0$. This is for all measures supported on $[0,T] \times X \times Z$, $\{0\} \times X_0 \times Z_0$, and $\{T\} \times X_T \times Z_T$ respectively. As discussed in [29], (5.3) can be solved using a hierarchy of LMI relaxations.

The main takeaway here is that an abstract problem of measures can be manipulated by its corresponding moments generated by a finite number of truncated sequences. To avoid large magnitude semi-definite constraints in the final problem, a normalizing matrix $D = \text{diag}(a_1, \ldots, a_5)$, $a_1, \ldots, a_5 \in \mathbb{R}_+$ is employed such that all trajectories, including the time domain, are constrained on the interval $\begin{bmatrix} -1 & 1 \end{bmatrix}$.

The procedure for expressing the validation problem in Gloptipoly 3 is no different. The script in appendix A can be used to solve the the polynomial dynamical optimization problem (5.2) with our framework using [30] as our main SDP solver. The computed upper bounds without parsimony can be found in Table 5.1. As k_{max} is increased, it is expected that the upper bound J will grow with it. Since the computational time scales exponentially with the size of the largest moment SDP block, this problem cannot be solved beyond the fourth relaxation order. This procedure is analogous to searching the worst case eigenvalues $\lambda_{\max} = \max(\text{re}(\text{eig}(A(k))))$, which can be found in Table 5.2. The resulting script that solves the validation problem in section 5.2, with some scaling strategies to improve numerical behavior, can be found in appendix A.

Table 5.2: Largest Eigenvalues for section 5.2

$k_{\max}$	$\lambda_{\max}$
0.1	-2.07×10^{-1}
0.5	-1.55×10^{-1}
5	3

5.2.1 Exploiting Parsimony for ODEs

The results of section 5.2 will now be repeated by exploiting parsimony for ODEs. The main advantage to this approach is that it reduces the size of the largest SDP block. Consequently, our framework can be used to validate problems that are larger in size. First, (5.1) can be rewritten as

$$\dot{\mathbf{x}}(t) = \mathbf{f_1}(t, \mathbf{x}(t), k), \quad y(t) = x_2(t) \tag{5.4}$$

$$\dot{\mathbf{z}}(t) = \mathbf{f_2}(t, \mathbf{z}(t), y(t)), \tag{5.5}$$

where dynamics $\mathbf{f_1}(\cdot) \in \mathbb{R}\begin{bmatrix} t & \mathbf{x}(t) & k \end{bmatrix}$ are autonomous and $y(t) = x_2(t) \in \mathbb{R}$ can be interpreted as a control input to $\mathbf{f_2}(\cdot) \in \mathbb{R}\begin{bmatrix} t & \mathbf{z}(t) & y(t) \end{bmatrix}$. Using the same polynomial dynamical optimization problem (5.2) and partitioned dynamics (5.5), the problem of measures can be written as

$$\begin{aligned} J_\infty = \inf_{\mu_T} \quad & -\int x_1(T)^2 d\mu_T \\ \text{s.t.} \quad & \frac{\partial \mu}{\partial t} + \text{div}\mathbf{f_1}\mu(t, \mathbf{x}, k) + \mu_T = \mu_0 \\ & \frac{\partial \nu}{\partial t} + \text{div}\mathbf{f_2}\nu(t, \mathbf{z}, y) + \nu_T = \nu_0 \\ & \pi_{t,\mathbf{y}\#}\mu = \pi_{t,\mathbf{y}\#}\nu \\ & \int \mu_0 = 1, \quad \int \nu_0 = 1, \end{aligned} \tag{5.6}$$

with marginal $\pi_{t,\mathbf{y}\#}\mu$, respectively, $\pi_{t,\mathbf{y}\#}\nu$, of measure μ, respectively, ν, with respect to variables t, $\mathbf{y}$. The moment LMI relaxation problem is modified accordingly. The results can be found in Table 5.3. As illustrated, similar upper bounds can be achieved. Since the size of the largest moment SDP block is reduced in this configuration, the problem size can be solved up to the fifth relaxation order. The overall maximum problem size is reduced by 2. This property will be exploited to solve problems with a large number of states in the proceeding sections.

The theoretical background for these results were first noted in [36]. In the proceeding section, this methodology for exploiting parsimony for ODEs is unchanged. If our problem can be written in the form similar to (5.5) and (5.6), then it is possible to proceed by solving our V&V problem in Gloptipoly 3 using our framework.

Table 5.3: Gloptipoly 3 + MOSEK Upper Bounds for section 5.2.1

	$k_{\max} = 0.1$		$k_{\max} = 0.5$		$k_{\max} = 5$	
Rel Ord	**Upper Bnd J**	**CPU [s]**	**Upper Bnd J**	**CPU [s]**	**Upper Bnd J**	**CPU [s]**
1	1.41×10^{-2}	1.64	1.71×10^{-2}	5.32×10^{-1}	1	4.00×10^{-1}
2	8.03×10^{-4}	1.10	1.44×10^{-3}	9.17×10^{-1}	1	8.29×10^{-1}
3	2.87×10^{-4}	2.86	8.38×10^{-4}	2.61	1	2.49
4	2.67×10^{-4}	9.58	8.31×10^{-4}	1.01×10^{1}	1	8.64
5	2.67×10^{-4}	4.50×10^{1}	8.30×10^{-4}	4.88×10^{1}	1	5.04×10^{1}

5.3 Flexible Dynamics for a F-16 Linear Model

Our objective is to validate a linear F-16 short period aircraft model augmented with adaptive feedback, uncertain parameters, and flexible dynamics using our V&V framework. The procedure for implementing our framework is rather straight forward. In section 5.3.1 we discuss the simplified uncertain aeroelastic model and its closed loop configuration. Although the rigid body and flexible modes are well-defined, their coupling is not. For the coupling uncertain, bounded parameters $k_1,\ k_2,\ k_3 \in \begin{bmatrix} -k_{max} & k_{max} \end{bmatrix}$, $k_{max} \in \mathbb{R}_+$ are used. After writing the problem in its compact form, control law validation problem is explicitly stated in section 5.3.2. The problem is then partitioned by exploiting parsimony for ODEs. The number of uncertain parameters are gradually increased. Finally, the model and its uncertainties are addressed explicitly using our framework and then validated under adverse flight conditions. In total, there are three cases:

1. k_1 is *uncertain*, k_2 and k_3 are *known*;
2. k_1 and k_3 are *uncertain*, k_2 is *known*;
3. k_1, k_2, and k_3 are *uncertain*.

5.3.1 Closed-Loop Configuration

Consider the short-period dynamics of a linear F-16 aircraft coupled with flexible dynamics

$$\dot{\mathbf{x}}_{\mathbf{p}}(t) = \underbrace{\begin{bmatrix} -1.0189 & +0.9051 \\ +0.8223 & -1.0774 \end{bmatrix}}_{A_{\mathrm{p}}} \mathbf{x}_{\mathbf{p}}(t) + \underbrace{\begin{bmatrix} -0.0022 \\ -0.1756 \end{bmatrix}}_{B_{\mathrm{p}}} \underbrace{0.7}_{\Lambda} \big(u(t) + \delta(\mathbf{x}_{\mathbf{p}}(t))\big) \quad (5.7)$$

$$+ \underbrace{\begin{bmatrix} -0.0022k_1 & 0 \\ -0.1756k_1 & 0 \end{bmatrix}}_{B_{\mathrm{p}}H(k_1)^T} \mathbf{z}(t), \quad \mathbf{x}_{\mathbf{p}}(0) = \mathbf{x}_{\mathbf{p}_0} \quad (5.8)$$

$$\dot{\mathbf{z}}(t) = \underbrace{\begin{bmatrix} -0.5 & 6.3 \\ -6.3 & -0.5 \end{bmatrix}}_{F} \mathbf{z}(t) + \underbrace{\begin{bmatrix} k_3 \\ k_2 \end{bmatrix}}_{G(k_2,k_3)^T} \mathbf{x}_{\mathbf{p}}(t), \quad \mathbf{z}(0) = \mathbf{z}_0 \quad (5.9)$$

where $\mathbf{x}_{\mathbf{p}}(t) = \begin{bmatrix} \alpha(t) & q(t) \end{bmatrix} \in \mathbb{R}^2$ are the short period dynamics, $\alpha(t)$ is the angle of attack, $q(t)$ is the pitch-rate, $\mathbf{z}(t) = \begin{bmatrix} z_1(t) & z_2(t) \end{bmatrix} \in \mathbb{R}^2$ are states related to the modal form of a considered dominant aeroelastic mode. Matrix F represents a 5.2 Hz first bending mode of the aircraft [61]. There is also measurable control input $u(t) \in \mathbb{R}$, control effectiveness $\Lambda \in \mathbb{R}_+$, the in state uncertainty

$$\delta(\mathbf{x}_{\mathbf{p}}(t)) = \underbrace{\begin{bmatrix} -0.0468 & -0.0982 \end{bmatrix}}_{K_{pert}} \mathbf{x}_{\mathbf{p}}(t), \quad (5.10)$$

and uncertain parameters representing the coupling of the rigid body and flexible dynamics $k_1, k_2, k_3 \in \begin{bmatrix} -k_{max} & k_{max} \end{bmatrix}$.

Our control objective is design a control law $u(t)$ to reject the in state disturbance (5.10) and asymptotically track the reference trajectory $\mathbf{x}_{\mathbf{r}}(t) = \begin{bmatrix} \alpha_{\mathrm{r}}(t) & q_{\mathrm{r}}(t) \end{bmatrix}$ generated by the dynamics

$$\dot{\mathbf{x}}_{\mathbf{r}}(t) = A_{\mathrm{r}}\mathbf{x}_{\mathbf{r}}(t) + B_{\mathrm{r}}c(t) \quad (5.11)$$

where $c(t) \in \mathbb{R}$ is a bounded command signal. The *desired closed loop* dynamics are derived using the nominal feedback control law [62]

$$u_{\mathrm{n}}(t) = \underbrace{\begin{bmatrix} -4.7432 & 2.3163 \end{bmatrix}}_{K_1} \mathbf{x}_{\mathbf{p}}(t) - \underbrace{4.3396}_{K_2} c(t), \quad (5.12)$$

such that $A_{\mathrm{r}} = A_{\mathrm{p}} - B_1$ is Hurwitz and $B_{\mathrm{r}} = B_{\mathrm{p}}K_2$. To reject exogenous disturbance and improve tracking performance an the adaptive feedback control law

$$u_{\mathrm{a}}(t) = -\hat{\mathbf{W}}(t)^T \Phi(\mathbf{x}_{\mathbf{p}}(t)) \quad (5.13)$$

is also included with basis function $\Phi_i(\mathbf{x_p}(t)) = (1 + e^{\mathbf{x}_{\mathrm{p}i}})^{-1}$ and $\hat{\mathbf{W}}(t) \in \mathbb{R}^2$ satisfies the weight update law

$$\dot{\hat{\mathbf{W}}}(t) = \underbrace{\begin{bmatrix} \epsilon & \\ & 100 \end{bmatrix}}_{\Gamma} \big(\Phi\big(\mathbf{x_p}(t)\big)\mathbf{e}^T(t)PB_{\mathrm{p}} + \underbrace{5(\mathbf{e}^T(t)PB_{\mathrm{p}})^2\hat{\mathbf{W}}(t)}_{\dot{\hat{\mathbf{W}}}_m(t)}\big), \quad \hat{\mathbf{W}}(0) = \hat{\mathbf{W}}_0 \tag{5.14}$$

where $\epsilon << 1$, error dynamics $\mathbf{e}(t) = \mathbf{x_p}(t) - \mathbf{x_r}(t)$, $\dot{\hat{\mathbf{W}}}_m(t)$ is the error modification [37], and positive definite symmetric $P \in \mathbb{R}^{2\times 2}$ is the unique solution to the Lyapunov equation

$$0 = A_{\mathrm{r}}^T P + PA_{\mathrm{r}} + 10I_{2\times 2}. \tag{5.15}$$

The *combined* nominal/adaptive feedback control law can be written as

$$u(t) = u_{\mathrm{n}}(t) + u_{\mathrm{a}}(t) \tag{5.16}$$

which was used in (5.8). In practice, Lyapunov analysis only informs us about the ultimate stability of the closed-loop system if the unmodeled dynamics are neglected. There at least exists a Lyapunov candidate function such that the longitudinal dynamics (5.8) subject to the control and weight update law (5.14) and (5.16) has the property $\lim_{t\to\infty} e(t) = 0$. Consequently, learning rates of (5.14) were tuned to reject disturbances and achieve tracking without the flexible dynamics.

It is of practical interest to know if the MRAC can tolerate unmodeled dynamics and uncertain parameters of a certain magnitude. In proceeding section it is shown numerically when the unmodeled dynamics with uncertain parameters can be neglected without using control modifications. These achieved upper bounds are significantly less conservative than norm approximations found in the Lyapunov analysis.

To set up the problem for our V&V framework, the compact form of the closed-loop model can now be written by combining (5.8), (5.9), (5.11),(5.14), and (5.16) to get

$$\begin{aligned}
&\dot{\mathbf{x}}_{\mathbf{1}}(t) = \mathbf{f_1}(t, \mathbf{x_1}(t), c(t)), && y_1(t) = \alpha_{\mathrm{r}}(t), && \mathbf{x_1}(0) = \mathbf{x}_{\mathbf{1}0} \\
&\dot{\mathbf{x}}_{\mathbf{2}}(t) = \mathbf{f_2}(t, \mathbf{x_2}(t), y_1(t), y_3(t), k_1), && \mathbf{y_2}(t) = \mathbf{x_p}(t), && \mathbf{x_2}(0) = \mathbf{x}_{\mathbf{2}0} \\
&\dot{\mathbf{x}}_{\mathbf{3}}(t) = \mathbf{f_3}(t, \mathbf{x_3}(t), \mathbf{y_2}(t), k_2, k_3), && y_3(t) = z_1(t), && \mathbf{x_3}(0) = \mathbf{x}_{\mathbf{3}0}
\end{aligned} \tag{5.17}$$

where $\mathbf{x_1}(t) = \mathbf{x_r}(t) \in \mathbb{R}^2$, $\mathbf{x_2}(t) = \big[\mathbf{x_p}(t), \quad \hat{\mathbf{W}}(t)\big] \in \mathbb{R}^3$, $\mathbf{x_3}(t) = \mathbf{z}(t) \in \mathbb{R}^2$, and $\mathbf{y_2}(t) \in \mathbb{R}^2$.

5.3.2 Validation Problem & Main Results

We want to validate our closed-loop model in its compact form (5.17) by finding the initial state that maximizes the norm of the concave cost function of the

error dynamics $J = -\|\mathbf{e}(T)\|_2^2$ with given command signal $c(t) = 0.1$ and terminal time $T = 20$. If it can be shown that for every chosen initial state

$$\begin{aligned}
\mathbf{x_1}(0) &\in \begin{bmatrix} -0.2 & 0.2 \end{bmatrix}^2 \triangleq X_{10} \\
\mathbf{x_2}(0) &\in \begin{bmatrix} -0.2 & 0.2 \end{bmatrix}^2 \times \begin{bmatrix} -1 \times 10^{-6}, & 1 \times 10^{-6} \end{bmatrix} \triangleq X_{20} \\
\mathbf{x_3}(0) &\in \begin{bmatrix} -0.2 & 0.2 \end{bmatrix}^2 \triangleq X_{30}
\end{aligned}$$

all trajectories remain bounded in the box

$$\begin{aligned}
\mathbf{x_1}(t) &\in \begin{bmatrix} -1 & 1 \end{bmatrix}^2 \triangleq X_1 \\
\mathbf{x_2}(t) &\in \begin{bmatrix} -1 & 1 \end{bmatrix}^2 \times \begin{bmatrix} -5, & 5 \end{bmatrix} \triangleq X_2 \\
\mathbf{x_3}(t) &\in \begin{bmatrix} -1 & 1 \end{bmatrix}^2 \triangleq X_3
\end{aligned}$$

until they reach the final state belonging to the set $\mathbf{e}(T) \in \{J \leq 3 \times 10^{-3}\} \triangleq X_{1T}$, then the control law is validated. The overall description can be expressed by its polynomial dynamical optimization problem

$$\begin{aligned}
J = \inf_{\mathbf{e}(T)} \quad & -\|\mathbf{e}(T)\|_2^2 \\
\text{s.t.} \quad & \dot{\mathbf{x}}_1(t) = \mathbf{f_1}(t, \mathbf{x_1}(t), c(t)) \\
& \dot{\mathbf{x}}_2(t) = \mathbf{f_2}(t, \mathbf{x_2}(t), y_1(t), y_3(t), k_1) \\
& \dot{\mathbf{x}}_3(t) = \mathbf{f_3}(t, \mathbf{x_3}(t), \mathbf{y_2}(t), k_2, k_3) \\
& \mathbf{x_1}(0) \in X_{10}, \quad \mathbf{x_1}(t) \in X_1, \quad \mathbf{x_1}(T) \in X_{1T}, \\
& \mathbf{x_2}(0) \in X_{20}, \quad \mathbf{x_2}(t) \in X_2, \quad \mathbf{x_2}(T) \in X_2, \\
& \mathbf{x_3}(0) \in X_{30}, \quad \mathbf{x_3}(t) \in X_3, \quad \mathbf{x_3}(T) \in X_3, \\
& t \in \begin{bmatrix} 0, & T \end{bmatrix}, \quad u \in \begin{bmatrix} -k_{max} & k_{max} \end{bmatrix}.
\end{aligned} \tag{5.18}$$

Its approximation in the space of infinite dimensional measures using parsimony can be written as

$$
\begin{aligned}
J_\infty = \inf_{\mu_T} \quad & -\int \|\mathbf{e}(T)\|_2^2 \, d\mu_T \\
\text{s.t.} \quad & \frac{\partial \mu}{\partial t} + \text{div}\mathbf{f_1}\mu(t, \mathbf{x_1}) + \mu_T = \mu_0 \\
& \frac{\partial \nu}{\partial t} + \text{div}\mathbf{f_2}\nu(t, \mathbf{x_2}, y_1, y_3, k_1) + \nu_T = \nu_0 \\
& \frac{\partial \xi}{\partial t} + \text{div}\mathbf{f_3}\xi(t, \mathbf{x_3}, \mathbf{y_2}, k_2, k_3) + \xi_T = \xi_0 \\
& \pi_{t,y_1,\#}\mu = \pi_{t,y_1,\#}\nu \\
& \pi_{t,\mathbf{y_2},y_3,\#}\mu = \pi_{t,\mathbf{y_2},y_3,\#}\xi \\
& \int \mu_0 = 1, \quad \int \nu_0 = 1, \quad \int \xi_0 = 1
\end{aligned}
\tag{5.19}
$$

and its respective moment LMI relaxations problem is modified accordingly. The same marginals of their respective measures from section 5.3 are also used. In total the overall size of the problem is reduced by 5 variables using parsimony. and its respective moment LMI relaxations problem is modified accordingly. The marginal $\pi_{t,y_1,\#}\mu$, respectively, $\pi_{t,y_1,\#}\nu$, on measure μ, respectively, ν, are with respect to variables t, y_1. There is also marginal $\pi_{t,\mathbf{y_2},y_3,\#}\mu$, respectively, $\pi_{t,\mathbf{y_2},y_3,\#}\xi$, on measure μ, respectively, ξ, with respect to variables t, $\mathbf{y_2}$, andy_3. Similar to chapter 4, partitioning the dynamics and approximating the reference trajectory chapter 4 allows using a command signal without using piecewise approximations chapter 3. In total the problem is reduced by 4 variables using parsimony.

The main results can be found below. In Table 5.4 an uncertain $k_1 \in \begin{bmatrix} -k_{max} & k_{max} \end{bmatrix}$ is considered with fixed $k_2 = -0.1$, $k_3 = 0.1$. Similar upper bounds were achieved for all values of k_{max}, which indicates tolerance from the MRAC in the presence of unmodeled flexible dynamics. Likewise, in Table 5.5 let $k_1,\ k_3 \in \begin{bmatrix} -k_{max} & k_{max} \end{bmatrix}$ and fix $k_2 = -0.1$. Lastly, in Table 5.6 there is also $k_1,\ k_3,\ k_2 \in \begin{bmatrix} -k_{max} & k_{max} \end{bmatrix}$. The upper bounds achieved are larger than those obtained for the one uncertain parameter case. At $k_{max} = 10$, the upper bound violates the terminal constraint which indicates the presence of unstable trajectories for two or three uncertain parameters.

The simulation results using Monte-Carlo can be found in Table 5.7 and Figs. 5.1 to 5.9. These simulations were obtained using evenly spaced initial conditions and Newton's Method. Red lines in the plot represent the desired closed loop performance. The maximum costs were obtained by finding the worst case trajectories in the simulation. In Figs. 5.6 and 5.9 and Table 5.7, the system becomes unstable for $k_{max} = 10$. This reflects our results obtained in Table 5.6. As shown in Table 5.7, increasing the number of uncertainties

Table 5.4: Gloptipoly 3 + MOSEK LQR + MRAC Upper Bounds for section 5.3 - Uncertain k_1 ($k_2,\ k_3 = -0.1$)

	$k_{\max} = 0.1$		$k_{\max} = 1$		$k_{\max} = 10$	
Rel Ord	**Upper Bnd J**	**CPU [s]**	**Upper Bnd J**	**CPU [s]**	**Upper Bnd J**	**CPU [s]**
1	1.96×10^{-1}	2.24	2.04×10^{-1}	7.34×10^{-1}	3.19×10^{-1}	6.13×10^{-1}
2	8.14×10^{-4}	4.80	9.46×10^{-4}	5.03	7.29×10^{-3}	4.15
3	2.01×10^{-4}	1.14×10^{2}	1.76×10^{-4}	1.18×10^{2}	7.04×10^{-4}	1.09×10^{2}

Table 5.5: Gloptipoly 3 + MOSEK LQR + MRAC Upper Bounds for section 5.3 - Uncertain $k_1,\ k_3$ ($k_2 = -0.1$)

	$k_{\max} = 0.1$		$k_{\max} = 1$		$k_{\max} = 10$	
Rel Ord	**Upper Bnd J**	**CPU [s]**	**Upper Bnd J**	**CPU [s]**	**Upper Bnd J**	**CPU [s]**
1	3.19×10^{-1}	1.90	2.08×10^{-1}	1.40	1.24	6.83×10^{-1}
2	7.29×10^{-3}	7.54	1.09×10^{-3}	7.73	1.24	5.57
3	7.04×10^{-4}	1.62×10^{2}	1.09×10^{-3}	1.41×10^{2}	1.24	1.25×10^{2}

becomes costly. Conversely, you also risk missing unsafe trajectories if your parameter spacing is too sparse. In juxtaposition, similar upper bounds can be achieved using our framework with equivalent or less computation time.

5.4 Flexible Dynamics for an F-16 Polynomial Model

A nonlinear polynomial short period F-16 aircraft model augmented with adaptive feedback and in the presence of flexible dynamics is now considered.

Table 5.6: Gloptipoly 3 + MOSEK LQR + MRAC Upper Bounds for section 5.3 - Uncertain $k_1,\ k_3,\ k_2$

	$k_{\max} = 0.1$		$k_{\max} = 1$		$k_{\max} = 10$	
Rel Ord	**Upper Bnd J**	**CPU [s]**	**Upper Bnd J**	**CPU [s]**	**Upper Bnd J**	**CPU [s]**
1	1.96×10^{-1}	1.75	2.14×10^{-1}	9.82×10^{-1}	1.24	8.14×10^{-1}
2	7.49×10^{-4}	8.72	1.93×10^{-3}	9.17	1.24	8.89
3	1.03×10^{-4}	2.55×10^{2}	3.10×10^{-4}	2.18×10^{2}	1.24	2.97×10^{2}

Table 5.7: Monte-Carlo Upper Bounds for section 5.3

	Uncertain κ		**Uncertain $\kappa,\ \zeta$**		**Uncertain $\kappa,\ \eta,\ \zeta$**	
$k_{\max}$	**Upper Bnd J**	**CPU [s]**	**Upper Bnd J**	**CPU [s]**	**Upper Bnd J**	**CPU [s]**
0.1	3.75×10^{-8}	4.09×10^{1}	3.75×10^{-8}	1.76×10^{2}	3.75×10^{-8}	8.81×10^{2}
1	4.00×10^{-8}	4.08×10^{1}	4.36×10^{-8}	4.99×10^{2}	5.40×10^{-8}	9.21×10^{2}
10	7.70×10^{-8}	4.06×10^{1}	6.82×10^{-1}	2.58×10^{2}	1.13	8.77×10^{2}

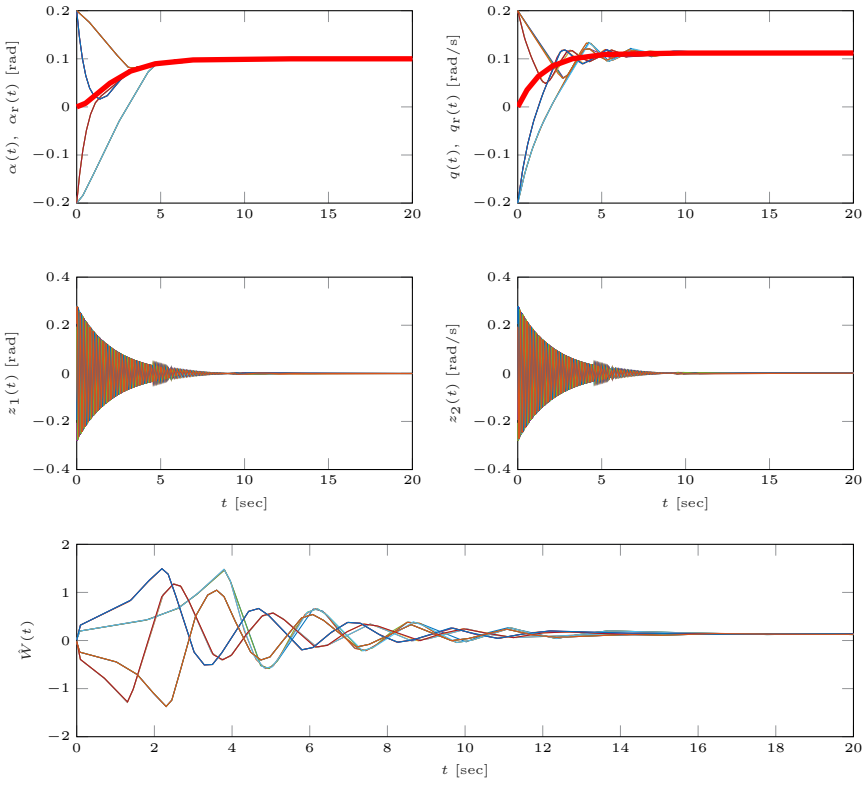

Figure 5.1: Monte-Carlo Worst Case for section 5.3 - Uncertain k_1 - ($k_1 = 0.1$, $k_2 = -0.1$, $k_3 = -0.1$)

The model itself and its feedback were used previously in chapter 3. The same flexible dynamics from (5.9) and the uncertain parameters $k_1,\ k_2,\ k_3 \in \begin{bmatrix} -k_{max} & k_{max} \end{bmatrix}$, $k_{max} \in \mathbb{R}_+$ are used. The procedure remains similar. After problem is presented in its compact form, it is written as a polynomial dynamical optimization problem, and then as its approximated partitioned form in the space of infinite measures using parsimony. Lastly, the model and its uncertainties are addressed explicitly using our framework and then validated under adverse flight conditions. In total, there are two cases:

1. k_1 is *uncertain*, k_2 and k_3 are *known*;
2. k_1 and k_3 are *uncertain*, k_2 is *known*.

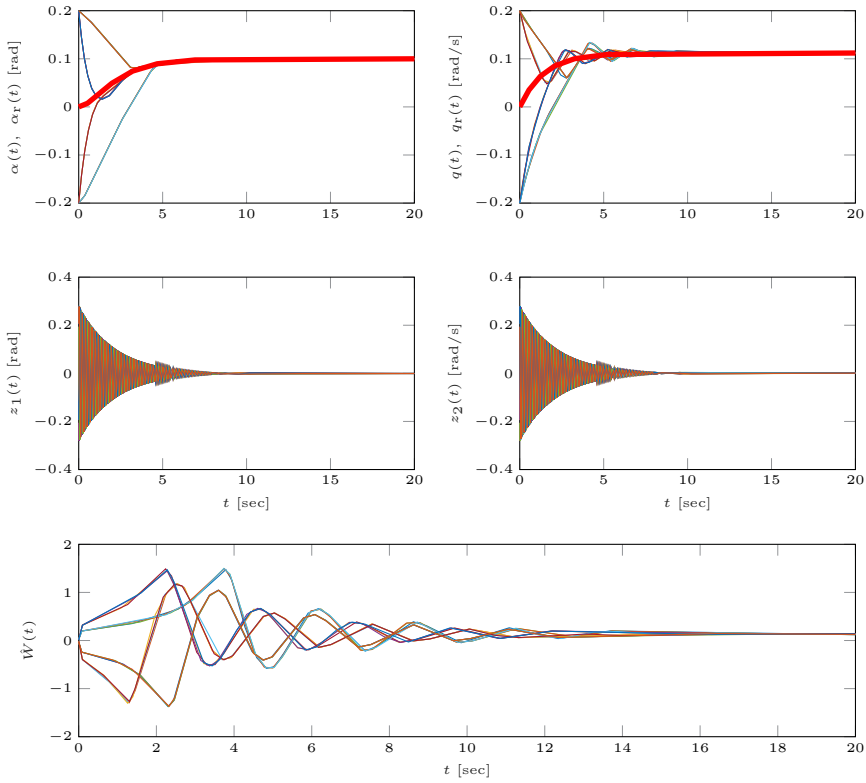

Figure 5.2: Monte-Carlo Worst Case for section 5.3 - Uncertain k_1 - ($k_1 = 1$, $k_2 = -0.1$, $k_3 = -0.1$)

5.4.1 Closed-Loop Configuration

Now consider a polynomial F-16 model with flexible dynamics

$$\dot{e}_\alpha(t) = \alpha(t) - c(t) \tag{5.20}$$

$$\dot{\mathbf{x}}_\mathbf{p}(t) = \mathbf{f}_\mathbf{p}(t, \mathbf{x}_\mathbf{p}(t), \Lambda u(t)) + B_\mathrm{p} H(k_1)^T \mathbf{z}(t) \tag{5.21}$$

$$\dot{\mathbf{z}}(t) = F\mathbf{z}(t) + G(k_2, k_3)^T \mathbf{x}_\mathbf{p}(t) \tag{5.22}$$

where $\mathbf{x}_\mathbf{p}(t) = \begin{bmatrix}\alpha(t), & q(t)\end{bmatrix}$ and polynomial $\mathbf{f}_\mathbf{p}(t, \mathbf{x}(t), \Lambda u(t)) \in \mathbb{R}^2$ $\begin{bmatrix}t, & \mathbf{x}_\mathbf{p}\end{bmatrix}$ are taken from chapter 3. The same matrices from section 5.3.1 B_p, F, $H(k_1)$, and $G(k_2, k_3)$ were used. The same uncertain parameter $k_1,\ k_2,\ k_3 \in \begin{bmatrix}-k_{max} & k_{max}\end{bmatrix}$ and reduced control effectiveness $\Lambda = 0.7$ were also used.

Our control objective is similar. We want to asymptotically track the reference dynamics (5.11) and command signal $c(t)$. With the *augmented* angle

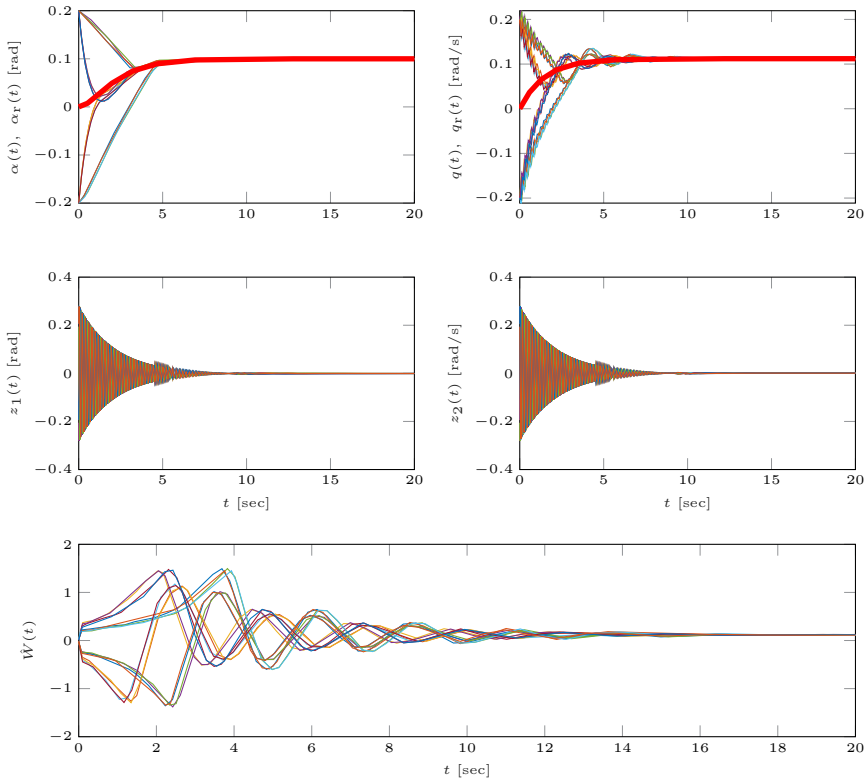

Figure 5.3: Monte-Carlo Worst Case for section 5.3 - Uncertain k_1 - ($k_1 = 10$, $k_2 = -0.1$, $k_3 = -0.1$)

of attack tracking dynamics (5.20), the new nominal control law becomes

$$u_{\mathrm{n}}(t) = -\underbrace{\begin{bmatrix} -10.0000 & -10.8756 & -6.0565 \end{bmatrix}}_{K} \mathbf{x_p}(t) \tag{5.23}$$

and was obtained using the LQR method [46]. Likewise, $A_{\mathrm{r}} = A_{\mathrm{p}} - B_{\mathrm{p}}K$ is Hurwitz, $B_{\mathrm{p}} = \begin{bmatrix} 0 & B_{\mathrm{p}} \end{bmatrix}^T$ and $B_{\mathrm{r}} = \begin{bmatrix} -1 & 0 & 0 \end{bmatrix}^T$ for (5.11). A similar adaptive feedback law $u_{\mathrm{a}}(t) = \hat{\mathbf{W}}(t)^T \Phi(\mathbf{x_p}(t))$ is also used

$$\dot{\hat{\mathbf{W}}}(t) = \underbrace{\begin{bmatrix} \epsilon & & \\ & \epsilon & \\ & & 100 \end{bmatrix}}_{\Gamma} \left(\Phi(\mathbf{x_p}(t))\mathbf{e}(T)^T PB\right), \quad \hat{\mathbf{W}}(0) = \hat{\mathbf{W}}_0 \tag{5.24}$$

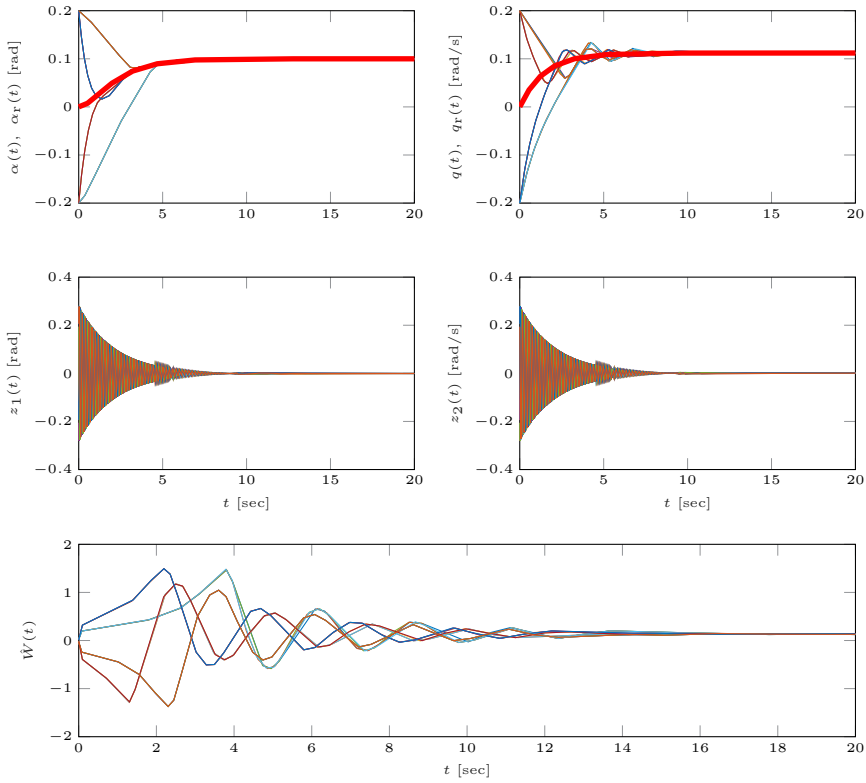

Figure 5.4: Monte-Carlo Worst Case for section 5.3 - Uncertain $k_1,\ k_3$ - ($k_1 = 0.1$, $k_2 = -0.1$, $k_3 = 0.1$)

where positive definite P is the unique solution to the Lyapunov equality

$$0 = A_r^T P + P A_r + \underbrace{\begin{bmatrix} 100 & & \\ & 10 & \\ & & 0.1 \end{bmatrix}}_{Q}. \tag{5.25}$$

Like before the MRAC is tuned for the longitudinal dynamics (5.21) while neglecting the unmodeled dynamics. The polynomial uncertainties from the dimensionless coefficients do not satisfy the matching condition. Combined with the unmodeled dynamics, the ultimate stability properties of the MRAC cannot be derived using Lyapunov. In the proceeding section, it is shown numerically that the MRAC can tolerate both. With the combined nominal/adaptive control law $u(t) = u_n(t) + u_a(t)$ the new closed loop dynamics (5.20), (5.21), (5.22),

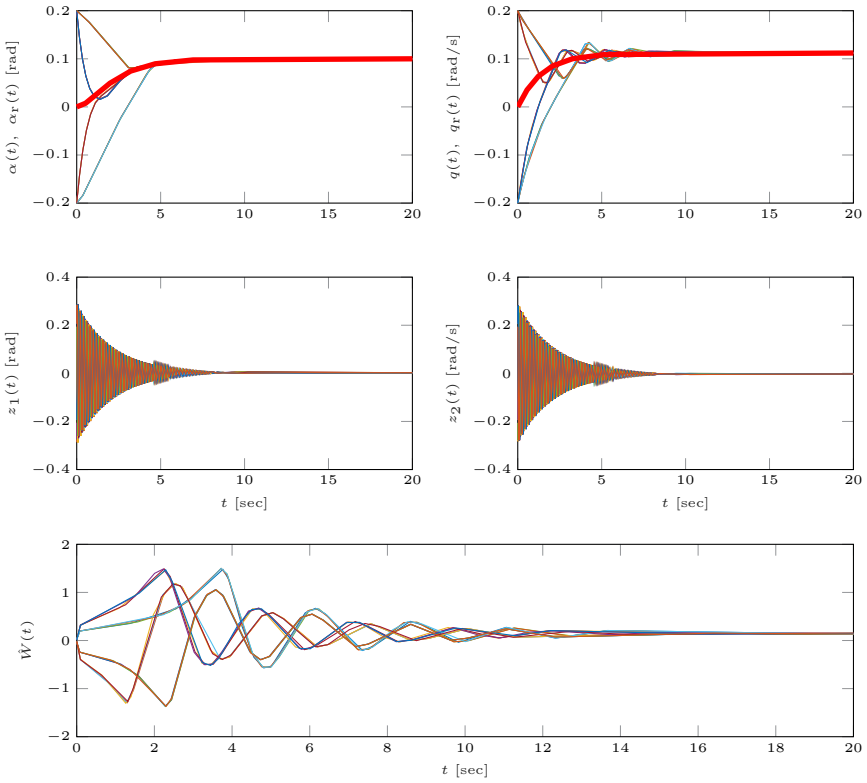

Figure 5.5: Monte-Carlo Worst Case for section 5.3 - Uncertain $k_1,\ k_3$ - ($k_1 = 1$, $k_2 = -0.1,\ k_3 = -1$)

and (5.24) can now be written in their compact form

$$\begin{aligned}
\dot{\mathbf{x}}_{\mathbf{1}}(t) &= \mathbf{f}_{\mathbf{1}}(t, \mathbf{x}_{\mathbf{1}}(t), c(t)), & y_1(t) &= \alpha_r(t), & \mathbf{x}_{\mathbf{1}}(0) &= \mathbf{x}_{\mathbf{1}0} \\
\dot{\mathbf{x}}_{\mathbf{2}}(t) &= \mathbf{f}_{\mathbf{2}}(t, \mathbf{x}_{\mathbf{2}}(t), y_1(t), y_3(t), k_1), & \mathbf{y}_{\mathbf{2}}(t) &= \mathbf{x}_{\mathbf{p}}(t), & \mathbf{x}_{\mathbf{2}}(0) &= \mathbf{x}_{\mathbf{2}0} \\
\dot{\mathbf{x}}_{\mathbf{3}}(t) &= \mathbf{f}_{\mathbf{3}}(t, \mathbf{x}_{\mathbf{3}}(t), \mathbf{y}_{\mathbf{2}}(t), k_2, k_3), & y_3(t) &= z_1(t), & \mathbf{x}_{\mathbf{3}}(0) &= \mathbf{x}_{\mathbf{3}0}
\end{aligned} \tag{5.26}$$

where $\mathbf{x}_{\mathbf{1}}(t) = \mathbf{x}_{\mathbf{r}}(t) \in \mathbb{R}^2$, $\mathbf{x}_{\mathbf{2}}(t) = \left[e_\alpha(t),\ \ \mathbf{x}_{\mathbf{p}}(t),\ \ \hat{\mathbf{W}}(t)\right] \in \mathbb{R}^3$, $\mathbf{x}_{\mathbf{3}}(t) = \mathbf{z}(t) \in \mathbb{R}^2$, and $\mathbf{y}_{\mathbf{2}}(t) \in \mathbb{R}^2$.

5.4.2 Validation Problem & Main Results

We want to validate our closed-loop model in its compact form (5.26) by finding the initial state that maximizes the norm of the concave cost function of the

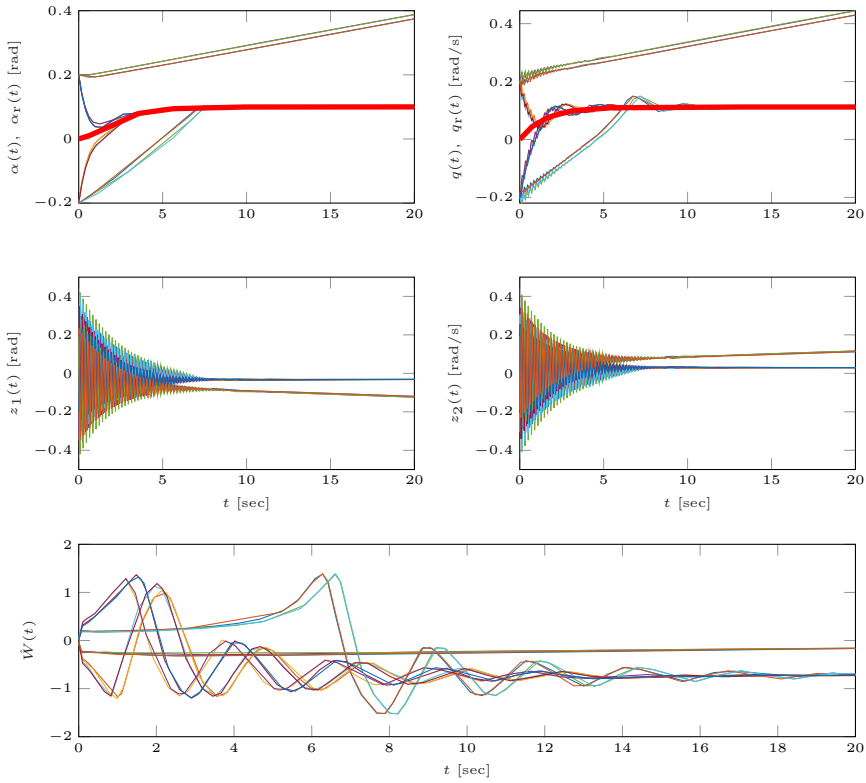

Figure 5.6: Monte-Carlo Worst Case for section 5.3 - Uncertain $k_1,\ k_3$ - ($k_1 = 10,\ k_2 = -0.1,\ k_3 = -10$)

tracking error $J = -(\alpha(T) - c(t))^2$ with given command signal $c(t) = 10\frac{\pi}{180}$ and terminal time $T = 10$. If we can show that for every chosen initial state

$$\mathbf{x_1}(0) \in \left[-1 \times 10^{-6},\quad 1 \times 10^{-6}\right]^3 \frac{\pi}{180} \triangleq X_{10}$$
$$\mathbf{x_2}(0) \in \left[-5,\quad 5\right]^3 \frac{\pi}{180} \times \left[-1 \times 10^{-6},\quad 1 \times 10^{-6}\right] \triangleq X_{20}$$
$$\mathbf{x_3}(0) \in \left[-0.01,\quad 0.01\right]^2 \triangleq X_{30}$$

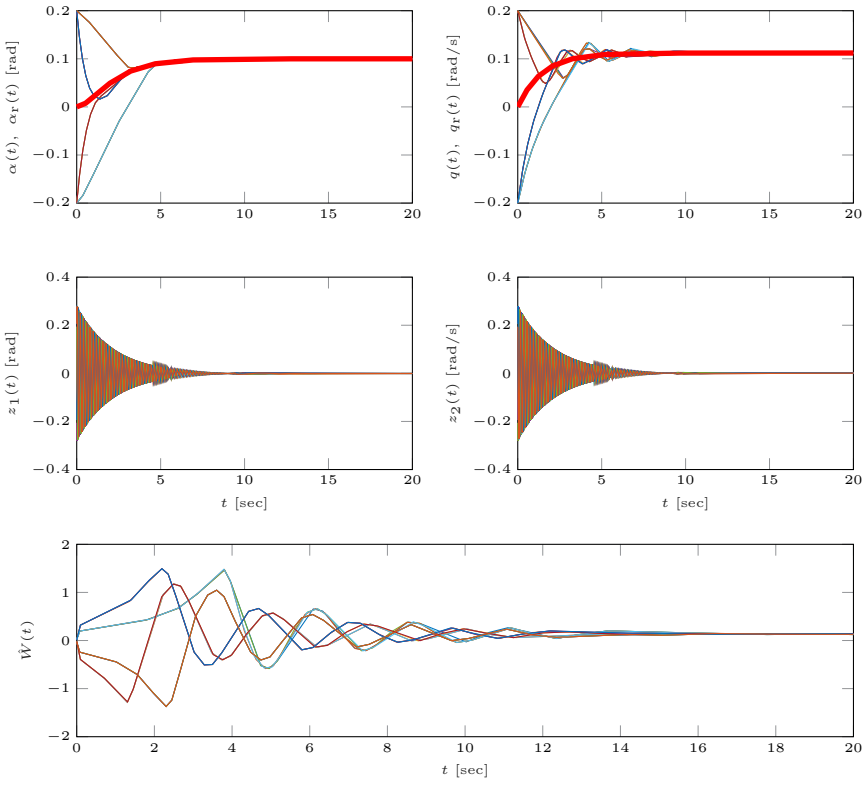

Figure 5.7: Monte-Carlo Worst Case for section 5.3 - Uncertain $k_1,\ k_2,\ k_3$ - $(k_1 = 0.1,\ k_2 = -0.1,\ k_3 = -0.1)$

all trajectories remain bounded in the box

$$\mathbf{x_1}(t) \in \left[-30,\quad 30\right]^2 \frac{\pi}{180} \times \left[-60,\quad 60\right] \frac{\pi}{180} \triangleq X_1$$
$$\mathbf{x_2}(t) \in \left[-30,\quad 30\right]^2 \frac{\pi}{180} \times \left[-60,\quad 60\right] \frac{\pi}{180} \times \left[-5,\quad 5\right] \triangleq X_2$$
$$\mathbf{x_3}(t) \in \left[-3,\quad 3\right]^2 \triangleq X_3$$

until they reach the final state belonging to the set $\alpha(T) \in \{J \leq 3 \times 10^{-3}\} \triangleq X_{1T}$, then the control law is validated. This general description can be expressed

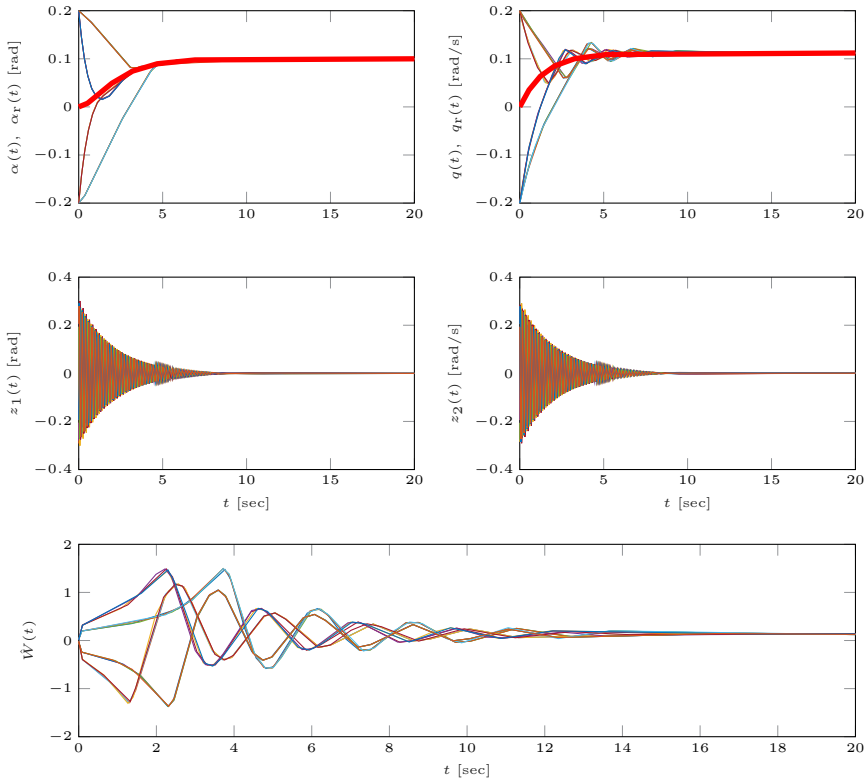

Figure 5.8: Monte-Carlo Worst Case for section 5.3 - Uncertain $k_1,\ k_2,\ k_3$ - $(k_1 = 1,\ k_2 = -1,\ k_3 = -1)$

by its polynomial dynamical optimization problem

$$
\begin{aligned}
J = \inf_{\alpha(T)} \quad & -(\alpha(T) - c(t))^2 \\
\text{s.t.} \quad & \dot{\mathbf{x}}_1(t) = \mathbf{f_1}(t, \mathbf{x_1}(t), c(t)) \\
& \dot{\mathbf{x}}_2(t) = \mathbf{f_2}(t, \mathbf{x_2}(t), y_1(t), y_3(t), k_1) \\
& \dot{\mathbf{x}}_3(t) = \mathbf{f_3}(t, \mathbf{x_3}(t), \mathbf{y_2}(t), k_2, k_3) \\
& \mathbf{x_1}(0) \in X_{10}, \quad \mathbf{x_1}(t) \in X_1, \quad \mathbf{x_1}(T) \in X_{1T}, \\
& \mathbf{x_2}(0) \in X_{20}, \quad \mathbf{x_2}(t) \in X_2, \quad \mathbf{x_2}(T) \in X_2, \\
& \mathbf{x_3}(0) \in X_{30}, \quad \mathbf{x_3}(t) \in X_3, \quad \mathbf{x_3}(T) \in X_3, \\
& t \in \left[0, \quad T\right], \quad u \in \left[-k_{max} \quad k_{max}\right].
\end{aligned}
\tag{5.27}
$$

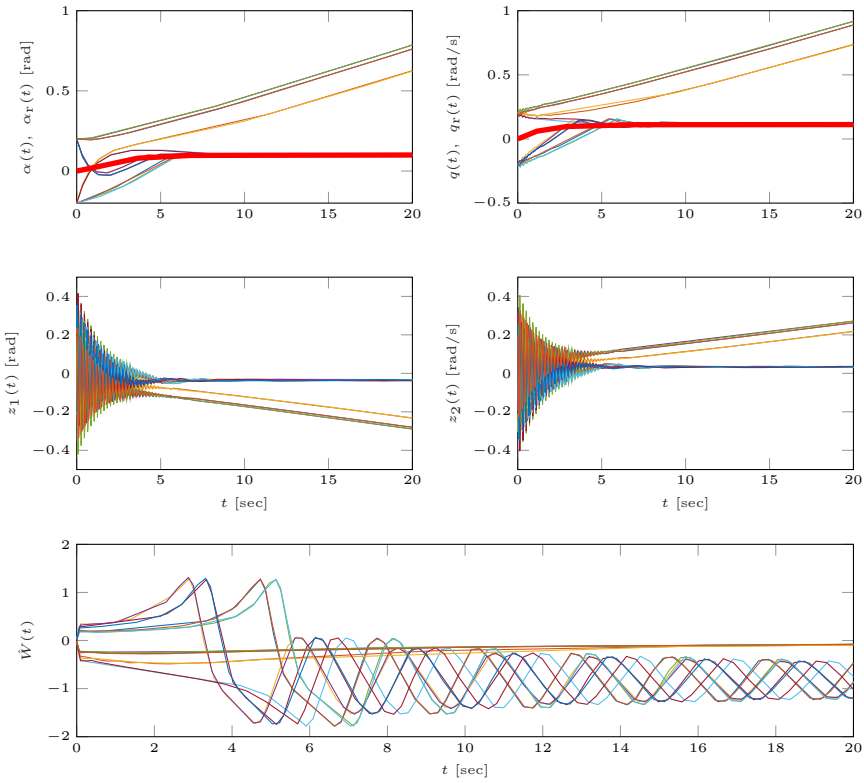

Figure 5.9: Monte-Carlo Worst Case for section 5.3 - Uncertain $k_1,\ k_2,\ k_3$ - $(k_1 = 10,\ k_2 = -10,\ k_3 = -10)$

Its approximation in the space of infinite dimensional measures using parsimony can be written as

$$
\begin{aligned}
J_\infty = \inf_{\mu_T} \quad & -\int (\alpha(T) - c(t))^2 d\mu_T \\
\text{s.t.} \quad & \frac{\partial \mu}{\partial t} + \mathrm{div}\mathbf{f_1}\mu(t, \mathbf{x_1}) + \mu_T = \mu_0 \\
& \frac{\partial \nu}{\partial t} + \mathrm{div}\mathbf{f_2}\nu(t, \mathbf{x_2}, y_1, y_3, k_1) + \nu_T = \nu_0 \\
& \frac{\partial \xi}{\partial t} + \mathrm{div}\mathbf{f_3}\xi(t, \mathbf{x_3}, \mathbf{y_2}, k_2, k_3) + \xi_T = \xi_0 \\
& \pi_{t,y_1,\#}\mu = \pi_{t,y_1,\#}\nu \\
& \pi_{t,\mathbf{y_2},y_3,\#}\mu = \pi_{t,\mathbf{y_2},y_3,\#}\xi \\
& \int \mu_0 = 1, \quad \int \nu_0 = 1, \quad \int \xi_0 = 1
\end{aligned}
\tag{5.28}
$$

Table 5.8: Gloptipoly 3 + MOSEK LQR Upper Bounds for section 5.4 - Unknown k_1 ($k_2 = -0.1$ $k_3 = 0.1$)

	$k_{\max} = 0.1$		$k_{\max} = 1$		$k_{\max} = 200$	
Rel Ord	**Upper Bnd J**	**CPU [s]**	**Upper Bnd J**	**CPU [s]**	**Upper Bnd J**	**CPU [s]**
1	1.78	1.25×10^{1}	1.78	9.56	1.78	9.32
2	1.72×10^{-4}	5.22×10^{2}	1.60×10^{-4}	5.52×10^{2}	9.78×10^{-4}	6.92×10^{2}
3	1.00×10^{-5}	1.74×10^{4}	1.03×10^{-5}	1.80×10^{4}	1.06×10^{-5}	1.81×10^{4}

Table 5.9: Gloptipoly 3 + MOSEK LQR + MRAC Upper Bounds for section 5.4 - Uncertain k_1, k_3 ($k_2 = -0.1$)

	$k_{\max} = 0.1$		$k_{\max} = 1$		$k_{\max} = 200$	
Rel Ord	**Upper Bnd J**	**CPU [s]**	**Upper Bnd J**	**CPU [s]**	**Upper Bnd J**	**CPU [s]**
1	1.42	1.13×10^{1}	1.42	8.77	9.07×10^{-1}	1.17×10^{1}
2	9.23×10^{-4}	7.98×10^{2}	9.29×10^{-4}	7.45×10^{2}	9.07×10^{-1}	4.68×10^{2}
3	1.51×10^{-5}	1.82×10^{4}	1.52×10^{-5}	1.59×10^{4}	6.42×10^{-1}	1.73×10^{4}

Like the results in chapter 4, main advantage of this parsimony approach

The upper bounds for the F-16 polynomial model, coupled flexible dynamics, and combined LQR + MRAC control law can all be found in Tables 5.8 and 5.9. The upper bounds obtained using Monte-Carlo can be found in Table 5.10. The figures for the worst case Monte-Carlo can be found in Figs. 5.10 to 5.15. The procedure for finding the maximum upper bound is the same as in section 5.3.

The increased damping inherent from the polynomial model allows for more uncertainty in the unmodeled dynamics. The only case where where the LQR + MRAC cannot tolerate the unmodeled dynamics is when $k_1 = 200$, $k_3 = -200$.

5.5 Conclusion

We validated both a linear and polynomial F-16 model coupled with uncertain flexible dynamics and MRAC using our V&V framework. The state dynamics were approximated and partitioned by exploiting parsimony for ODEs. These results were compared to the upper bounds obtained using traditional Monte-Carlo simulation. This approach allows engineers to address explicitly MRAC

Table 5.10: F-16 Polynomial Monte-Carlo Upper Bounds for section 5.4

	Uncertain k_1		**Uncertain k_1, k_3**	
$k_{\max}$	**Upper Bnd J**	**CPU [s]**	**Upper Bnd J**	**CPU [s]**
0.1	2.61×10^{-8}	4.82×10^{1}	2.61×10^{-8}	1.82×10^{3}
1	2.62×10^{-8}	4.54×10^{1}	2.70×10^{-8}	2.35×10^{3}
200	2.86×10^{-8}	4.54×10^{1}	1.70×10^{-11}	7.23×10^{3}

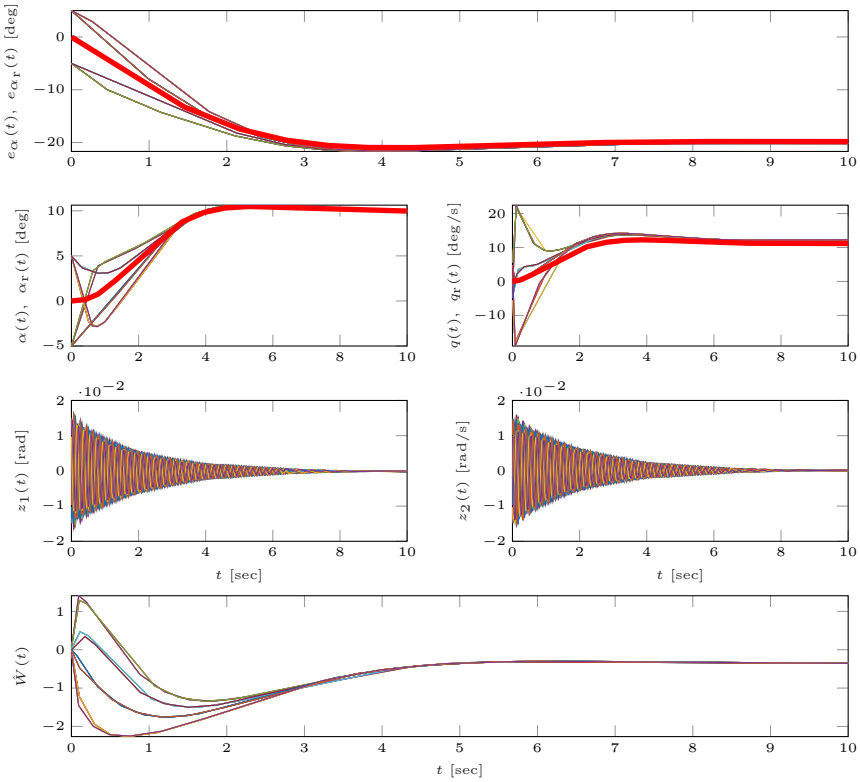

Figure 5.10: F-16 Polynomial Monte-Carlo Worst Case for section 5.4 - Uncertain k_1 - ($k_1 = -1$, $k_2 = -0.1$, $k_3 = 0.1$)

interacting with unmodeled dynamics without using costly Monte-Carlo simulations or complex controller modifications. In the future, we hope to use this same framework for validation of a full nonlinear F-16 model complete with MRAC and in-state uncertainties.

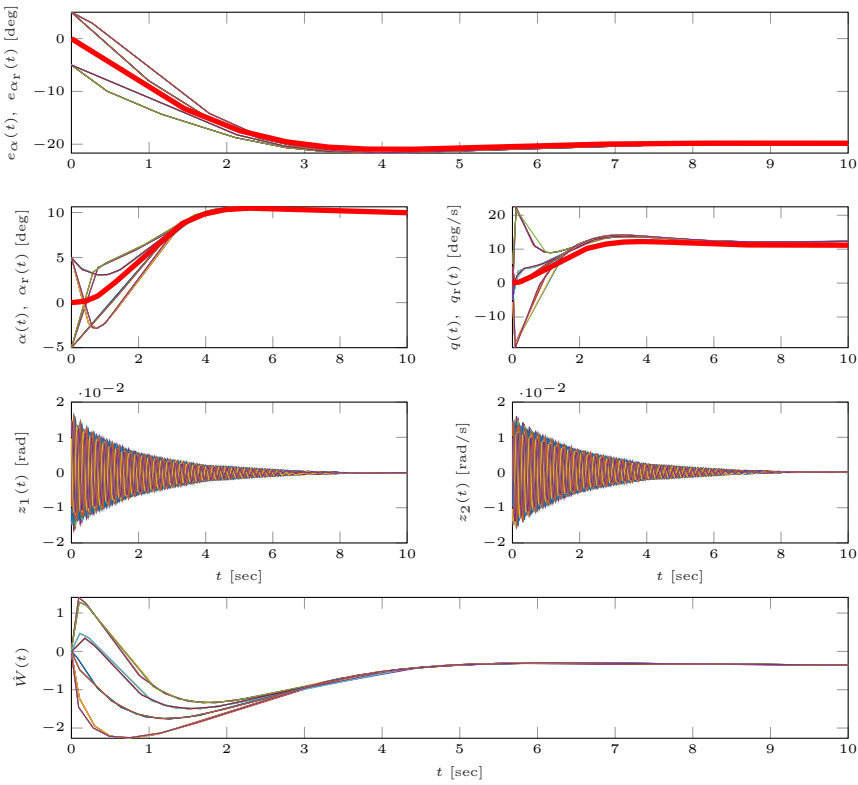

Figure 5.11: F-16 Polynomial Monte-Carlo Worst Case for section 5.4 - Uncertain k_1 - ($k_1 = -10$, $k_2 = -0.1$, $k_3 = 0.1$)

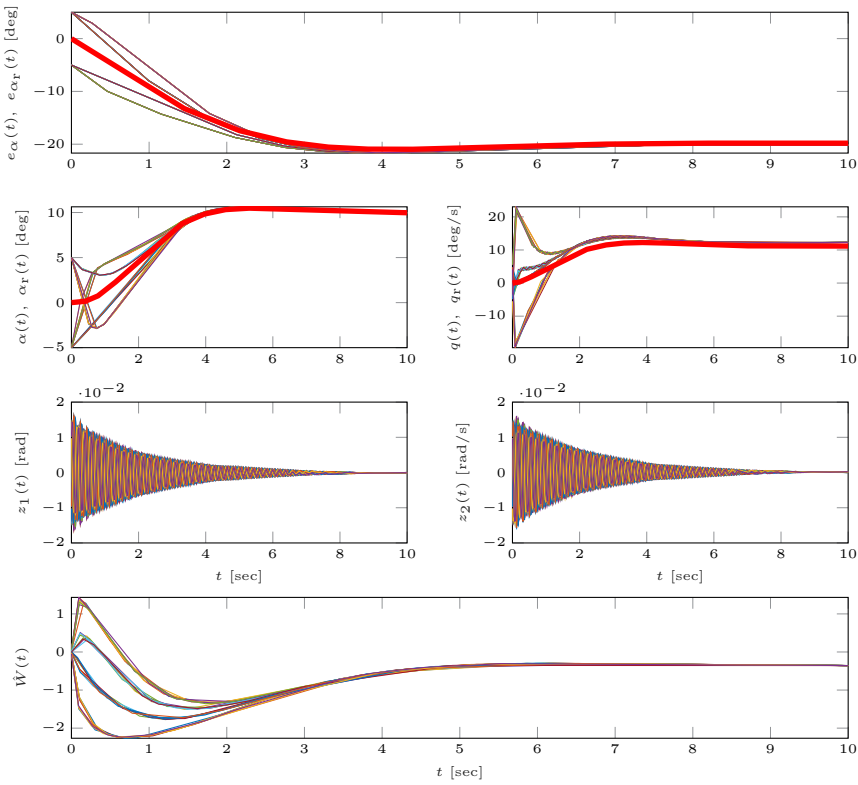

Figure 5.12: F-16 Polynomial Monte-Carlo Worst Case for section 5.4 - Uncertain k_1 - ($k_1 = 200$, $k_2 = -0.1$, $k_3 = 0.1$)

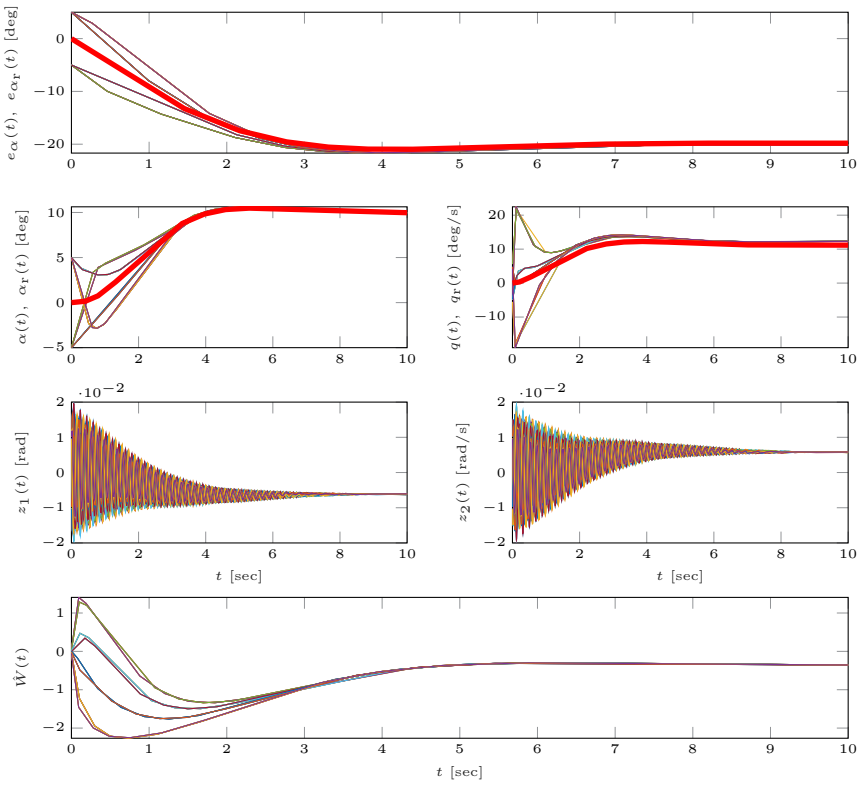

Figure 5.13: F-16 Polynomial Monte-Carlo Worst Case for section 5.4 - Uncertain $k_1,\ k_3$ - $(k_1 = -1,\ k_2 = -0.1,\ k_3 = -1)$

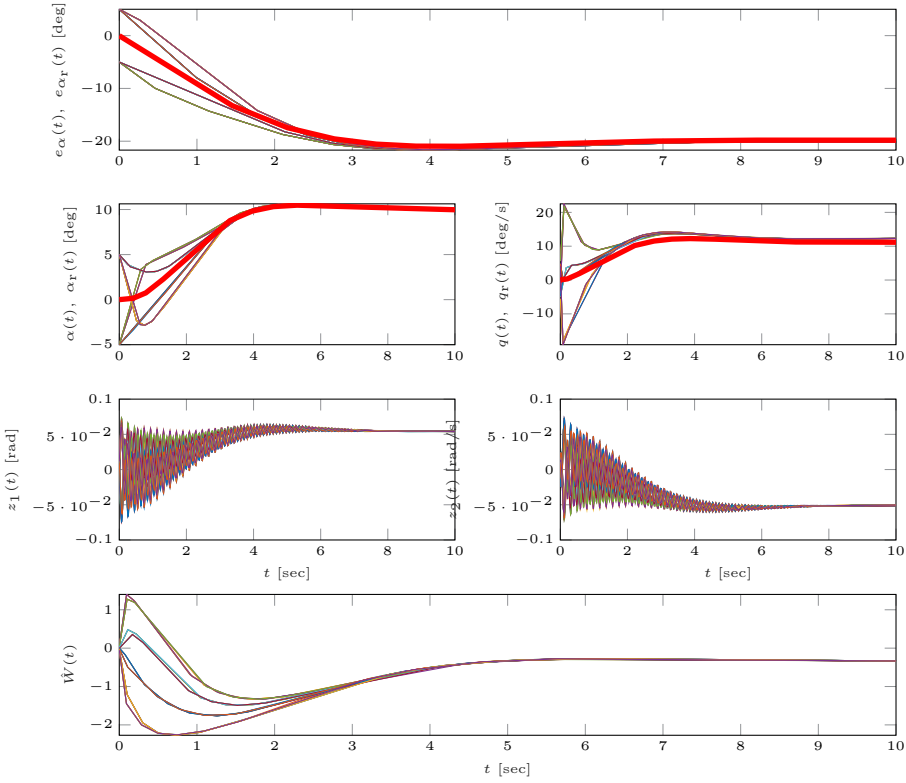

Figure 5.14: F-16 Polynomial Monte-Carlo Worst Case for section 5.4 - Uncertain $k_1,\ k_3$ - ($k_1 = 10,\ k_2 = -0.1,\ k_3 = 10$)

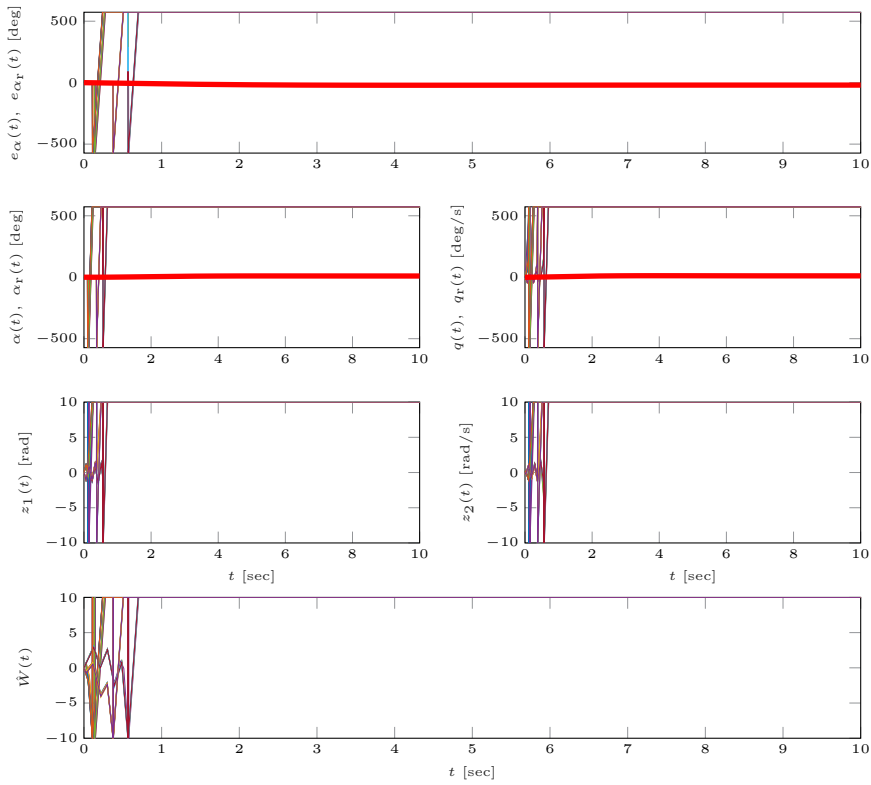

Figure 5.15: F-16 Polynomial Monte-Carlo Worst Case for section 5.4 - Uncertain $k_1,\ k_3$ - $(k_1 = 200,\ k_2 = -0.1,\ k_3 = -200)$

6

Aircraft with Uncertain Actuator Dynamics and MRAC

6.1 Introduction

As discussed in chapter 5, the main challenge in the design of adaptive control laws is addressing system stability and acceptable command following in the presence of uncertain, unmodeled actuator dynamics. In particular, degraded actuator performance can lead to poor tracking and even instability [21]. In real world applications, actuators seldom follow a first order model and their dynamics cannot be safely neglected, as they can limit achievable stability of model reference adaptive control (MRAC). Therefore, it remains imperative that there exists a way to ensure safe interaction between the higher order actuator and the MRAC in the design phase.

Current literature attempts to address this by using MRAC control modifications. See [63, 64] where the authors consider a pseudo control hedging modification to include actuator dynamics in the design phase of MRAC. The authors of [65, 28] revisit pseudo-control hedging with a novel Lyapunov LMI method to ensure ideal bounded reference trajectories for a range of admissible bandwidths, natural frequency, and damping inherent in the actuator dynamics.

Content of this chapter were accepted for publication to the Proceedings of the AIAA Guidance, Navigation, and Control Conference 2021 (Invited Session)

As discussed mainly in [28], the relationship between the damping and natural frequency can be bilinear. In other words, any variation in the damping can adversely affect the range of admissible natural frequencies required to maintain closed-loop stability for higher order actuators and vice-versa. There is also a relationship between the MRAC learning rate and the closed-loop stability. Consequently, traditional Monte-Carlo methods can become costly for systems with these parameter uncertainties inherent in their dynamics. Every combination of these parameters must be simulated, and there remains risk of state-space explosion or unexplored, unsafe trajectories for medium and large scale systems.

In this chapter, we focus on V&V of an F-16 longitudinal model with MRAC and uncertain third order elevator dynamics with deflection saturation. The elevator contains bounded uncertainties inherent in its damping and natural frequency. This approach is similar to that in chapter 5. Since uncertain parameters have an explicit representation in the space of occupation measures, we can identify numerically the worst case behavior caused by inherent uncertainties in damping and natural frequencies coming from the actuator. To avoid scaling problems, we exploit sparsity for ODEs to partition out the dynamics into a class of smaller systems that serve as control inputs for each other. In total, we are able to validate medium and large scale systems (up to 11 states) by using this approach.

Two examples are considered where the MRAC tolerates uncertainty in the natural frequency and damping, and one example where it obviously fails. Then, we compare our main results to those achieved using Monte-Carlo simulations and a search algorithm. The search algorithm locates the worst case damping and natural frequency behavior from the actuator.

Unlike the results of [63, 65, 28], we do not use the the pseudo control hedging modification to address actuator bandwidth uncertainty. Furthermore, none of the prior results take into account angle deflection saturation of the actuator. The results in [4, 6] provide only ultimate stability for aircraft models with linear feedback. The results in chapters 3 and 4 do not take into account uncertainties with a polynomial structure. In other words, our framework guarantees finite-time convergence for non-autonomous systems with piecewise dynamics. This is solution better than the solution provided by Barbalat's lemma [32] provided by the readily available Lyapunov certificate.

The organization of this work is as follows: section 6.2 discusses the short period of the F-16 with third order actuator dynamics, section 6.3 discusses our main results, and section 6.4 gives our main conclusions and suggestions for future research.

6.2 F-16 Short Period with Actuator Dynamics

The short-period mode of an F-16 aircraft can be expressed by the dynamics

$$\dot{\mathbf{x}}_{\mathbf{p}}(t) = A\mathbf{x}_{\mathbf{p}}(t) + Bv(t), \quad \mathbf{x}_{\mathbf{p}}(0) = \mathbf{x}_{\mathbf{p}0} \tag{6.1}$$

where $\mathbf{x}_{\mathbf{p}}(t) = \begin{bmatrix}\alpha(t) & q(t)\end{bmatrix}$ are the short period dynamics, $\alpha(t) \in \mathbb{R}$ is the angle of attack, $q(t) \in \mathbb{R}$ is the pitchrate,

$$A = \begin{bmatrix}-1.0189 & +0.9051 \\ +0.8223 & -1.0774\end{bmatrix}, \quad B = \begin{bmatrix}-0.0022 \\ -0.1756\end{bmatrix}$$

are the open loop short period dynamics. Elevator actuator output $v(t) \in \mathbb{R}$ is described the third order unmodeled actuator dynamics

$$\dot{\mathbf{x}}_{\mathbf{c}}(t) = (F + L(k_1, k_2))\,\mathbf{x}_{\mathbf{c}}(t) + Gu(t) \tag{6.2}$$

$$v(t) = H\mathbf{x}_{\mathbf{c}}(t), \quad v(0) = v_0 \tag{6.3}$$

where $u(t) \in \mathbb{R}$ is a measurable control input,

$$F = \begin{bmatrix} 0 & 1 & 0 \\ 0 & 0 & 1 \\ -a\omega_n^2 & \omega_n^2 + 2\zeta\omega_n a; & 2\zeta\omega_n + a \end{bmatrix}, \quad G = \begin{bmatrix}0\\0\\1\end{bmatrix}, \quad H = \begin{bmatrix} a\omega_n^2 \\ 0 \\ 0 \end{bmatrix},$$

$\zeta,\ \omega_n,\ a \in \mathbb{R}_+$ are the damping, natural frequency, and gain respectively,. Matrix

$$L = \begin{bmatrix} 0 & 1 & 0 \\ 0 & 0 & 1 \\ -ak_1^2 & k_1^2 + 2k_2k_1a; & 2k_2k_1 + a \end{bmatrix}$$

contains inherent uncertainties within damping and natural frequency of the actuator dynamics described by bounded parameters $k_1, k_2 \in \begin{bmatrix}-k_{max} & k_{max}\end{bmatrix}$, $k_{max} \in \mathbb{R}_+$. We assume that resulting matrix $(F + L)$ is Hurwitz, the DC gain between the control input $u(t)$ and actuator output $v(t)$ is unity, and pair (A, B) is controllable.

6.2.1 Model Reference Adaptive Control

Given a measurable command signal $c(t)$, we want to design a control law

$$u(t) = u_{\mathrm{n}}(t) + u_{\mathrm{a}}(t) \tag{6.4}$$

such that the combined nominal $u_{\mathrm{n}}(t)$ and adaptive control $u_{\mathrm{a}}(t)$ laws allow (6.1) to asymptotically track reference model

$$\dot{\mathbf{x}}_{\mathbf{r}}(t) = A_{\mathrm{r}}\mathbf{x}_{\mathbf{r}}(t) + B_{\mathrm{r}}c(t), \quad \mathbf{x}_{\mathbf{r}}(0) = \mathbf{x}_{\mathbf{r}0} \tag{6.5}$$

where $\mathbf{x_r}(t) = \begin{bmatrix}\alpha_\mathrm{r} & q_\mathrm{r}\end{bmatrix}$ and the error dynamics

$$\mathbf{e}(t) = \mathbf{x_p}(t) - \mathbf{x_r}(t) \tag{6.6}$$

satisfies $\lim_{t\to\infty} \mathbf{e}(t) = 0$. Matrices $A_\mathrm{r} = (A - BK_1)$ and $B_\mathrm{r} = BK_2$ are from the nominal controller

$$u(t) = K_1\mathbf{x_p}(t) + K_2 c(t) \tag{6.7}$$

with feedback/feedforward gains

$$K_1 = \begin{bmatrix}+4.7432 & -2.3163\end{bmatrix}, \quad K_2 = \begin{bmatrix}-4.3396\end{bmatrix}$$

obtained using the LQR method [62, 46]. We assume that there exists a feedback matrix K_1 such that matrix A_r is Hurwtiz.

The adaptive controller

$$u_\mathrm{a}(t) = -\hat{\mathbf{W}}^T(t)\Phi\big(\mathbf{x_p}(t)\big), \tag{6.8}$$

with the given basis function $\Phi_i(\mathbf{x_p}(t)) = (1 + e^{\mathbf{x_{p}}_i})^{-1}$, $i = 1, 2$ and weight estimate $\hat{\mathbf{W}}(t)$, satisfies the update law

$$\dot{\hat{\mathbf{W}}}(t) = \Gamma\Phi\big(\mathbf{x_p}(t)\big)\mathbf{e}^T(t)PB_\mathrm{p}, \quad \hat{\mathbf{W}}(0) = \hat{\mathbf{W}}_0 \tag{6.9}$$

where $\Gamma = \mathrm{diag}\left(\begin{bmatrix}\epsilon & 10\end{bmatrix}\right)$, $\epsilon << 1$ is the learning rate and positive definite matrix P is generated by the Lyapunov equality

$$0 = A_\mathrm{r}^T P + PA_\mathrm{r} + I_{2\times 2}. \tag{6.10}$$

Theorems that highlight the boundedness and long range stability of MRAC are discussed extensively in [47, 32]. For some discussion on control modifications, refer to [37]. For papers that discuss using these control modifications, refer to chapters 3 and 4.

6.3 Main Results

We wish to validate our existing closed loop polynomial aircraft model (6.1) with actuator dynamics (6.3) by finding the initial state that maximizes of the norm of the concave cost function $J = -\left\|\hat{\mathbf{e}}(T)\right\|_2^2$ where

$$\hat{\mathbf{e}}(t) = \begin{bmatrix}\alpha(t) - \alpha_\mathrm{r}(t) \\ q(t) - q_\mathrm{ss}(t)\end{bmatrix} \approx \mathbf{e}(t)$$

approximates the error dynamics and $q_{ss} = \lim_{t\to\infty} q_{\mathrm{r}}(t)$. We also have given terminal time $T = 25$ s, $c(t) = 0.1$ and actuator constants

$$a = 5, \quad \omega_n = 20, \quad \zeta = 0.1,$$

which are all guaranteed feasible solutions from [28]. If we can show that for every chosen initial state

$$\underbrace{\begin{bmatrix}\mathbf{x_p}(0) & \mathbf{x_c}(0) & \mathbf{x_r}(0) & \hat{\mathbf{W}}(0)\end{bmatrix}}_{\mathbf{x}(0)} \in X_0 \triangleq \begin{bmatrix}-0.2 & 0.2\end{bmatrix}^2 \times \begin{bmatrix}-1\times 10^{-6} & 1\times 10^{-6}\end{bmatrix}^6$$

that all trajectories remain bounded in the box

$$\underbrace{\begin{bmatrix}\mathbf{x_p}(t) & \mathbf{x_c}(t) & \mathbf{x_r}(t) & \hat{\mathbf{W}}(t)\end{bmatrix}}_{\mathbf{x}(t)} \in X \triangleq \begin{bmatrix}-2 & 2\end{bmatrix}^7 \times \begin{bmatrix}-3 & 3\end{bmatrix}$$

until they reach the terminal cost target $\hat{\mathbf{e}}(T) \in \{J \leq 4\times 10^{-3}\}$, then our control law is validated. For our main results, we consider a 1% and 10% increase in the uncertainty the elevator dynamics by increasing k_{max}. We also include an example where the MRAC *fails* due to severe degraded actuator performance invoked by a 5000% increase in the dynamic uncertainty.

To include saturation in the elevator deflection, we partition the dynamics using locally affine functions in three cells $X_j, j = 1,\ldots,3$ corresponding to linear, upper saturation, lower regimes

$$X_1 \triangleq \{\mathbf{x}(t) \in \mathbb{R}^8 : |v(t)| \leq \theta_{max}\}, \quad v(t) = H\mathbf{x_c}(t) \tag{6.11}$$

$$X_2 \triangleq \{\mathbf{x}(t) \in \mathbb{R}^8 : v(t) \geq \theta_{max}\}, \quad v(t) = \theta_{max} \tag{6.12}$$

$$X_3 \triangleq \{\mathbf{x}(t) \in \mathbb{R}^8 : v(t) \leq -\theta_{max}\}, \quad v(t) = -\theta_{max} \tag{6.13}$$

where $\theta_{max} = \frac{25\pi}{180}$.

With the *combined* short period dynamics (6.1), actuator dynamics, in-state actuator uncertainties k_1 and k_2, and controller dynamics all partitioned into the saturation regimes, we can write (2.9) as

$$\begin{aligned} J = \inf_{\hat{\mathbf{e}}(T)} \quad & -\|\hat{\mathbf{e}}(T)\|_2^2 \\ \text{s.t.} \quad & \dot{\mathbf{x}}_{\mathbf{p}}(t) = \mathbf{f_p}(t, \mathbf{x_p}(t), v(t)), \\ & \dot{\mathbf{x}}_{\mathbf{r}}(t) = \mathbf{f_r}(t, \mathbf{x_r}(t)), \\ & \begin{bmatrix}\dot{\mathbf{x}}_{\mathbf{c}}(t) \\ \dot{\hat{\mathbf{W}}}(t)\end{bmatrix} = \mathbf{f}_j(t, \mathbf{x_c}(t), \mathbf{x_p}(t), \hat{\mathbf{W}}(t), \alpha_{\mathrm{r}}, k_1, k_2), \\ & \mathbf{x}(t) \in X_j, \quad k_1, k_2 \in \begin{bmatrix}-k_{max} & k_{max}\end{bmatrix}, \quad j = 1,\ldots,3 \\ & \mathbf{x}(0) \in X_0, \quad \mathbf{x}(t) \in X_T, \quad t \in [0, T], \end{aligned} \tag{6.14}$$

and the measure LP of parsimony (2.12) as

$$
\begin{aligned}
J_\infty = \inf_{\mu_T} \quad & -\int \|\hat{\mathbf{e}}(T)\|_2^2 \, d\mu_T \\
\text{s.t.} \quad & \frac{\partial \mu}{\partial t} + \text{div}_{\mathbf{p}} \mu(t, \mathbf{x_p}, v) + \mu_T = \mu_0 \\
& \frac{\partial \nu}{\partial t} + \text{div}_{\mathbf{r}} \nu(t, \mathbf{x_r}) + \nu_T = \nu_0 \\
& \frac{\partial \xi}{\partial t} + \text{div} \mathbf{f}_j \xi(t, \mathbf{x_c}, \hat{\mathbf{W}}, \mathbf{x_p}, \alpha_{\text{r}}, k_1, k_2) + \xi_T = \xi_0 \\
& \pi_{t,\mathbf{x_p},v\#}\mu = \pi_{t,\mathbf{x_p},v\#}\nu \\
& \pi_{t,\mathbf{x_r}\#}\nu = \sum_{j=1}^{3} \pi_{t,\mathbf{x_r}\#}\xi \\
& \int \mu_0 = 1, \quad \int \nu_0 = 1, \quad \int \xi_0 = 1
\end{aligned}
\tag{6.15}
$$

with respect to each occupation measure μ, ν, ξ. Marginal $\pi_{t,\mathbf{x_p},v\#}\mu$ (respectively, $\pi_{t,\mathbf{x_p},v\#}\nu$) of measure μ (respectively, ν) with respect to variables t, $\mathbf{x_p}$, and v. Marginal $\pi_{t,\mathbf{x_r}\#}\mu$ (respectively, $\pi_{t,\mathbf{x_r}\#}\xi$) of measure μ (respectively, ξ) with respect to variables t, $\mathbf{x_r}$. As discussed in chapter 2 we use this strategy to address scaling issues inherited from the problem. With this approach, we can reduce the overall size of the problem by 3 variables. As discussed in chapters 3 to 5, we also employ some basic scaling strategies so that all dynamics are normalized on the interval $\begin{bmatrix}-1 & 1\end{bmatrix}$.

The Monte-Carlo use a fixed time step and evenly distributed initial conditions to simulate the trajectories. For every simulation, we also use a search algorithm to find the matrix $L(k_1, k_2)$ that maximizes the terminal cost J. The worst case Monte-Carlo simulations and upper bounds are given in Figs. 6.1 to 6.3 and Table 6.2, respectively,. Worst case parameters for natural frequency and damping are also shown in the captions.

As shown in Table 6.1, the upper bounds obtained using our framework (Gloptipoly 3 + MOSEK) show the MRAC can tolerate a 0.1% and 10% uncertainty in damping and natural frequency. At $k_{max} = 50$, the actuator performance degrades significantly and tracking is lost. We can also extract the time spent in the saturation regime, by extracting the mass of each occupation measure [40].

6.4 Conclusion

We validated a short period F-16 model with MRAC and a higher order elevator dynamics. The elevator contained parameter uncertainties and deflection

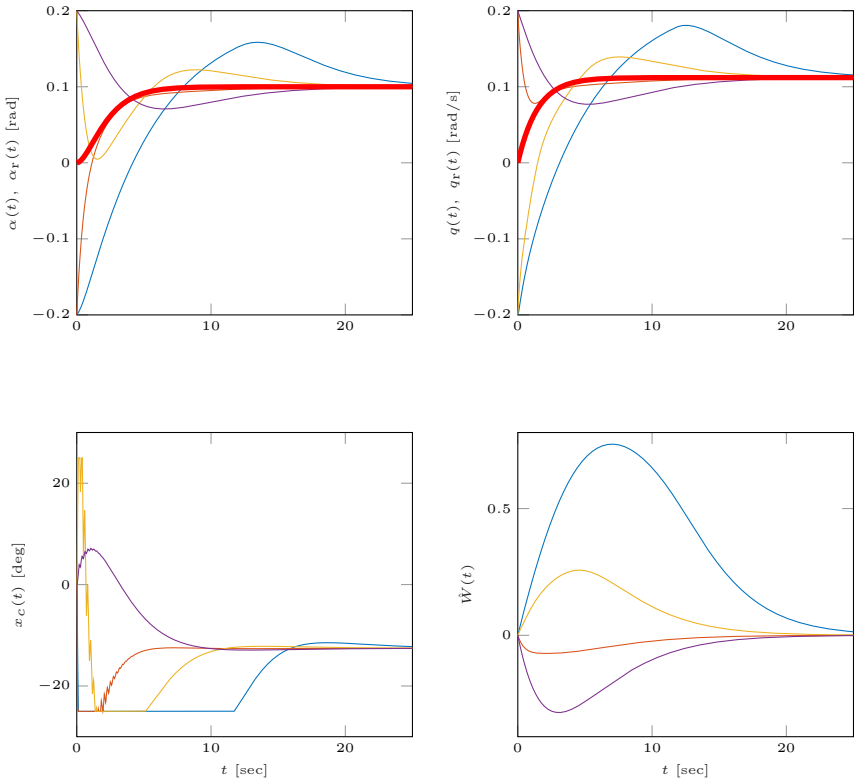

Figure 6.1: F-16 Monte-Carlo ($k_{max} = 0.01$, $k_1 = -0.01$, $k_2 = 0.01$)

	$k_{\max} = 0.01$		$k_{\max} = 0.1$		$k_{\max} = 50$	
Rel Ord	**Upper Bnd J**	**CPU [s]**	**Upper Bnd J**	**CPU [s]**	**Upper Bnd J**	**CPU [s]**
1	3.00×10^{-2}	2.81	3.10×10^{-2}	3.59	1.13	3.82
2	9.78×10^{-3}	3.17×10^{2}	9.66×10^{-3}	3.36×10^{2}	1.03×10^{-1}	4.34×10^{2}
3	1.98×10^{-3}	1.38×10^{5}	2.91×10^{-3}	1.15×10^{5}	2.86×10^{-2}	1.20×10^{5}

Table 6.1: Gloptipoly 3 + MOSEK Upper Bounds for section 6.3

saturation. We compared the results using our framework with those obtained using Monte-Carlo and a search algorithm. We also showed an example where the MRAC obviously fails due to poor performance from the elevator. For future results, we wish to find new ways to partition the dynamical problem to solve even larger scale systems and use region of attraction framework to find the numerical upper bounds for the uncertain parameters.

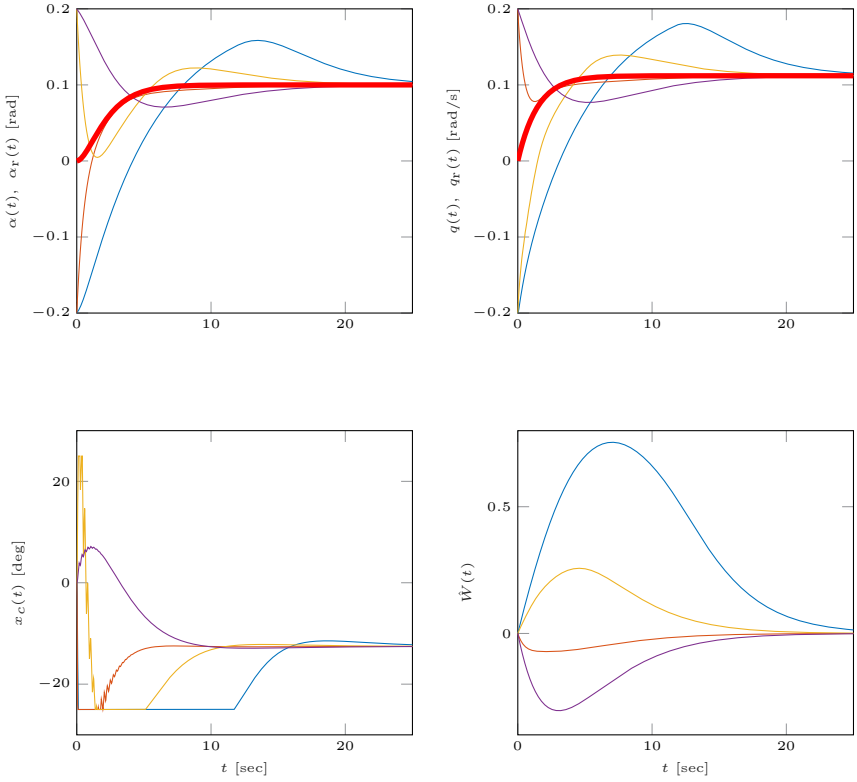

Figure 6.2: F-16 Monte-Carlo ($k_{max} = 0.1$, $k_1 = -0.1$, $k_2 = 0.1$)

$k_{\max}$	Upper Bound J (LQR + MRAC)	CPU Time [s]
0.01	3.13×10^{-5}	7.74×10^{1}
0.1	3.13×10^{-5}	7.96×10^{1}
50	2.27×10^{-2}	7.43×10^{1}

Table 6.2: Monte-Carlo Upper Bounds for section 6.3

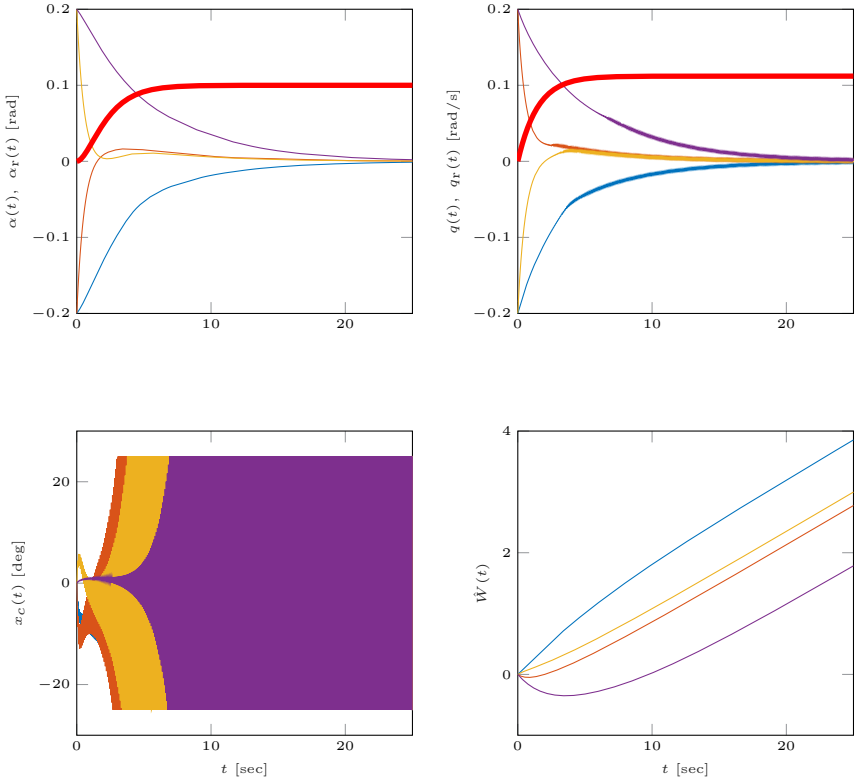

Figure 6.3: F-16 Monte-Carlo ($k_{max} = 50$, $k_1 = -50$, $k_2 = 0$)

7

Final conclusion

This chapter summarizes the main contributions of this thesis and discusses some potential future research directions.

7.1 Contributions

This thesis employed moment SOS hierarchies (in particular, Gloptipoly 3 with a SDP solver such as SeDuMi or MOSEK) for V&V of aerospace problems with adaptive control laws such as MRAC. Generating the numerical certificates for the polynomial aircraft model with adaptive feedback relies on using our framework. The main contributions of this thesis are outlined below:

1. This thesis proposes the use of advanced algorithms and our framework for V&V of polynomial aircraft models with nonlinear control laws such as MRAC. This serves as an alternative to traditional methods that are insufficient for adaptive control, such as Monte-Carlo, or infinite time convergence of non-piecewise polynomial systems. Specifically our framework was used to validate both longitudinal and lateral F-16 plants with MRAC. The numerical certificates we produce guarantee boundedness of all trajectories and convergence in finite time.

2. The computational cost for solving these polynomial dynamical optimization problems using our framework depends on size of the closed-loop system and the largest moment SDP block it generates. MRAC, at the very least, doubles the number of states we need to optimize over. By exploiting sparsity of ODEs, we are able to solve moderate to large scale systems (of up to 9 states depending on the problem) that are otherwise numerically intractable. In particular, we used our framework to solve a lateral F-16 plant with piecewise disturbances and MRAC feedback.

3. Unmodeled dynamics have an adverse affect on a closed-loop system with MRAC. Specifically, it is well established MRAC with the presence of unmodeled dynamics can lead to instability. Since bounded uncertain parameters have explicit representation in the space of occupation measures, we can guarantee the MRAC can tolerate at least sufficiently small unmodeled dynamics within the dynamical system. We solved for a longitudinal polynomial F-16 plant with known flexible dynamics but uncertain coupling. This approach was also applied to a longitudinal F-16 plant with MRAC and actuator dynamics that contain uncertain parameters.

7.2 Future Research

There are some interesting directions to take this research in the future:

1. Exploiting sparsity for ODEs using parsimony for MRAC relies on approximating the reference trajectory. Although we can write this off as initial condition mismatch, it would be interesting ways to find other ways to divide up the flight control problem using state estimators and observer based MRAC. The end goal would be generating a numerical certificate for a full polynomial aircraft model with longitudinal/lateral adaptive feedback. Since MRAC exhibits closed-loop phenomena invoked by numerical problems, such as initial condition mismatch, traditional V&V methods such as Monte-Carlo are out of the question.

2. Hi-fidelity models for high performance aircraft (such as hypersonic vehicles) are typically unavailable to the public. Using our framework to solve for a polynomial longitudinal hypersonic vehicle model could yield notable results.

3. Throughout this thesis, our generated numerical certificate are the terminal costs of our polynomial dynamical optimization problem. We should revisit the same results using our framework with the region-of-attraction (ROA) problem.

Appendix A

Validation Script

```
% inputs
r = input('Relaxation order r = '); T = input('Terminal time T = ');

ki  = 0.1; % uncertain parameter u upper bound

TScaled = 1; % normalized time

xmax = 1 * ones(2,1); x0max = 0.1 * ones(2,1);
zmax = 1 * ones(3,1); z0max = 0.1 * ones(3,1);

Dx  = diag(1./xmax); Dxinv = inv(Dx);
Dz  = diag(1./zmax); Dzinv = inv(Dz);

xmax = Dx * xmax; x0max = Dx * x0max; % normalize all states
zmax = Dz * zmax; z0max = Dz * z0max;

mpol('x1', 2); mpol('z1', 3); mpol('k1', 1); % dynamics

mpol('x0', 2); mpol('z0', 3); mpol('k0', 1); % initial
mpol('xT', 2); mpol('zT', 3); mpol('kT', 1); % terminal

mpol('t1', 1); % measures depend on time

m1 = meas([x1; z1; k1; t1]); % occupation measures

m0 = meas([x0; z0; k0]); mT = meas([xT; zT; kT]); %initial/terminal measures

% dynamics
x = Dxinv * x1; z = Dzinv * z1; u = k1; t = t1;

A = [0 -1+u 0 0 0; 1+u -5 0 0 0; 0 0.1 -10 0.1 0; 0 0 0.1 -1 -0.1; 0 0 0 1 -1];

f1 = T * blkdiag(Dx, Dz) * A * [x; z];

d = 2*r; % order of relaxation

p1 = genpow(8,d); p1 = p1(:,2:end); % powers

g1 = mmon([x1; z1; k1; t1],d); % bkild test functions

y10 = ones(size(p1,1),1)*[x0; z0; k0; 0]';  % unknown moments of initial measure
y10 = mom(prod((y10.^p1)'));

y1T = ones(size(p1,1),1)*[xT; zT; kT; TScaled]'; % unknown moments of terminal measure
y1T = mom(prod((y1T.^p1)'));

cost = mom(xT'*xT); % input LMI moment problem

A1y = mom(diff(g1,[x1;z1])*f1) + mom(diff(g1,t1)); % linear regime

% bounds on states
X0 = [x0.^2 <= x0max.^2; z0.^2 <= z0max.^2];
XT = [xT.^2 <= xmax.^2; zT.^2 <= zmax.^2];
B  = [x1.^2 <= xmax.^2; z1.^2 <= zmax.^2];
```

```
% bounds on time variables [normalized]
Tlim = [t1 >= 0, t1 <= TScaled];

% bounds on uncertain parameter
K0 = k0.^2 <= ki.^2; KT = kT.^2 <= ki.^2; K  = k1.^2 <= ki.^2;

tic % timer
P = msdp(max(cost),...
    mass(m0) == 1,...
    A1y - y1T + y10 ==  0,...
    X0, XT, B, K, K0, KT, Tlim);

% solve LMI moment problem
[status,obj] = msol(P);
```

Bibliography

[1] M. Heller, P. K. Niewoehner, and P. K. Lawson, "On the validation of safety critical aircraft systems, part I: An overview of analytical & simulation methods," Proceedings of the AIAA Guidance Navigation and Control Conference, (Austin, TX), August 11–14 2003.

[2] G. S. Tallant, P. Bose, J. M. Buffington, V. W. Crum, R. A. Hull, T. Johnson, B. Krogh, and R. Prasanth, "Validation & verification of intelligent and adaptive control systems," Proceedings of the IEEE Aerospace Conference, (Big Sky, MT), March 5–12 2005.

[3] S. A. Jacklin, "Closing certification gaps in adaptive flight control software," Proceedings AIAA Guidance, Navigation and Control Conference, (Honolulu, HI), August 18–21 2012.

[4] A. Chakraborty, *Nonlinear Robustness Analysis Tools for Flight Control Law Validation and Verification.* PhD thesis, University of Minnesota, 2012.

[5] AIAA Intelligent Systems Technical Committee, "Roadmap for intelligent systems in aerospace," tech. rep., AIAA, 2016.

[6] A. Chakraborty, P. Seiler, and G. J. Balas, "Susceptibility of F/A-18 flight controllers to the falling-leaf mode: Nonlinear analysis," *AIAA Journal of Guidance, Control, and Dynamics*, vol. 32, no. 1, pp. 73–85, 2011.

[7] H. P. Whitaker, J. Yamron, and A. Kezer, "Design of model reference control systems for aircraft," tech. rep., Instrumentation Laboratory, Massachusetts institution of Technology, Cambridge, MA, 1958.

[8] P. V. Osburn, H. P. Whitaker, and A. Kezer, "New developments in the design of adaptive control systems," tech. rep., Institution of Aeronautical Sciences, 1961.

[9] P. V. Kokotović, *Foundations of Adaptive Control*. New York: Springer-Verlag, 1991.

[10] M. Krstić, I. Kanellakopoulos, and P. V. Kokotović, *Nonlinear and Adaptive Control Design*. New York: Wiley, 1995.

[11] G. Tao, *Adaptive Control Design and Analysis*. New York: John Wiley & Sons, 2003.

[12] P. Ioannou and B. Fidan, *Adaptive Control Tutorial*. Philadelphia, PA: SIAM, 2006.

[13] N. Hovakimyan and C. Cao, $\mathcal{L}_1$ *Adaptive Control Theory: Guaranteed Robustness with Fast Adaptation*. Philadelphia, PA: SIAM, 2010.

[14] S. Sastry and M. Bodson, *Adaptive Control: Stability, Convergence and Robustness*. New York: Dover Publications, 2011.

[15] K. S. Narendra and A. M. Annaswamy, *Stable Adaptive Systems*. New York: Dover Publications, 2012.

[16] K. J. Åström and B. Wittenmark, *Adaptive Control*. New York: Dover Publications, 2013.

[17] K. A. Wise, E. Lavretsky, and N. Hovakimyan, "Adaptive control of flight: Theory, applications, and open problems," Proceedings of the American Control Conference, (Minneapolis, MN), June 14–16 2006.

[18] B. D. Anderson and A. Dehghani, "Challenges of adaptive control–past, permanent and future," *Annual Reviews in Control*, vol. 32, no. 2, pp. 123–135, 2008.

[19] W. S. Black, P. Haghi, and K. B. Ariyur, "Adaptive systems: History, techniques, problems, and perspectives," *Systems*, vol. 2, no. 4, pp. 606–660, 2014.

[20] G. Tao, "Multivariable adaptive control: A survey," *Automatica*, vol. 50, no. 411, pp. 2737–2754, 2014.

[21] Z. Drydek, A. Annaswamy, and E. Lavretsky, "Adaptive control and the NASA X-15-3 flight revisited," *IEEE Control Systems Magazine*, vol. 30, no. 3, p. 32–48, 2010.

[22] J. Bosworth and P. Williams-Hayes, "Flight test results from the NF-15B intelligent flight control system (IFCS) project with adaptation to a simulated stabilator failure," Proceedings of the AIAA Infotech@Aerospace Conference, May 7–10 2007.

[23] A. J. Calise, S. Lee, and M. Sharma, "Development of a reconfigurable flight control law for tailless aircraft," *AIAA Journal of Guidance, Control, and Dynamics*, vol. 24, no. 5, pp. 896–902, 2011.

[24] M. Sharma, E. Lavretsky, and K. A. Wise, "Application and flight testing of an adaptive autopilot on precision guided munitions," Proceedings of the AIAA Guidance Navigation and Control Conference, (Keystone, CO), 2006.

[25] J. H. Wall, J. S. Orr, and T. VanZweiten, "Space launch system implementation of adaptive augmenting control," Proceedings of the AIAA Guidance Navigation and Control Conference, (Breckenridge, CO), January 31–February 5 2014.

[26] N. Nguyen and J. S. A, *Neural Net Adaptive Flight Control Stability, Verification and Validation Challenges, and Future Research.* Berlin: Springer-Verlag, 2015.

[27] C. Rohrs, L. Valavani, M. Athans, , and G. Stein, "Robustness of continuous-time adaptive control algorithms in the presence of unmodeled dynamics," *IEEE Transactions on Automatic Control*, vol. 30, no. 9, pp. 881–889, 1985.

[28] B. Gruenwald, T. Yucelen, J. A. Muse, and D. Wagner, "Computing stability limits for adaptive control laws with high-order actuator dynamics," *Automatica*, vol. 101, pp. 409–416, 2019.

[29] D. Henrion, J. B. Lasserre, and J. Löfberg, "Gloptipoly 3: moments, optimization and semidefinite programming," *Optimization Methods and Software*, vol. 24, no. 4–5, pp. 761–779, 2009.

[30] M. ApS, "The MOSEK optimization toolbox for Matlab manual," 2019. www.mosek.com/, (accessed November 8, 2020).

[31] J. Sturm, "Using SeDuMi 1.02, a MATLAB toolbox for optimization over symmetric cones," *Optimization Methods and Software*, vol. 11–12, pp. 625–653, 1999.

[32] W. M. Haddad and V. S. Chellaboina, *Nonlinear dynamical systems and control: A Lyapunov-based approach.* Princeton, NJ: Princeton University Press, 2011.

[33] D. Henrion, "Optimization on linear matrix inequalities for polynomial systems control," *Les cours du CIRM*, vol. 3, no. 1, pp. 1–44, 2013.

[34] J. B. Lasserre, *Moments, positive polynomials and their applications.* London: Imperial College Press, 2009.

[35] M. Adbalmoaty, D. Henrion, and L. Rodrigues, "Measures and LMIs for optimal control of piecewise-affine systems," Proceedings of the European Control Conference, (Zurich, CH), January 17–19 2013.

[36] M. Tacchi, C. Cardozo, D. Henrion, and J. B. Lasserre, "Approximating regions of attraction of a sparse polynomial differential system," IFAC World Congress, (Berlin, DE), July 12–17 2020.

[37] K. S. Narendra and A. M. Annaswamy, "A new adaptive law for robust adaptation without persistent excitation," *IEEE Transactions on Automatic Control*, vol. 32, no. 2, pp. 134–145, 1987.

[38] A. J. Calise, T. Yucelen, J. A. Muse, and B. J. Yang, "A loop recovery method for adaptive control," Proceedings of the AIAA Guidance Navigation and Control Conference, (Chicago, IL), 2009.

[39] D. Wagner, D. Henrion, and M. Hromčík, "Measures and LMIs for adaptive control validation," Proceedings of IEEE Conference on Decision and Control, (Nice FR), December 11–13 2019.

[40] D. Henrion, M. Ganet-Schoeller, and S. Bennani, "Measures and LMI for space launcher robust control validation," vol. 7 of *Proceedings of the IFAC Symposium on Robust Control Design*, (Copenhagen, DK), pp. 236–241, 2011.

[41] A. F. Gabernet, *Controllers for Systems with Bounded Actuators : Modeling and control of an F-16 aircraft*. PhD thesis, University of California, Irvine, 2007.

[42] E. A. Morelli, "Global nonlinear parametric modeling with application to F-16 aerodynamics," vol. 2 of *Proceedings of the American Control Conference*, (Philadelphia, PA), pp. 997–1001, 1998.

[43] T. Yucelen and A. J. Calise, "Derivative-free model reference adaptive control of a generic transport model," Proceedings of the AIAA Guidance Navigation and Control Conference, (Toronto, CA), 2010.

[44] E. Lavretsky, "Combined/composite model reference adaptive control," *IEEE Transactions on Automatic Control*, vol. 54, no. 11, pp. 2692–2697, 2009.

[45] D. Wagner, D. Henrion, and M. Hromčík, "Measures and LMIs for lateral F-16 mrac validation," Proceedings of the American Control Conference, (Denver, CO), July 1–3 2020.

[46] B. L. Stevens, F. L. Lewis, and E. N. Johnson, *Aircraft control and simulation: Dynamics, controls design, and autonomous systems: Third edition*. NY: Wiley, 3rd ed. ed., 2015.

[47] E. Lavretsky and K. Wise, *Robust and Adaptive Control With Aerospace Applications*. London: Springer-Verlag, 2013.

[48] A. Calise, N. Hovakimyan, and M. Idan, "Adaptive output feedback control of nonlinear systems using neural networks," *Automatica*, vol. 38, no. 8, pp. 1201–1211, 2001.

[49] N. Hovakimyan, F. Nardi, A. Calise, and N. Kim, "Adaptive output feedback control of uncertain nonlinear systems using single-hidden-layer neural networks," *IEEE Transactions on Neural Networks*, vol. 13, no. 6, pp. 1420–1431, 2002.

[50] S. Tong, T. Wang, Y. Li, and H. Zhang, "Adaptive output feedback control of uncertain nonlinear systems using single-hidden-layer neural networks," *IEEE Transactions on Neural Networks*, vol. 13, no. 6, pp. 1420–1431, 2014.

[51] S. Tong, T. Wang, and Y. Li, "Fuzzy adaptive actuator failure compensation control of uncertain stochastic nonlinear systems with unmodeled dynamics," *IEEE Transactions on Fuzzy System*, vol. 22, no. 3, pp. 563–574, 2014.

[52] Y. Li, S. Sui, and S. Tong, "Adaptive fuzzy control design for stochastic nonlinear switched systems with arbitrary switchings and unmodeled dynamics," *IEEE Transactions on Cybernetics*, vol. 47, no. 2, pp. 403–414, 2016.

[53] M. Matsutani, A. M. Annaswamy, T. E. Gibson, and E. Lavretsky, "Trustable autonomous systems using adaptive control," Proceedings of the IEEE Conference on Decision and Control, (Orlando, FL), December 12–15 2011.

[54] M. Matsutani and A. M. Annaswamy, "Guaranteed delay margins for adaptive control of scalar plants," Proceedings of the IEEE Conference on Decision and Control, (Maui, HI), December 10–13 2012.

[55] M. Matsutani, A. M. Annaswamy, and E. Lavretsky, "Robust adaptive control in the presence of unmodeled dynamics: A counter to Rohrs's counterexample," Proceedings of the AIAA Guidance Navigation and Control Conference, (Boston, MA), August 19–22 2013.

[56] K. Merve Dogan, B. C. Gruenwald, T. Yucelen, and J. A. Muse, "Relaxing the stability limit of adaptive control systems in the presence of unmodelled

dynamics," *International Journal of Control*, vol. 91, no. 8, pp. 1774–1784, 2018.

[57] K. Merve Dogan, B. C. Gruenwald, T. Yucelen, and J. A. Muse, "Relaxing the stability limit of adaptive control systems in the presence of unmodelled dynamics," *International Journal of Robust and Nonlinear Control*, vol. 91, no. 8, pp. 1774–1784, 2016.

[58] K. Merve Dogan, T. Yucelen, and J. A. Muse, "Performance guarantees in adaptive control of uncertain systems with unmodeled dynamics," Proceedings of the AIAA Guidance, Navigation, and Control Conference, (Orlando, FL), January 6–10 2020.

[59] K. Merve Dogan and J. A. Yucelen, T Muse, "Adaptive control of dynamical systems with unstructured uncertainty and unmodeled dynamics," Proceedings of the American Control Conference, (Philadelphia, PA), July 10–12 2019.

[60] K. Merve Dogan, T. Yucelen, J. Yildirim, and J. A. Muse, "Experimental results of a model reference adaptive control law on an uncertain system with unmodeled dynamics," Proceedings of the AIAA Guidance, Navigation, and Control Conference, (San Diego, CA), January 7–11 2019.

[61] J. Noel, L. Renson, G. Kerschen, B. Peeters, S. Manzato, and J. Debille, "Nonlinear dynamic analysis of an F-16 aircraft using GVT data," Proceedings of the International Forum on Aeroelasticity and Structural Dynamics, (Bristol, UK), 2014.

[62] M. L. Fravolini, E. Arabi, and T. Yucelen, "A model reference adaptive control approach for uncertain dynamical systems with strict component-wise performance guarantees," Proceedings of AIAA Guidance, Navigation, and Control Conference, (Kissimmee, FL), January 8–12, 2018.

[63] E. N. Johnson and A. J. Calise, "Pseudo-control hedging : a new method for adaptive control," Advances in Navigation Guidance and Control Technology Workshop, (Redstone, AL), November 1–2 2000.

[64] E. N. Johnson and A. J. Calise, "Limited authority adaptive flight control for reusable launch vehicles," *AIAA Journal of Guidance, Control, and Dynamics*, vol. 26, no. 6, pp. 906–913, 2003.

[65] B. C. Gruenwald, D. Wagner, T. Yucelen, and J. A. Muse, "An LMI-based hedging approach to model reference adaptive control with actuator dynamics," Proceedings of the ASME 8th Annual Dynamic Systems and Control Conference, (Columbus, OH), October 28–30 2015.

Publications and awards

Papers related to this thesis

Published conference papers

[1] D. Wagner, D. Henrion, and M. Hromčík, "Measures and LMIs for Validation of an Aircraft with MRAC and Uncertain Actuator Dynamics," Proceedings of the AIAA Guidance, Navigation, and Control Conference, (Kissimmee, FL), January 11-15 2021 (To Appear).

[2] D. Wagner, D. Henrion, and M. Hromčík, "Measures and LMIs for lateral F-16 MRAC validation," Proceedings of the American Control Conference, (Denver, CO) July 1-3 2020.

[3] D. Wagner, D. Henrion, and M. Hromčík, "Measures and LMIs for Adaptive Control Validation," Proceedings of the IEEE Conference on Decision and Control, (Nice, FR), December 11-13 2019.

Published journal papers

[4] B.C. Gruenwald, T. Yucelen, J.A. Muse, and D. Wagner, "Computing stability limits for adaptive control laws with high-order actuator dynamics," Automatica 101 (2019), 409–416.

Submited journal papers

[5] D. Wagner, D. Henrion, and M. Hromčík, "Measures and LMIs for Verification and Validation of a Flexible Aircraft with Model Reference Adaptive Control," submitted to *International Journal of Control*, in June 2020.

Papers not related to this thesis

Published conference papers

[6] B.C. Gruenwald, T. Yucelen, J.A. Muse, and D. Wagner, "Model reference adaptive control in the presence of high-order actuator dynamics," Proceedings of the IEEE Conference on Decision and Control, (Las Vegas, NV), December 12-14 2016.

[7] M.L. Fravolini, T. Yucelen, B.C. Gruenwald, D. Wagner, and M.R. Napolitano, "Comparison of Robust and Probabilistic LMI-Based Design of Adaptive Flight Controllers with Uncertain Input Dynamics," Proceedings of the AIAA Guidance, Navigation, and Control Conference. (San Diego, CA), January 4-8 2016.

[8] B.C. Gruenwald, D. Wagner, T. Yucelen, and J.A. Muse, "An LMI-Based Hedging Approach to Adaptive Control with Actuator Dynamics in the Presence of Unknown Control Effectiveness," Proceedings of the AIAA Guidance, Navigation, and Control Conference. (San Diego, CA), January 4-8 2016.

[9] B.C. Gruenwald, D. Wagner, T. Yucelen, and J.A. Muse, "An LMI-Based Hedging Approach to Model Reference Adaptive Control with Actuator Dynamics," Proceedings of the ASME 8th Annual Dynamic Systems and Control Conference, (Columbus, OH), October 28-30 2015.

[10] M.L. Fravolini, T. Yucelen, D. Wagner, B.C. Gruenwald, and N. Nguyen, "A design, analysis, and verification framework for adaptive flight control," Proceedings of the AIAA Guidance, Navigation, and Control Conference. (Kissimmee, FL), January 5-9 2015.

[11] M.L. Fravolini, T. Yucelen, D. Wagner, A. Albattat, and P. Valigi, "Verifiable frequency-limited adaptive control performance based on LMIs," Proceedings of the IEEE Conference on Decision and Control, (Los Angeles, CA), December 15-17 2014.

Published journal papers

[12] B.C. Gruenwald, D. Wagner, T. Yucelen, and J.A. Muse, "Computing Actuator Bandwidth Limits for Model Reference Adaptive Control," International Journal of Control vol. 89, no. 12, pp. 2434–2452, 2016.

Published book chapters

[13] B.C. Gruenwald, J.A. Muse, D. Wagner, and T. Yucelen, "Adaptive Architectures for Control of Uncertain Dynamical Systems with Actuator Dynamics," in *Advances in Computational Intelligence and Autonomy for Aerospace Systems*. Valasek, J., Renton, VA: AIAA, 2015.

Awards

- NASA-Missouri Space Grant Consortium (MOSGC), 2017.

Czech Technical University in Prague
Faculty of Electrical Engineering
Department of Control Engineering
Karlovo Náměstí 13E
121 35 Praha 2